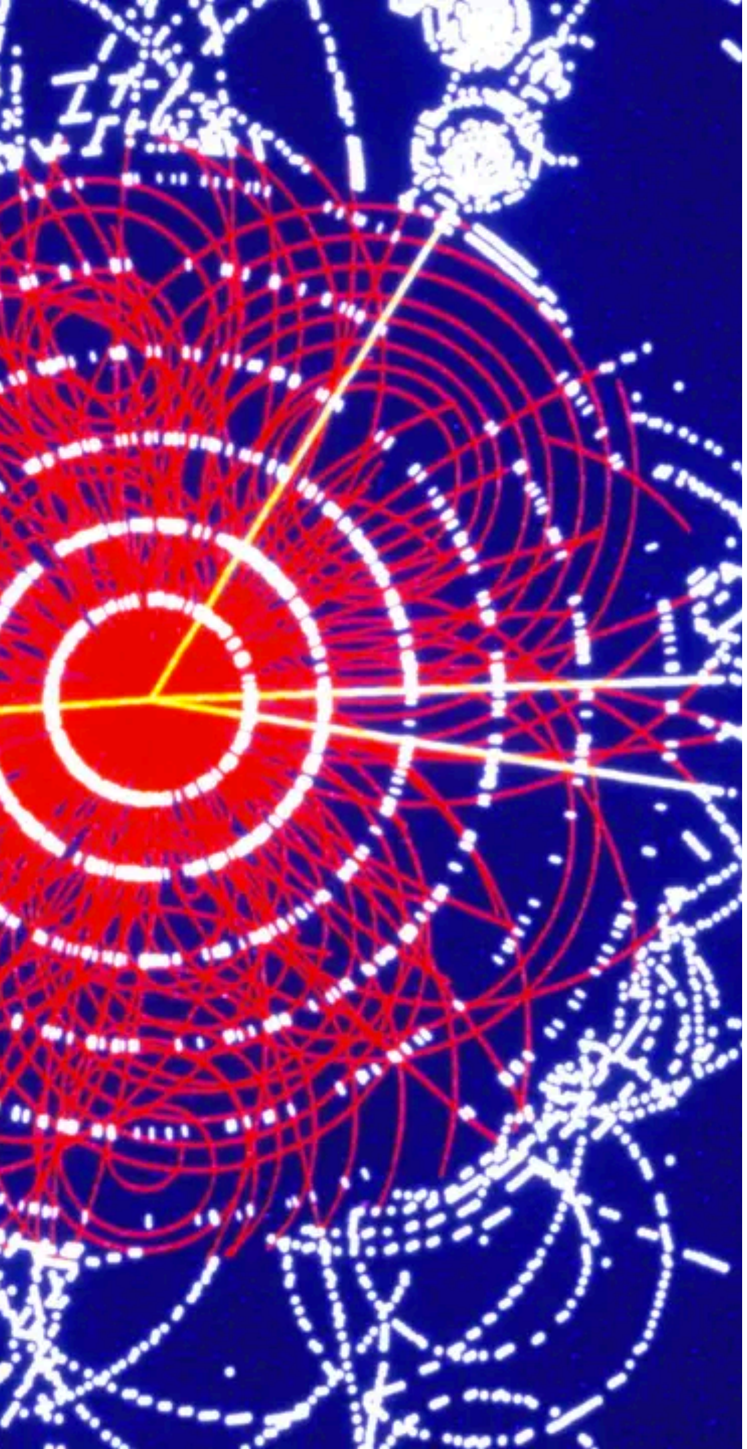

Exploring long-lived BSM Particles at the LHC

Rafał Masełek

PostDoc seminar, 23.01.2024, Grenoble

CLASSICAL PHYSICS

ISAAC NEWTON

LAWS OF MOTION

LAW OF UNIVERSAL GRAVITATION

ORBITS

GRAVITY

CALCULUS

$\int_0^6 x^2\,dx$ $\frac{dy}{dx}$

COSMOLOGY

ASTROPHYSICS

PRISM

OPTICS

REFLECTION
REFRACTION
DIFFRACTION

MICROSCOPE

TELESCOPE

CLASSICAL MECHANICS

WAVES

TRANSVERSE

LONGITUDINAL

ELECTRIC FIELDS

MAGNETIC FIELDS

JAMES CLERK MAXWELL

ELECTROMAGNETISM

FLUID MECHANICS

FLOW

LIFT

AERODYNAMICS

ELECTRICITY

LIGHT

THERMODYNAMICS

ENERGY

HEAT
TEMPERATURE

ENTROPY

CHAOS THEORY

RELATIVITY

CONSTANT SPEED OF LIGHT

ALBERT EINSTEIN

GENERAL THEORY OF RELATIVITY

SPECIAL THEORY OF RELATIVITY

$E=mc^2$

TIME

SPACE

SPACETIME

PHILOSOPHY

PHILOSOPHY OF SCIENCE

FREE WILL

HOW COME?

NATURE OF REALITY

JUST...WHY?

THE CHASM OF IGNORANCE

THE FUTURE

QUANTUM GRAVITY

STRING THEORY

SUPER SYMMETRY

LOOP QUANTUM GRAVITY

DARK ENERGY

DARK MATTER

AND MANY MORE...

QUANTUM FIELD THEORY

QUANTUM ELECTRO DYNAMICS

THE STANDARD MODEL

ATOMIC THEORY

NUCLEAR PHYSICS

FISSION

FUSION

CONDENSED MATTER PHYSICS

QUANTUM INFORMATION

COMPUTERS

LASERS

QUANTUM PHYSICS

@DominicWalliman

PARTICLE PHYSICS

Large Hadron Collider (LHC)

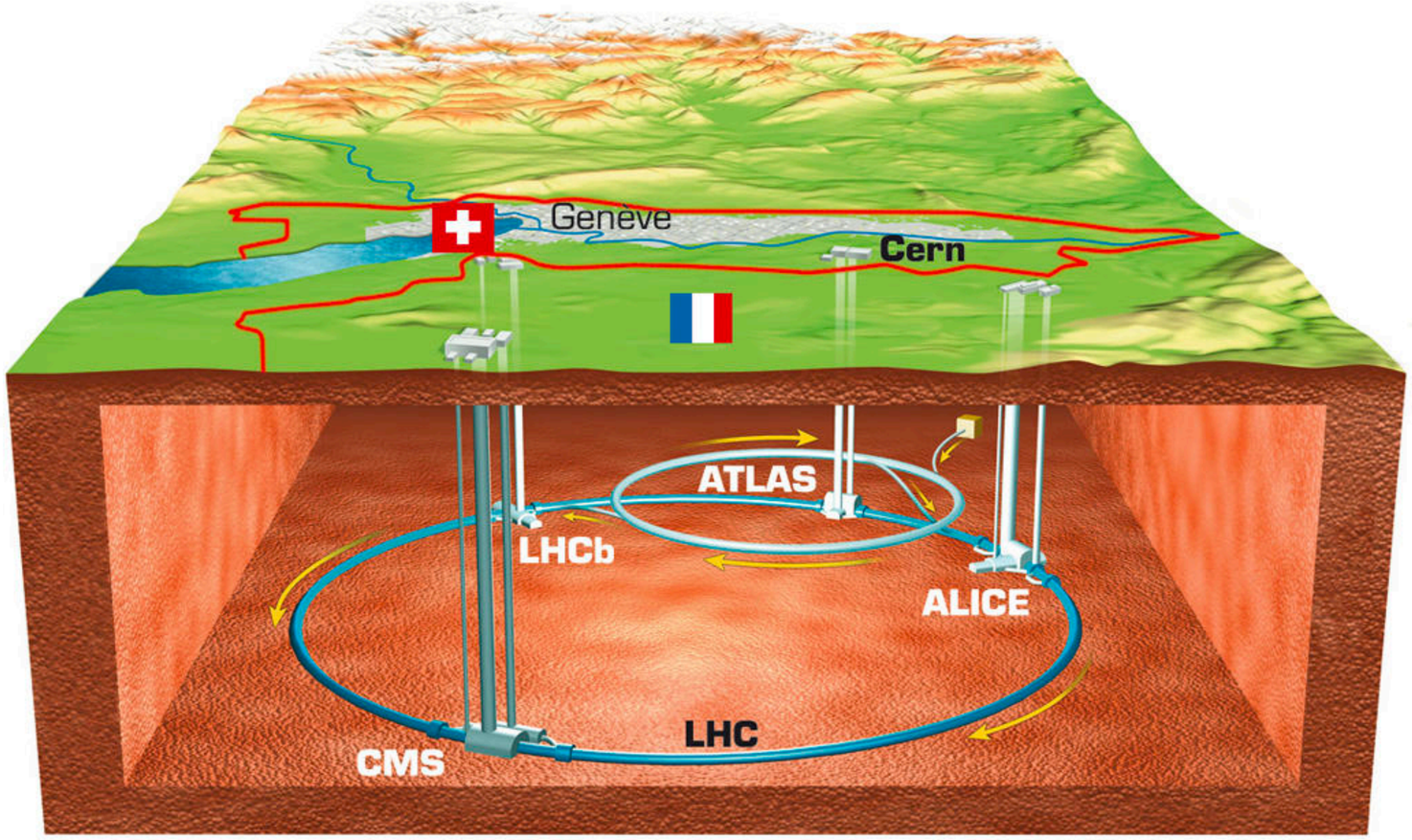

©CERN / Illustration Philippe Mouche

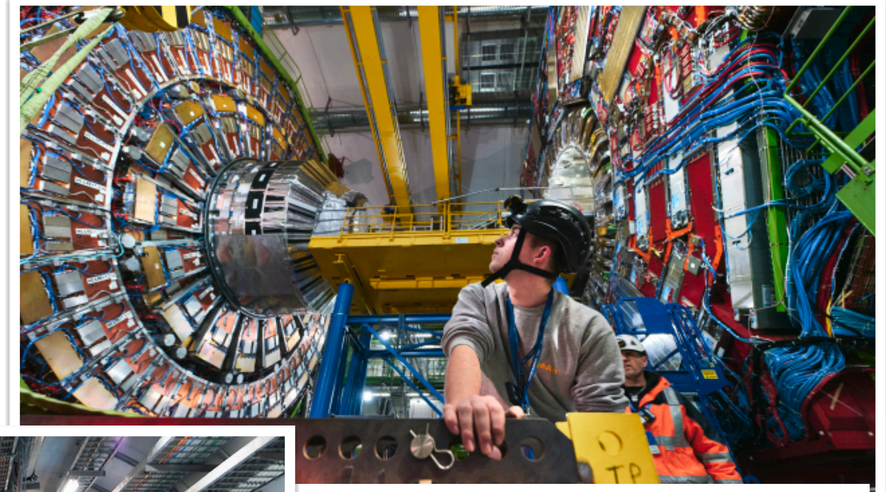

©CERN / Maximilien Brice

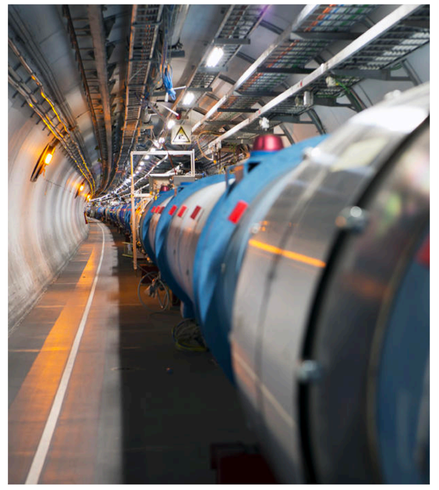

©CNRS Photothèque / Cyril FRÉSILLON

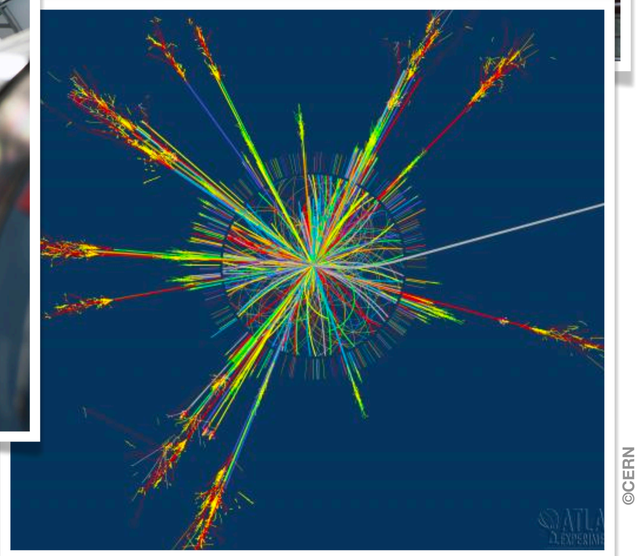

©CERN

Standard Model of Particle Physics (SM)

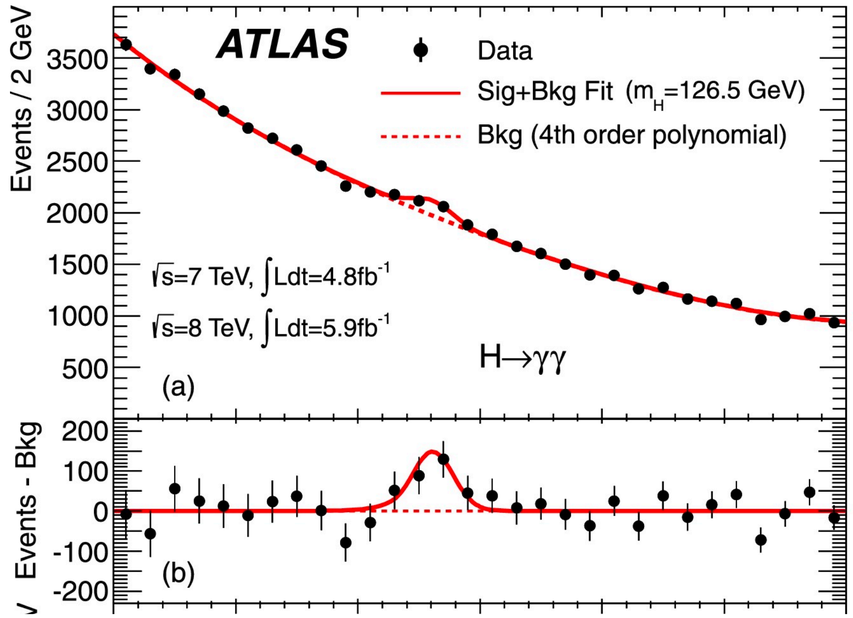

[ATLAS, Phys. Lett. B 716 (2012) 1–29]

© Denis Balibouse

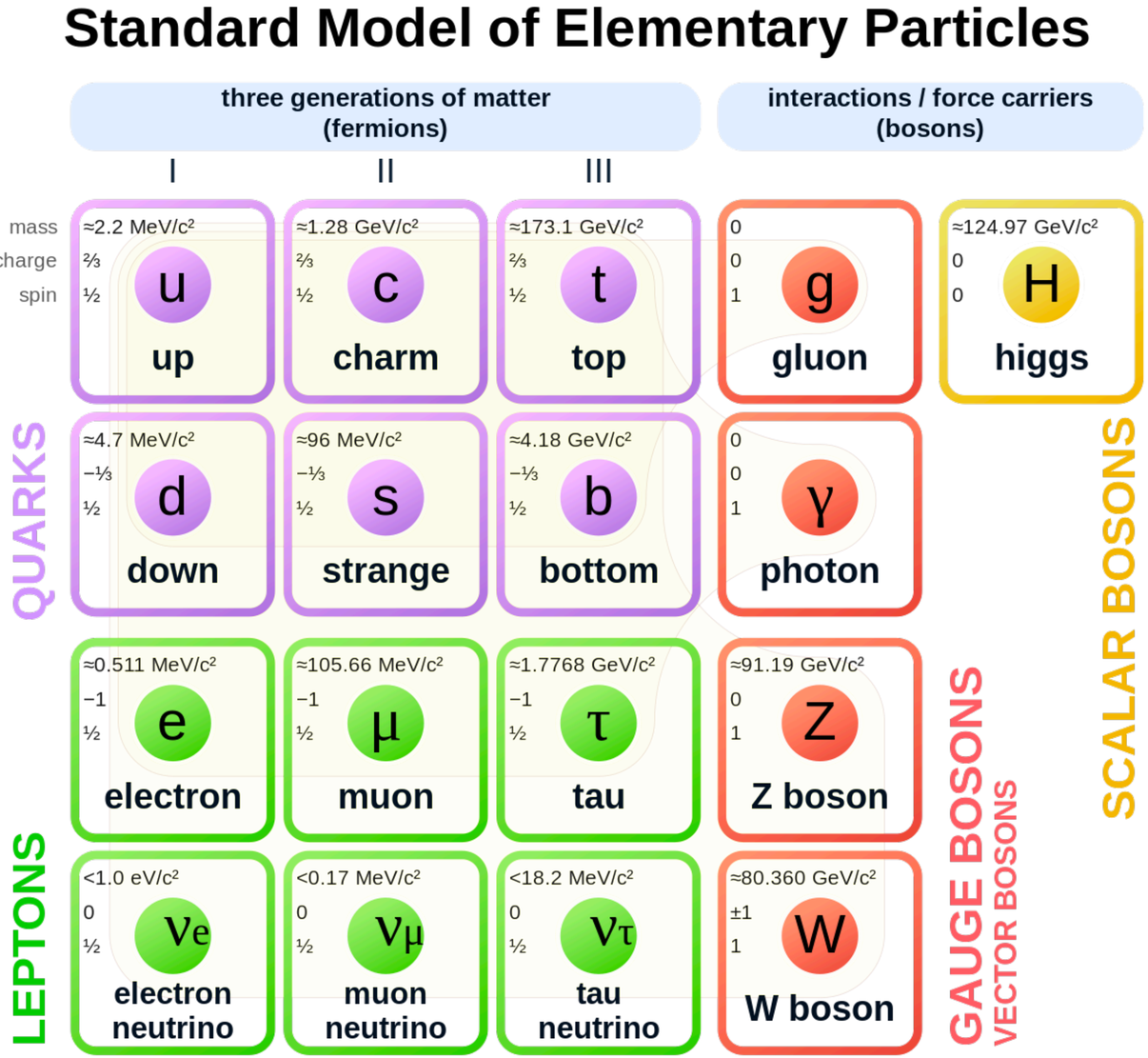

©Wikipedia / MissMJ

Issues with the Standard Model

- No unified description of gravity
- SM neutrino are massless
- Hierarchy problem -> why Higgs mass is so small?
- No viable Dark Matter candidate
- No explanation of Dark Energy
- ...

Issues with the Standard Model

- No unified description of gravity
- SM neutrino are massless
- Hierarchy problem -> w
- No viable D
- N ergy

Need for new theory —>
Beyond the Standard Model Physics (BSM)

LR-SYMMETRY

COMPOSITENESS

LEPTOQUARK

AXIONS

TWO HIGGS DOUBLETS

SUPERSYMMETRY

MILICHARGED PARTICLES

NEUTRINO MODELS

EXTRA DIMENSIONS

DARK SECTOR

WIMPs

Lack of BSM discoveries

No new physics
at the LHC scale

We are missing
something

New methods,
e.g. Machine Learning

New goals,
e.g. Long Lived Particles

Lack of BSM discoveries

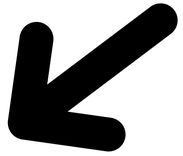

No new physics
at the LHC scale

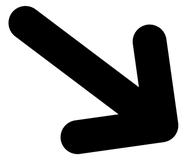

We are missing
something

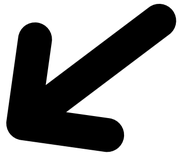

New methods,
e.g. Machine Learning

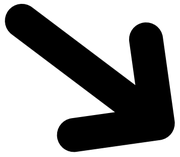

New goals,
e.g. Long Lived Particles

ATLAS detector

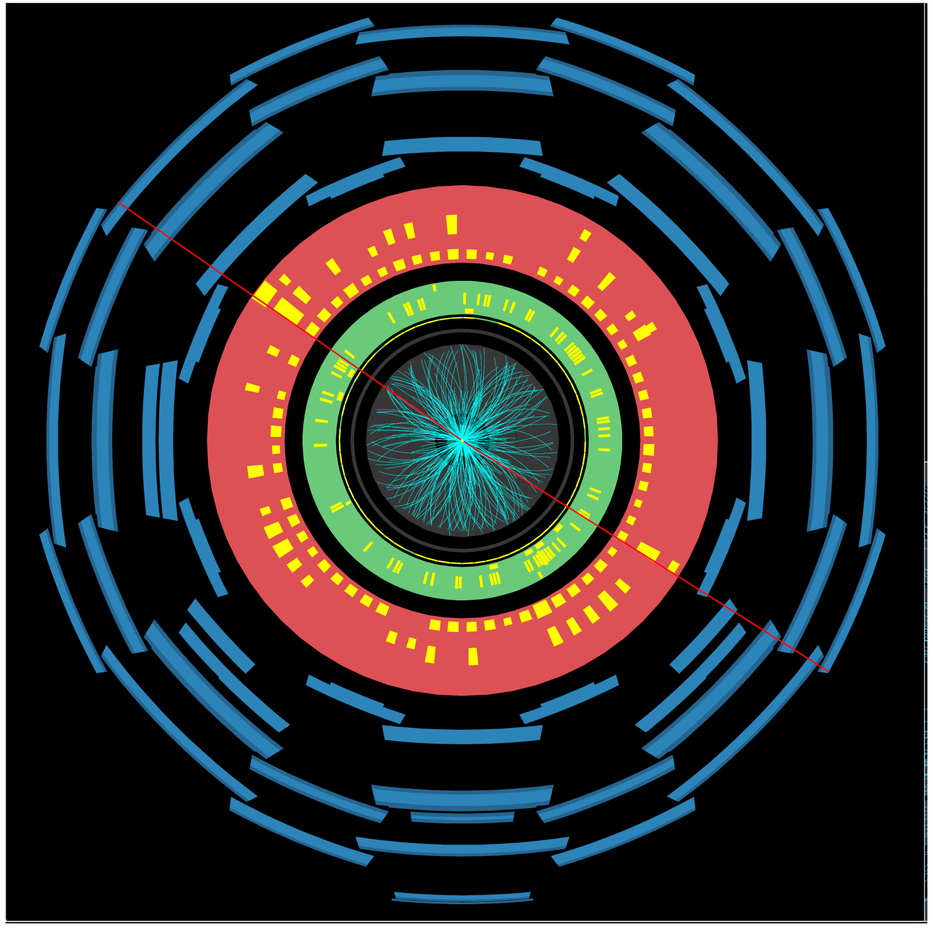

front view

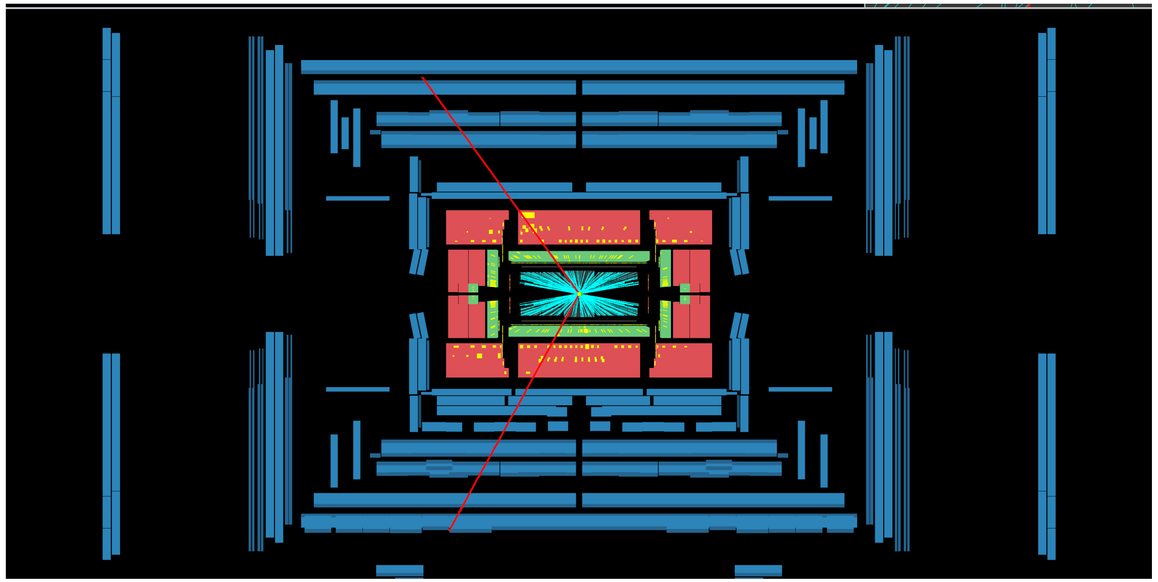

side view

LLPs @ ATLAS/CMS

- LLPs emerge in many models via:
  - small couplings
  - phase space suppression
  - small mass splitting between mother and daughter particles
- LLPs have been searched in ATLAS and CMS. They may result in many exotic signatures.

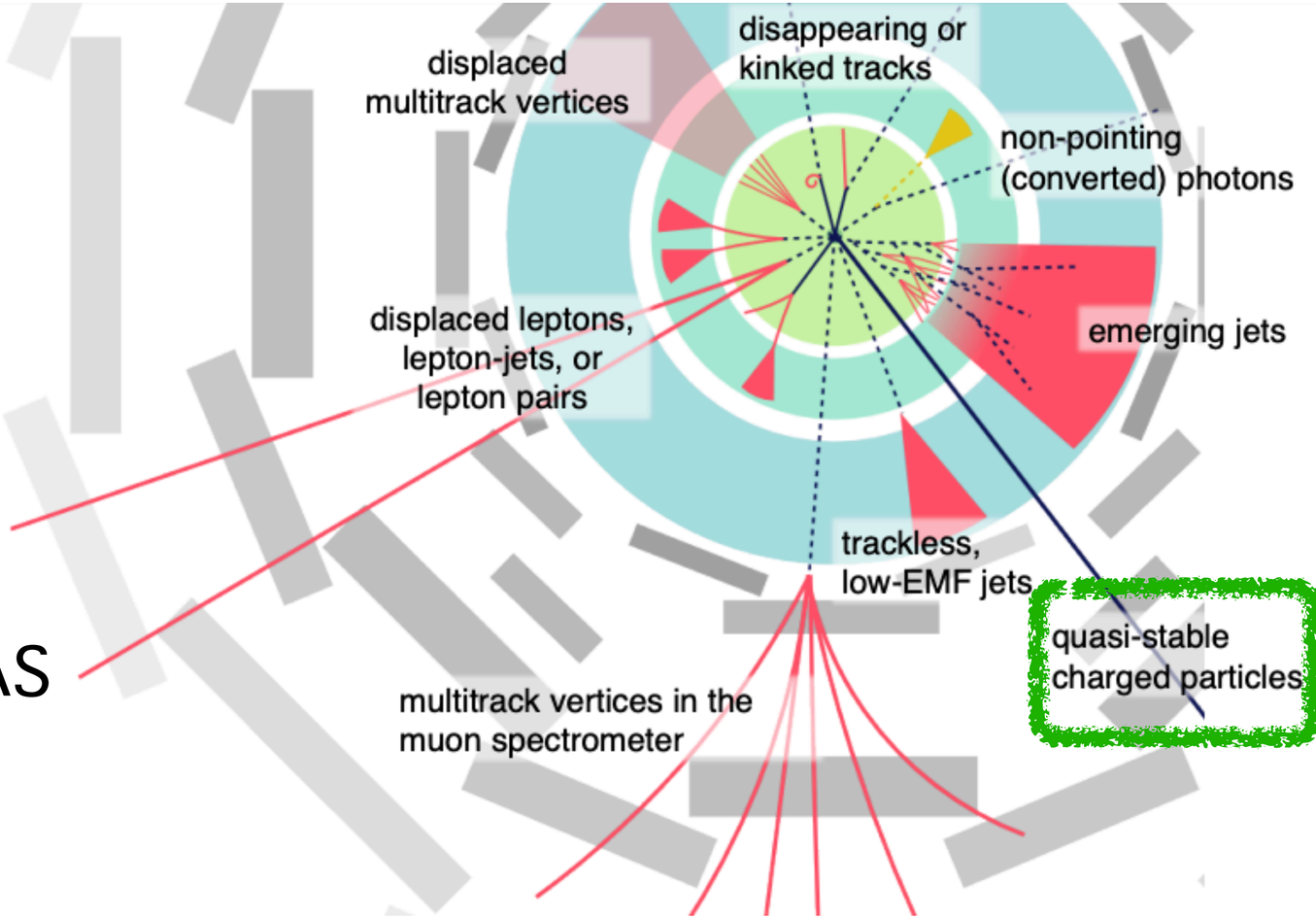

Monopole and Exotics Detector at the LHC (MoEDAL)

- designed primarly for magnetic monopoles
- can discover charged LLPs
- located ~2 m from IP8, outside LHCb VeLo detector
- passive, no trigger, no pile-up
- no SM background
- sensitive to highly ionising particles with $\beta \leq 0.15 \quad Q/e$

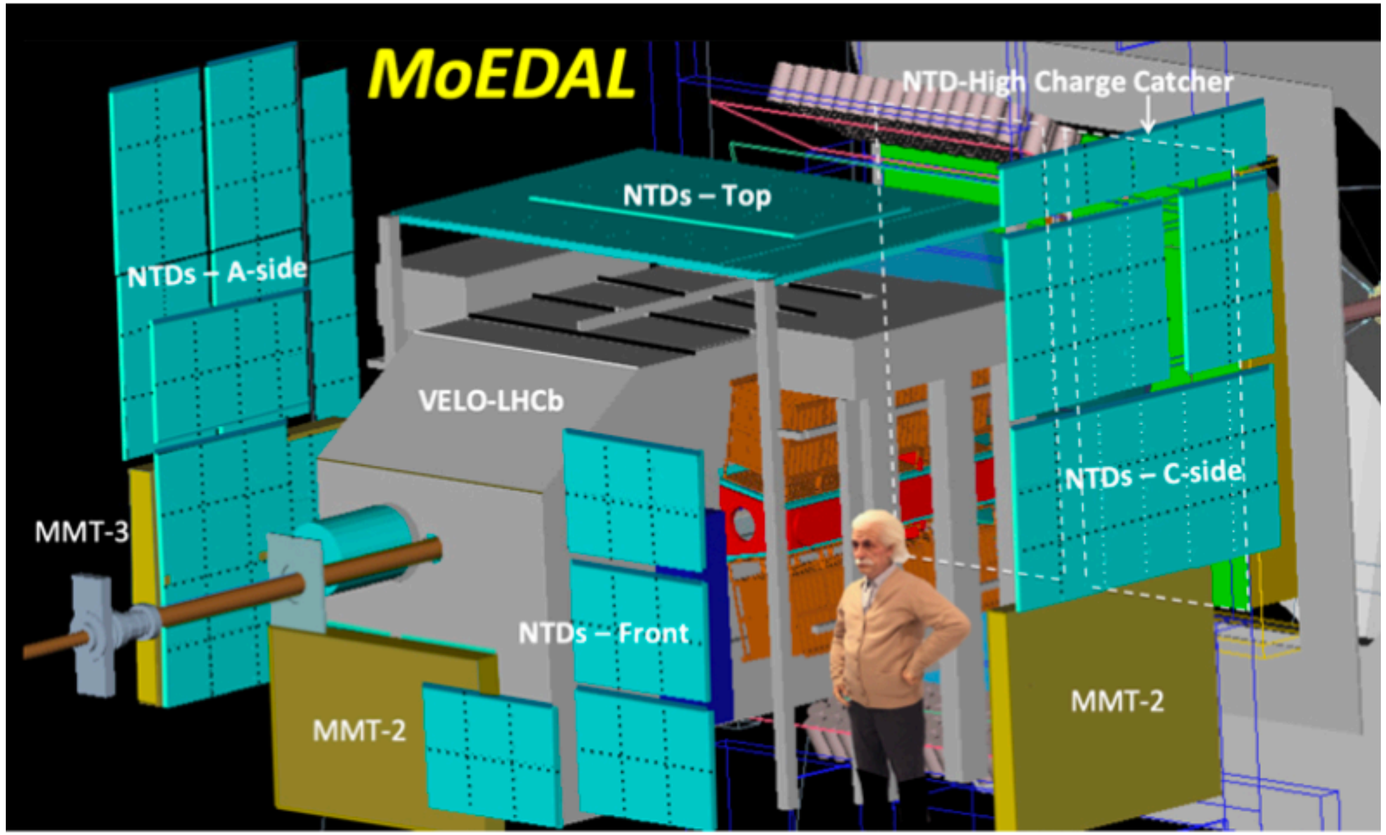

selected results

Morskie Oko, Tatra, Poland

UNIVERSITY OF WARSAW

Prospects for detecting long-lived particles at the Large Hadron Collider

Rafał Masełek

supervised by
Kazuki Sakurai

March 2023

arXiv:2310.13748 [hep-ph]

LPSC Grenoble

Prospects for discovering supersymmetric long-lived particles with MoEDAL

D. Felea, J. Mamuzic, R. Masełek, N. E. Mavromatos, V. A. Mitsou ✉, J. L. Pinfold, R. Ruiz de Austri, K. Sakurai, A. Santra & O. Vives

[10.1140/epjc/s10052-020-7994-7]

The European Physical Journal C **80**, Article number: 431 (2020) | Cite this article

Prospects of searches for long-lived charged particles with MoEDAL

B. S. Acharya, A. De Roeck, J. Ellis, D. K. Ghosh, R. Masełek, G. Panizzo, J. L. Pinfold, K. Sakurai ✉, A. Shaa & A. Wall

[10.1140/epjc/s10052-020-8093-5]

The European Physical Journal C **80**, Article number: 572 (2020) | Cite this article

Detecting long-lived multi-charged particles in neutrino mass models with MoEDAL

Martin Hirsch, Rafał Masełek ✉ & Kazuki Sakurai

[10.1140/epjc/s10052-021-09507-9]

The European Physical Journal C **81**, Article number: 697 (2021) | Cite this article

417 Accesses | **4** Citations | **2** Altmetric | Metrics

Discovery prospects for long-lived multiply charged particles at the LHC

Mohammad Mahdi Altakach, Priyanka Lamba, Rafał Masełek ✉, Vasiliki A. Mitsou & Kazuki Sakurai

The European Physical Journal C **82**, Article number: 848 (2022) | Cite this article

318 Accesses | **2** Citations | Metrics

[10.1140/epjc/s10052-022-10805-z]

Prospects for discovering supersymmetric long-lived particles with MoEDAL

- Can MoEDAL detect charged LLPs?
- Which BSM particles MoEDAL is sensitive to?
- What are the prospects for Run 3?
- Can MoEDAL compete with large experiments like ATLAS?

Prospects for discovering supersymmetric long-lived particles with MoEDAL

- Can MoEDAL detect charged LLPs?
- Which BSM particles MoEDAL is sensitive to?
- What are the prospects for Run 3?
- Can MoEDAL compete with large experiments like ATLAS?
- Fast simulation framework for MoEDAL
- Simplified SUSY scenario as our benchmark model

Supersymmetry

$$\phi \leftrightarrow \psi$$

gluon ↔ gluino
B boson ↔ Bino
W boson ↔ Wino
Higgs ↔ Higgsino
squark ↔ quark
slepton ↔ lepton

neutralino $\tilde{\chi}_j^0$ = mixture of wino, bino & higgsinos

Prospects for discovering supersymmetric long-lived particles with MoEDAL

- Can MoEDAL detect charged LLPs?
- Which BSM particles MoEDAL is sensitive to?
- What are the prospects for Run 3?
- Can MoEDAL compete with large experiments like ATLAS?

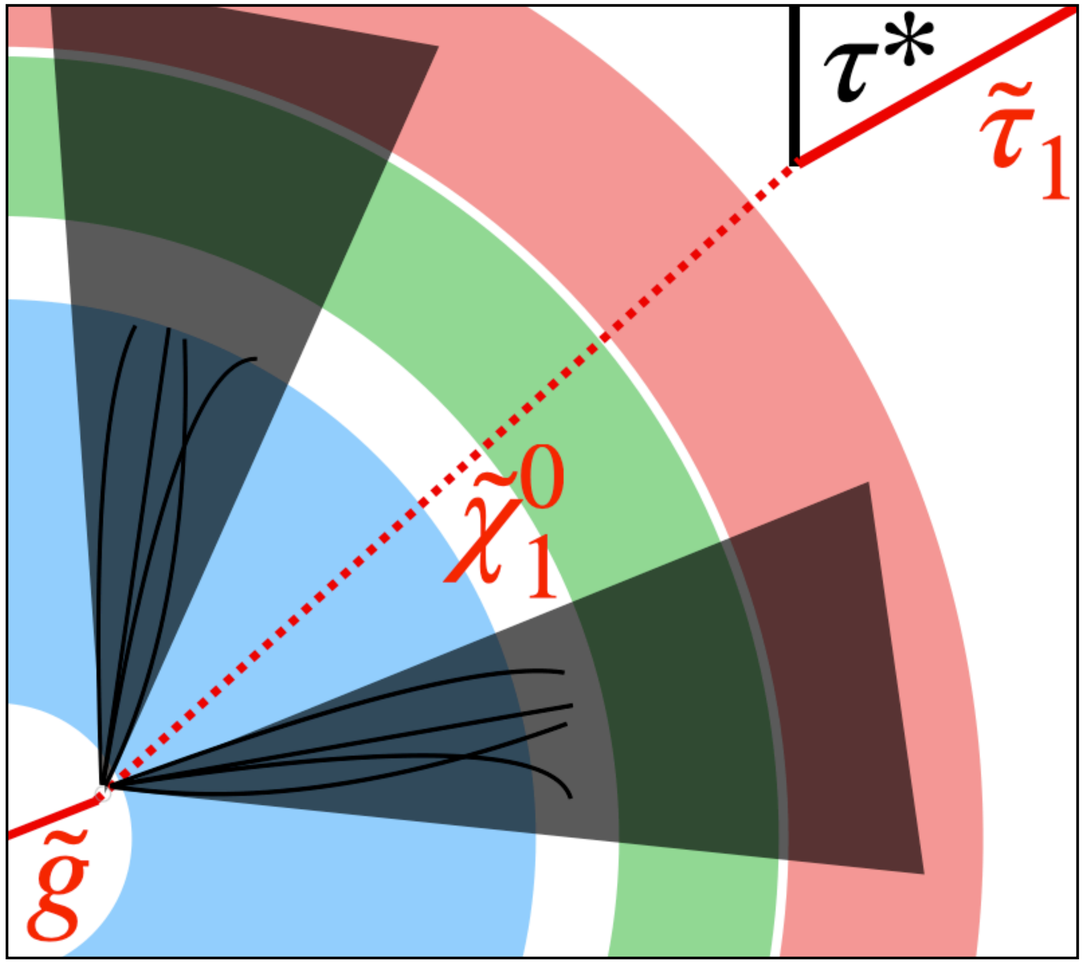

- Fast simulation framework for MoEDAL
- Simplified SUSY scenario as our benchmark model

$$pp \to \tilde{g}\tilde{g}, \quad \tilde{g} \to qq\tilde{\chi}_1^0, \quad \tilde{\chi}_1^0 \to \tau^*\tilde{\tau}_1$$

Prospects for discovering supersymmetric long-lived particles with MoEDAL

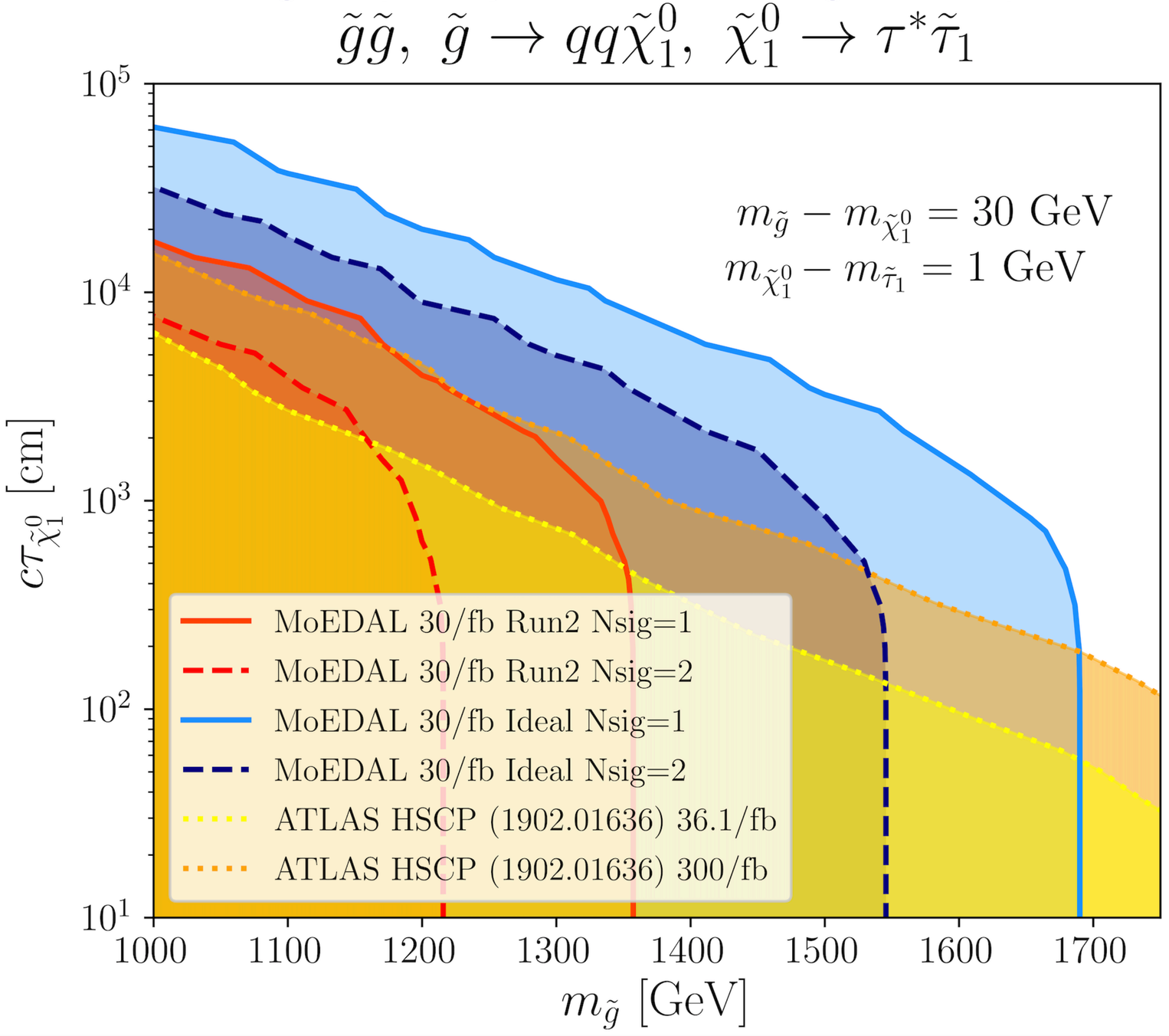

Prospects of searches for long-lived charged particles with MoEDAL

- What is the MoEDAL's sensitivity to supersymmetric particles in a general scenario?
- Can it detect doubly charged scalar/fermionic particles?
- Can it compete with ATLAS and CMS?

Prospects of searches for long-lived charged particles with MoEDAL

- What is the MoEDAL's sensitivity to supersymmetric particles in a general scenario?
- Can it detect doubly charged scalar/fermionic particles?
- Can it compete with ATLAS and CMS?

	MoEDAL	(ATLAS)	(CMS)
$\tilde{g}$	1600	(2000)	(1500)
$\tilde{q}$	1920	((2310))	-
$\tilde{t}$	920	(1350)	(1000)
$\widetilde{W}$	670	(1090)	-
$\tilde{h}$	530	((1170))	-
$\tilde{\tau}$	61	(430)	(230)

	MoEDAL	(CMS)
Scalar singlet	160	((320))
Fermion singlet	650	(680)
Scalar triplet	340	((590))
Fermion triplet	1130	((900))

Detecting long-lived multi-charged particles in neutrino mass models with MoEDAL

	$\mathbf{S_1}$	$\mathbf{S_3}$	$\mathbf{F_i}$	$\mathbf{\bar{F}_i}$
Spin	0	0	$\frac{1}{2}$	$\frac{1}{2}$
$\mathbf{SU(3)_C}$	1	1	1	1
$\mathbf{SU(2)_L}$	1	3	2	2
$\mathbf{U(1)_Y}$	2	3	$\frac{5}{2}$	$-\frac{5}{2}$

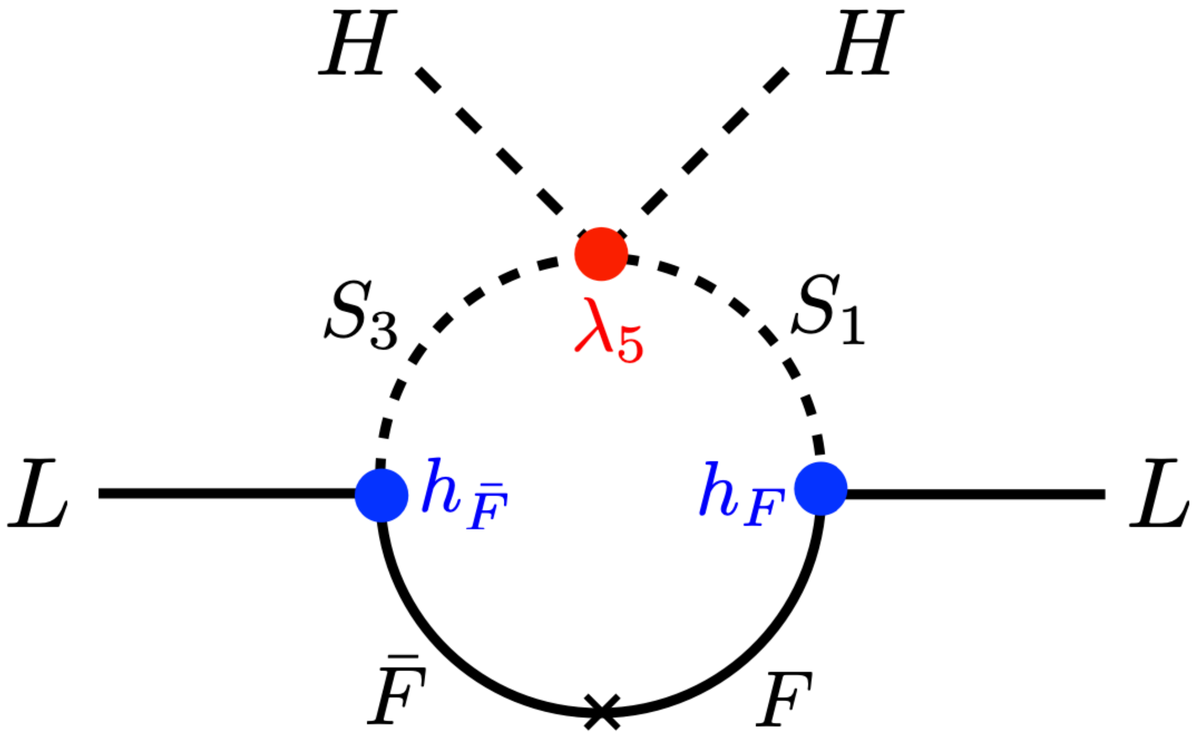

$$\mathscr{L}_{\mathrm{BSM}} \ni -(h_{ee})_{ij}(e_R^i)^C(e_R^j)^C S_1^\dagger - (h_F)_{ij} L_i F_j S_1^\dagger - (h_{\bar{F}})_{ij} L_i \bar{F}_j S_3^\dagger - \lambda_5 H H S_1 S_3^\dagger + h.c.$$

Detecting long-lived multi-charged particles in neutrino mass models with MoEDAL

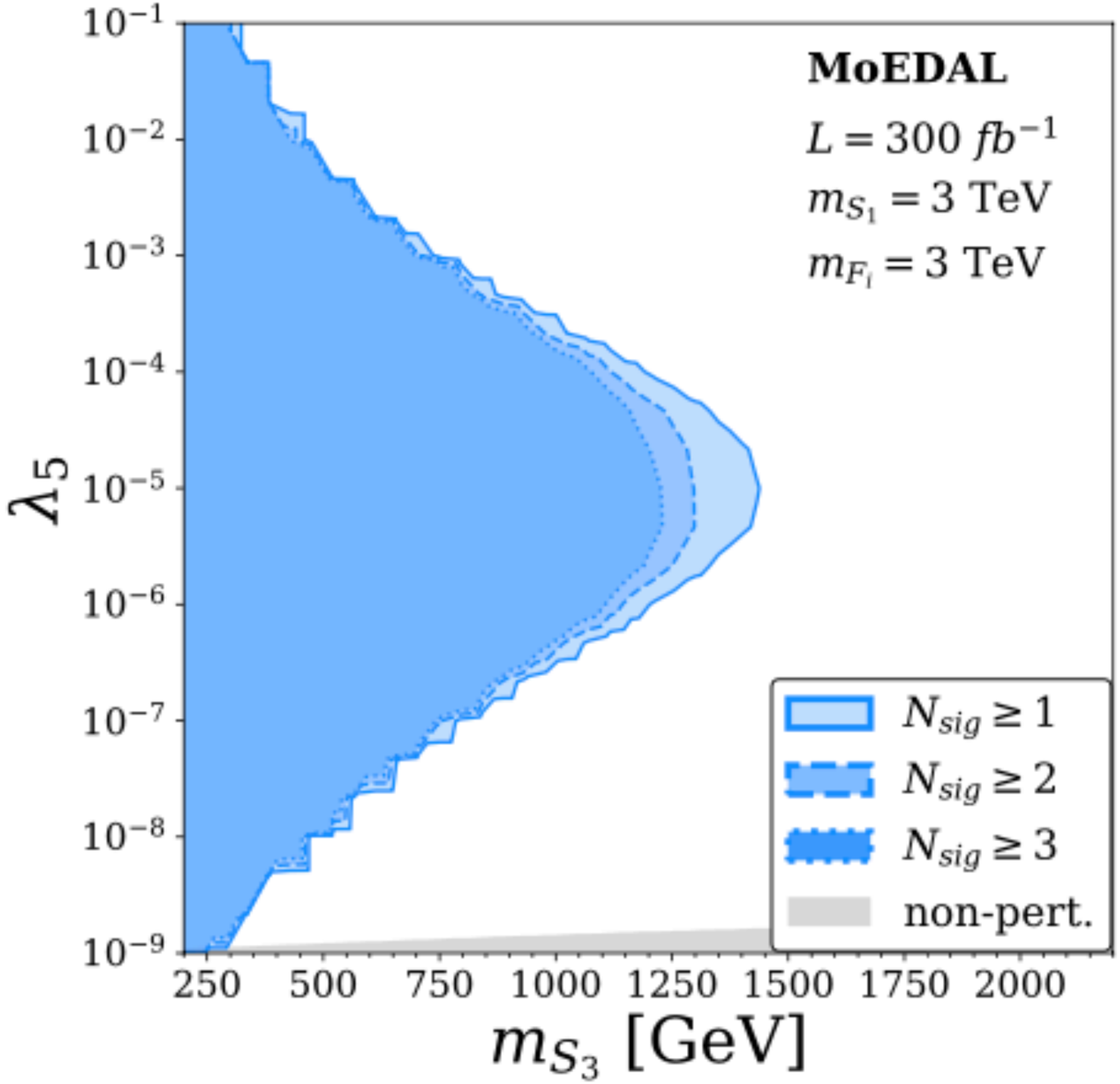

Discovery prospects for long-lived multiply charged particles at the LHC

- MoEDAL is sensitive to particles with $\beta \leq 0.15 \cdot \ Q/e$.
- Can MoEDAL outcompete ATLAS and CMS for large Q?
- We considered simplified models: coloured & uncoloured scalars & spin-1/2 fermions with charges $1e \leq \ Q \ \leq 8e$
- ATLAS and CMS constrainsts:
  - large dE/dx searches
  - di-photon decays of positronium/quarkonium-like bound states

Discovery prospects for long-lived multiply charged particles at the LHC

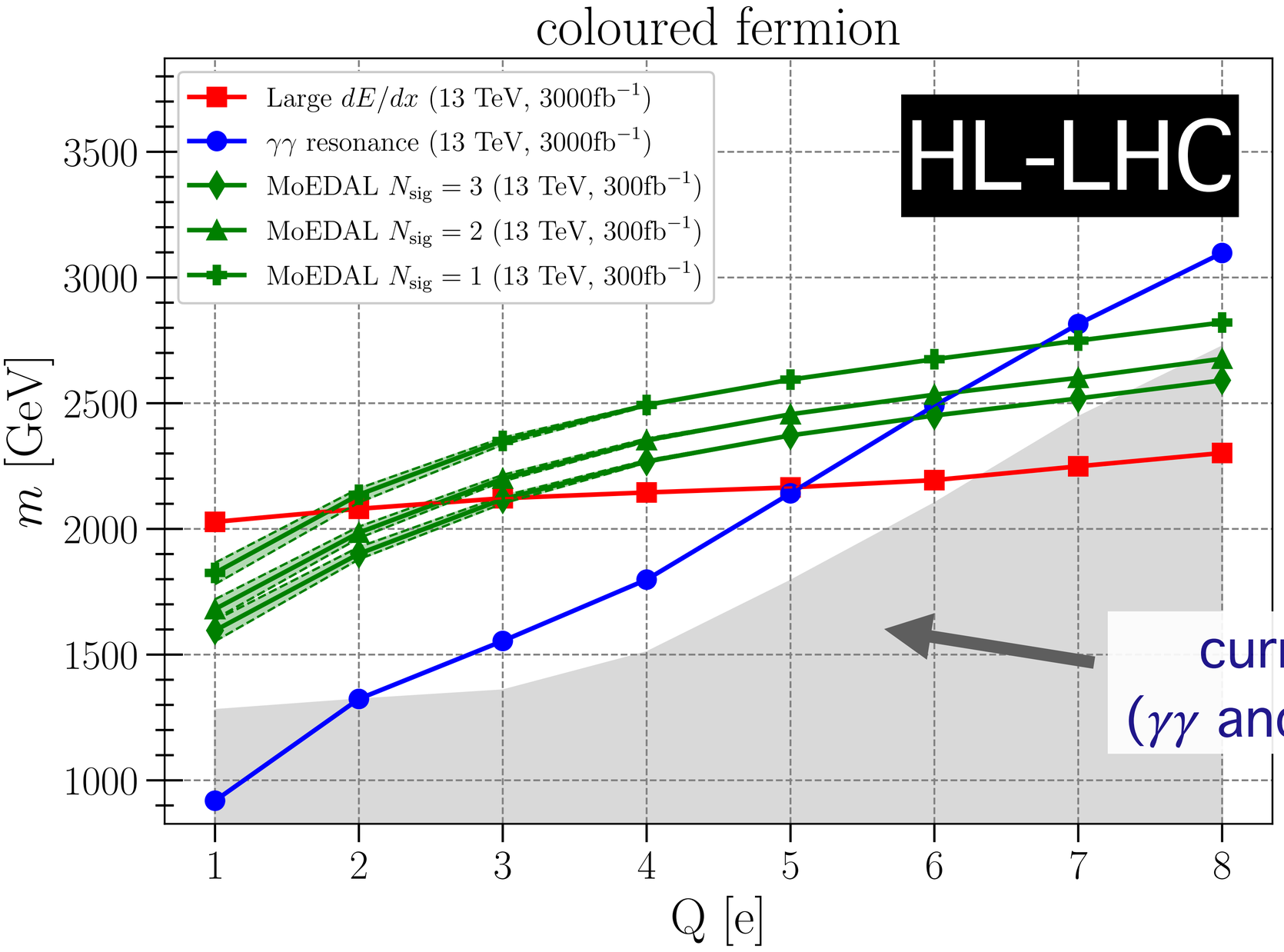

Larde dE/dx searches

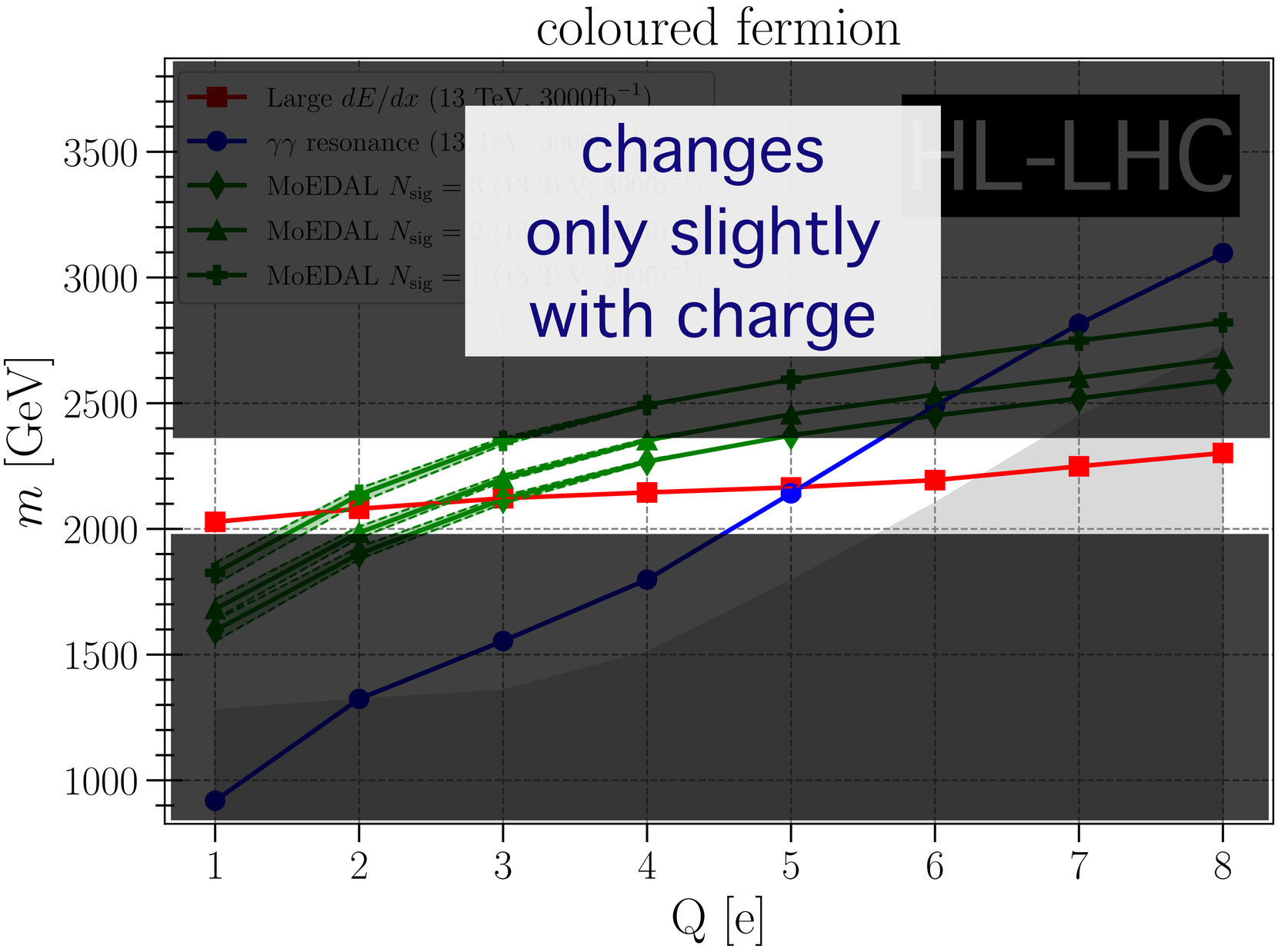

diphoton resonance search

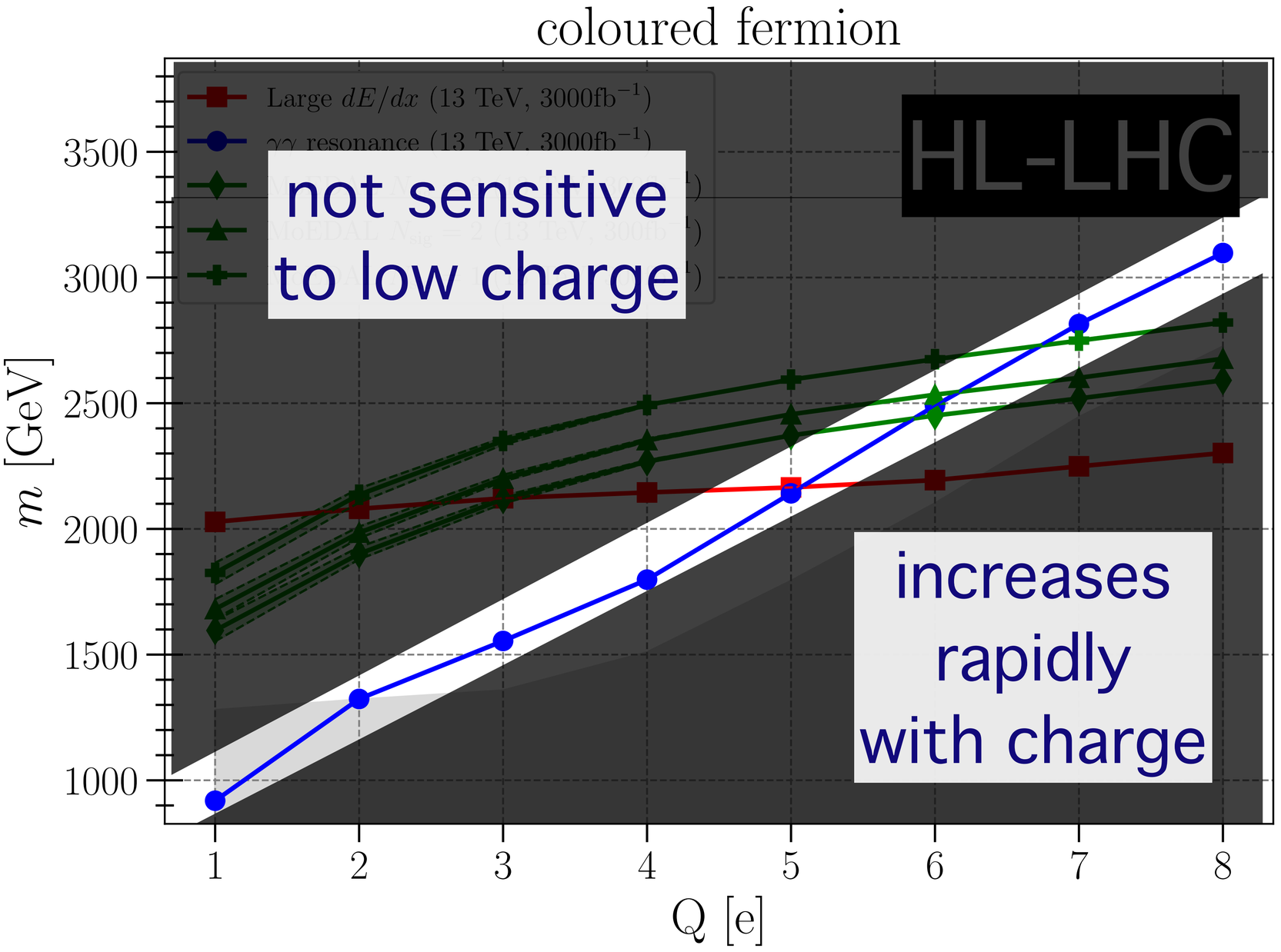

Discovery prospects for long-lived multiply charged particles at the LHC

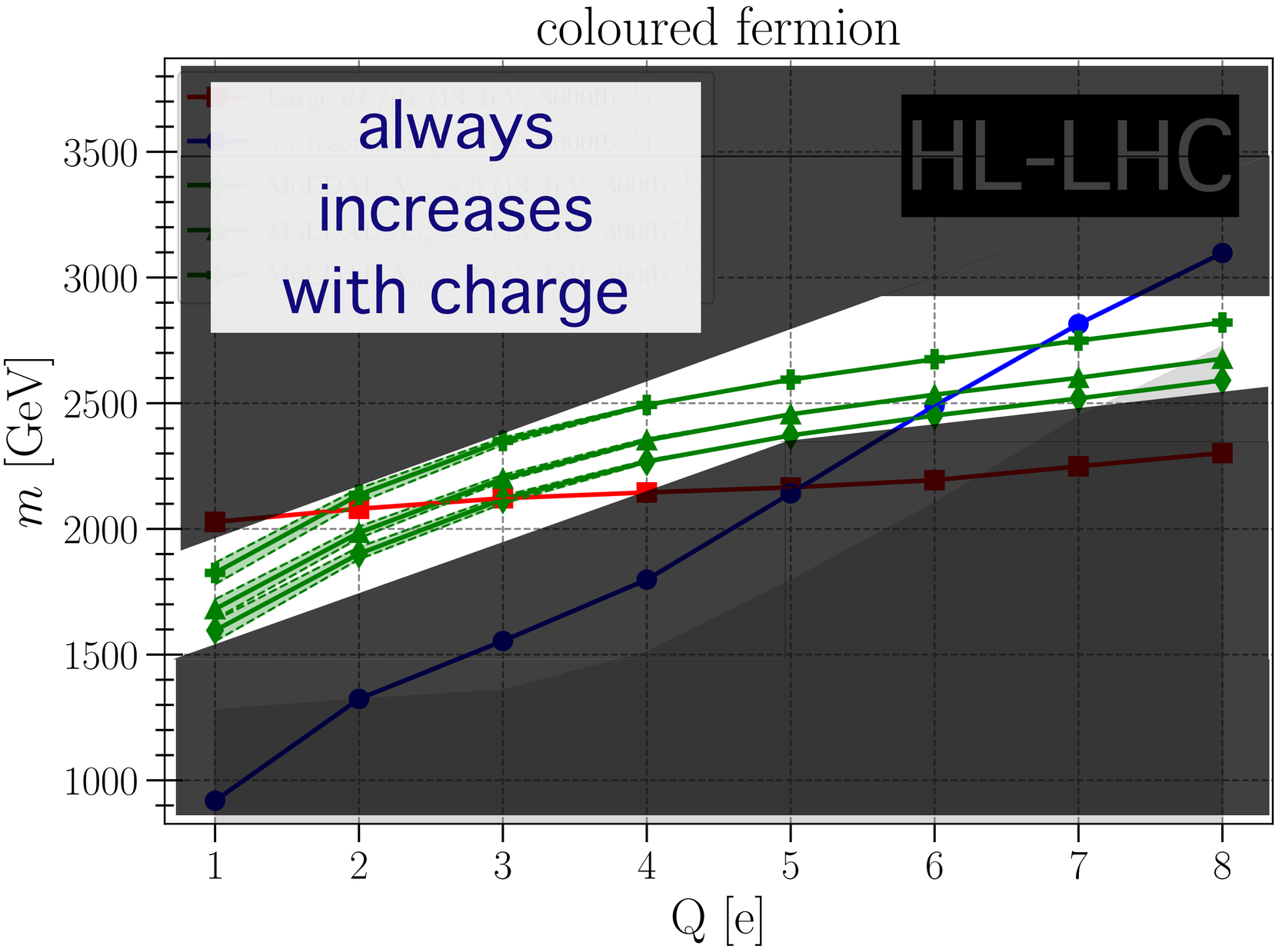

Discovery prospects for long-lived multiply charged particles at the LHC

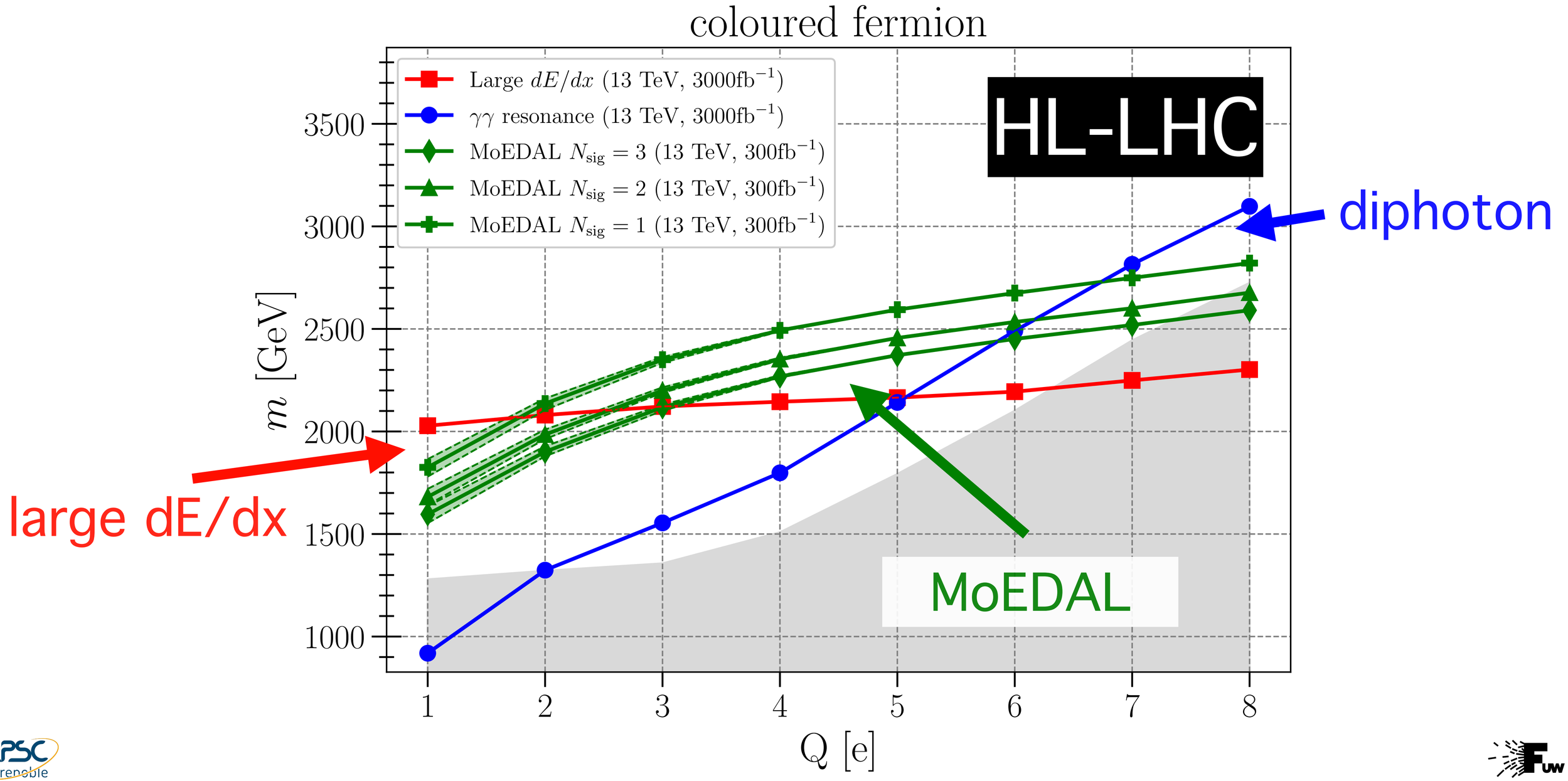

Summary

- MoEDAL can detect charged long-lived particles
- Sensitivity assessed for SUSY, neutrino mass models and simplified models
- Sensitivity depends on incidence angle, electric charge, velocity distribution
- Compared to ATLAS and CMS sensitivities:
  - in most cases, MoEDAL does worse, mainly because of the lower luminosity available
  - but for the specific SUSY scenario and multiply charged particles it can do better
  - MoEDAL will gain more in the High Luminosity phase because it's background free
- The presented research resulted in:
  - stimulating searches for LLPs in MoEDAL
  - rearrangement of NTD placement
  - understanding the impact of photon-induced production channels for multiply charged particles
  - providing a broad overview of the prospects for detection of quasi-stable charged LLPs at the Run 3 & HL-LHC

Now in LPSC

Sabine Kraml

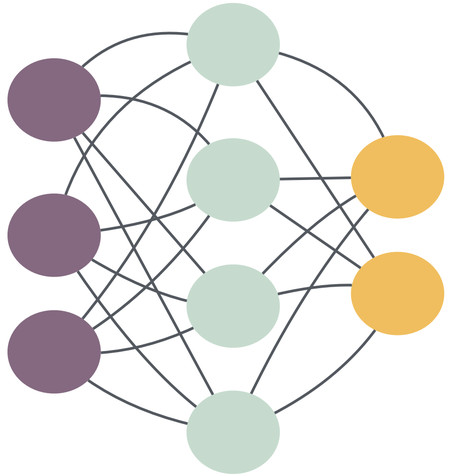

- Developing ML-based analyses for BSM searches
- Using NNs to speed up reinterpretation tools
- Unfolding of detector effects

Thank you for attention!

rafal.maselek@lpsc.in2p3.fr

Dolina Chochołowska, Poland
photo by Piotr Kałuża

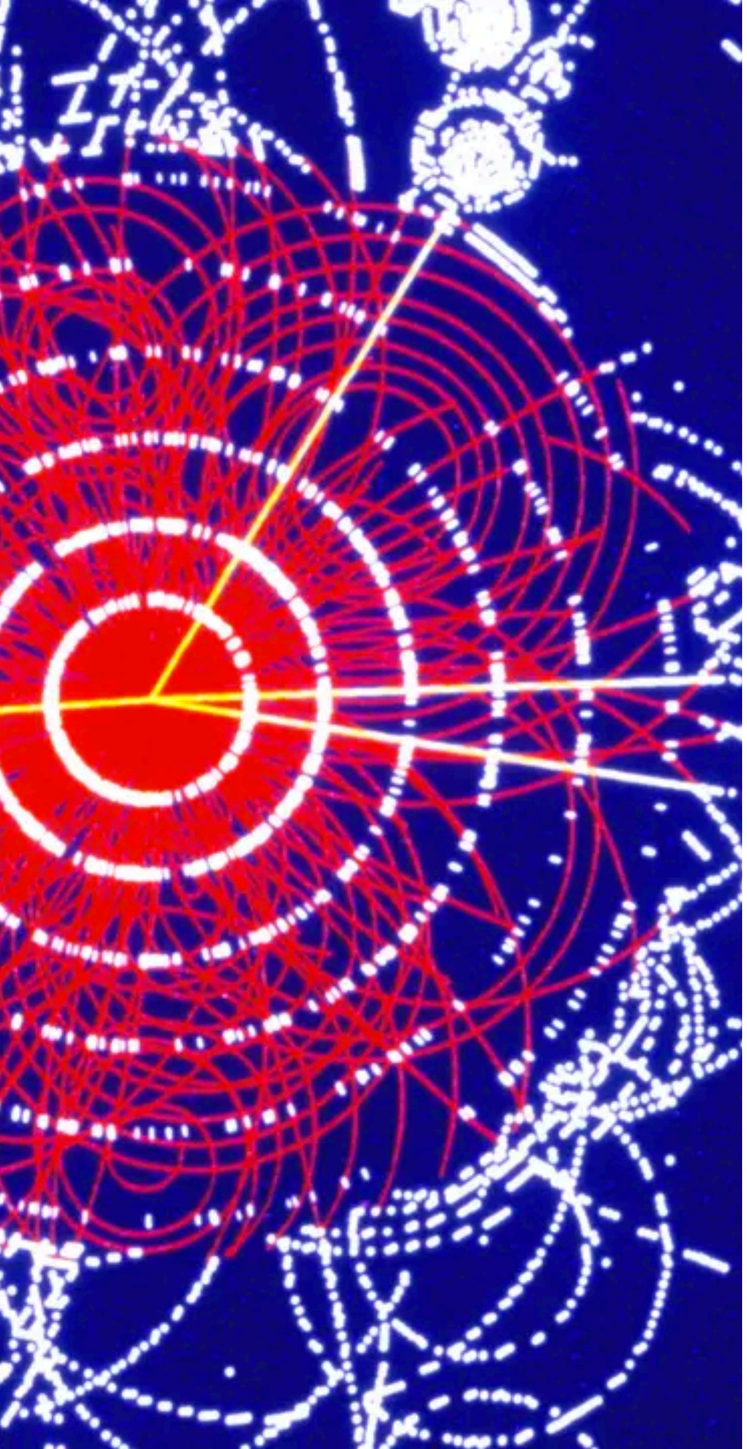

FACULTY OF PHYSICS
UNIVERSITY OF WARSAW

Backup slides

Rafał Masełek

PostDoc seminar, 23.01.2024, Grenoble

Experimental results

2112.05806 [hep-ex]

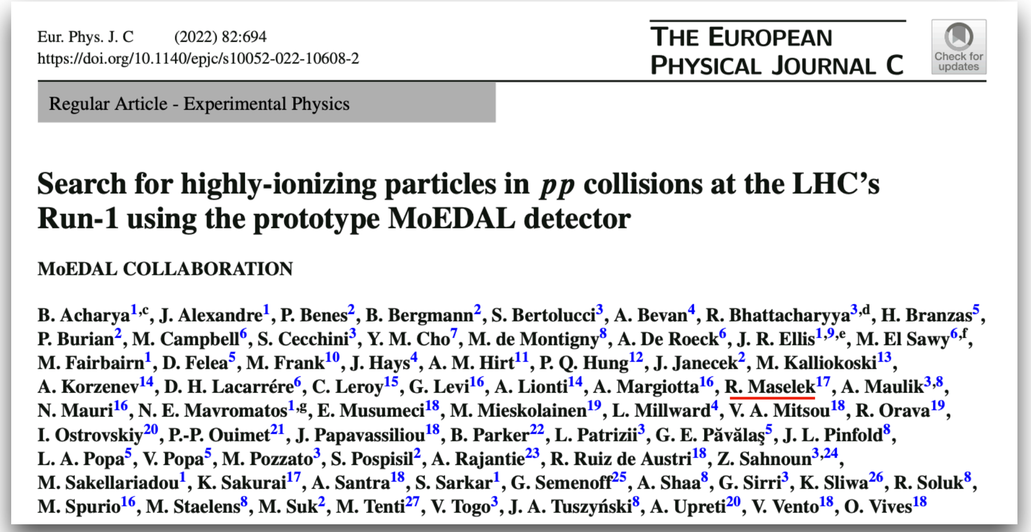

Eur. Phys. J. C (2022) 82:694
https://doi.org/10.1140/epjc/s10052-022-10608-2

THE EUROPEAN PHYSICAL JOURNAL C

Regular Article - Experimental Physics

Search for highly-ionizing particles in *pp* collisions at the LHC's Run-1 using the prototype MoEDAL detector

MoEDAL COLLABORATION

B. Acharya[1,c], J. Alexandre[1], P. Benes[2], B. Bergmann[2], S. Bertolucci[3], A. Bevan[4], R. Bhattacharyya[3,d], H. Branzas[5], P. Burian[2], M. Campbell[6], S. Cecchini[3], Y. M. Cho[7], M. de Montigny[8], A. De Roeck[6], J. R. Ellis[1,9,e], M. El Sawy[6,f], M. Fairbairn[1], D. Felea[5], M. Frank[10], J. Hays[4], A. M. Hirt[11], P. Q. Hung[12], J. Janecek[2], M. Kalliokoski[13], A. Korzenev[14], D. H. Lacarrére[6], C. Leroy[15], G. Levi[16], A. Lionti[14], A. Margiotta[16], R. Maselek[17], A. Maulik[3,8], N. Mauri[16], N. E. Mavromatos[1,g], E. Musumeci[18], M. Mieskolainen[19], L. Millward[4], V. A. Mitsou[18], R. Orava[19], I. Ostrovskiy[20], P.-P. Ouimet[21], J. Papavassiliou[18], B. Parker[22], L. Patrizii[3], G. E. Păvălaş[5], J. L. Pinfold[8], L. A. Popa[5], V. Popa[5], M. Pozzato[3], S. Pospisil[2], A. Rajantie[23], R. Ruiz de Austri[18], Z. Sahnoun[3,24], M. Sakellariadou[1], K. Sakurai[17], A. Santra[18], S. Sarkar[1], G. Semenoff[25], A. Shaa[8], G. Sirri[3], K. Sliwa[26], R. Soluk[8], M. Spurio[16], M. Staelens[8], M. Suk[2], M. Tenti[27], V. Togo[3], J. A. Tuszyński[8], A. Upreti[20], V. Vento[18], O. Vives[18]

2311.06509 [hep-ex]

Search for Highly-Ionizing Particles in *pp* Collisions During LHC Run-2 Using the Full MoEDAL Detector

B. Acharya,[1,*] J. Alexandre,[1] P. Benes,[2] B. Bergmann,[2] S. Bertolucci,[3] A. Bevan,[4] R. Brancaccio,[5] H. Branzas,[6] P. Burian,[2] M. Campbell,[7] S. Cecchini,[3] Y. M. Cho,[8] M. de Montigny,[9] A. De Roeck,[7] J. R. Ellis,[1,10] M. Fairbairn,[1] D. Felea,[6] M. Frank,[11] J. Hays,[4] A. M. Hirt,[12] D. L.-J. Ho,[13] P. Q. Hung,[14] J. Janecek,[2] M. Kalliokoski,[15] D. H. Lacarrère,[7] C. Leroy,[16] G. Levi,[5] A. Margiotta,[5] R. Maselek,[17,18] A. Maulik,[3,9] N. Mauri,[5] N. E. Mavromatos,[1,†] M. Mieskolainen,[19] L. Millward,[4] V. A. Mitsou,[20,†] A. Mukhopadhyay,[9] E. Musumeci,[20] I. Ostrovskiy,[21] P.-P. Ouimet,[22] J. Papavassiliou,[20] L. Patrizii,[3,‡] G. E. Păvălaş,[6] J. L. Pinfold,[9,§] L. A. Popa,[6] V. Popa,[6] M. Pozzato,[3] S. Pospisil,[2] A. Rajantie,[13] R. Ruiz de Austri,[20] Z. Sahnoun,[5] M. Sakellariadou,[1] K. Sakurai,[18] S. Sarkar,[1] G. Semenoff,[23] A. Shaa,[9] G. Sirri,[3] K. Sliwa,[24] R. Soluk,[9] M. Spurio,[5] M. Staelens,[20] M. Suk,[2] M. Tenti,[3] V. Togo,[3] J. A. Tuszyński,[9] A. Upreti,[21] V. Vento,[20] and O. Vives[20]

(THE MoEDAL COLLABORATION)

Outlook — new spherical detector for FCC

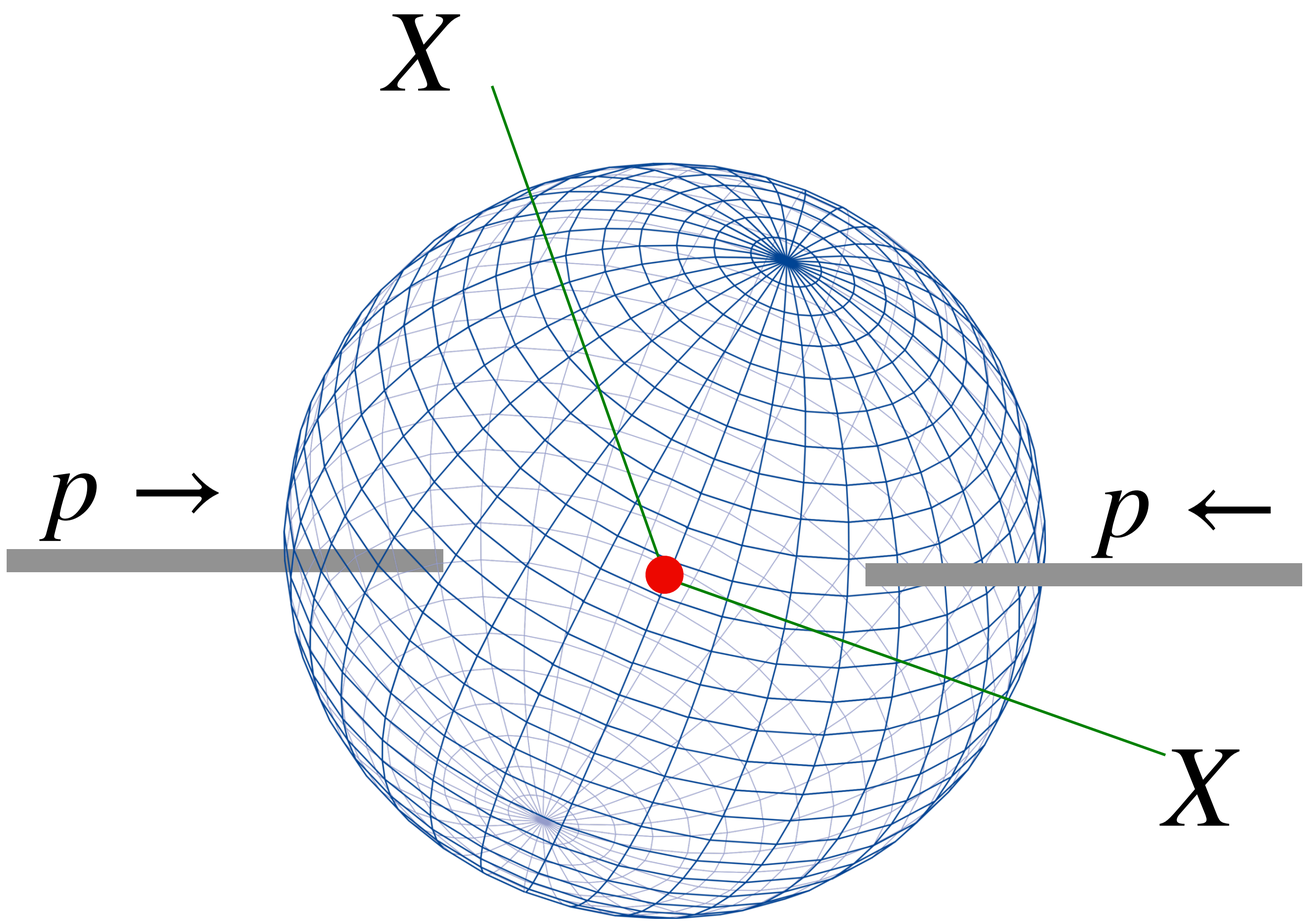

R = 10 m

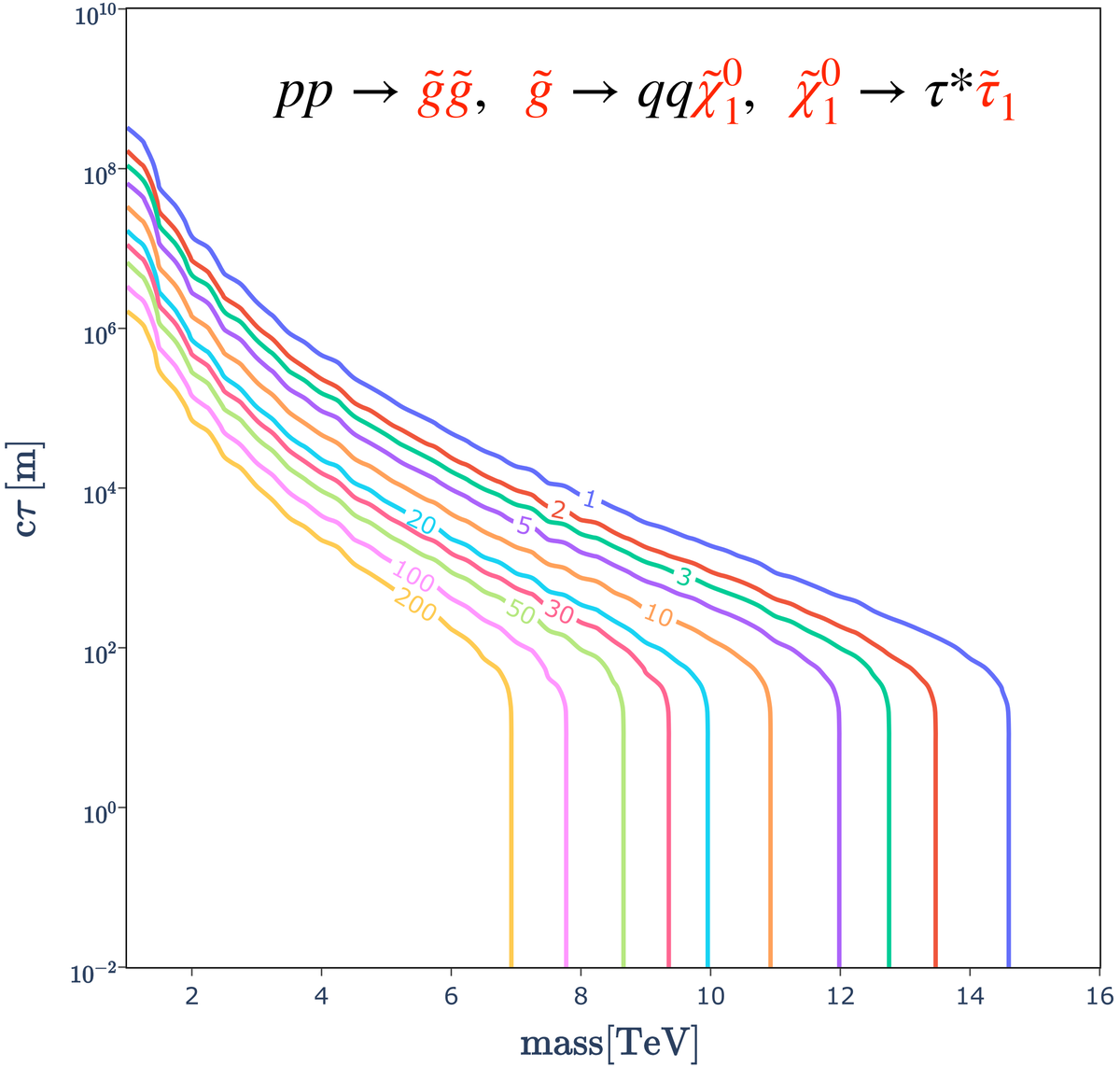

LPSC Grenoble

MoEDAL experiment

Beach in Dębki, Poland

Monopole and Exotics Detector at the LHC (MoEDAL)

- designed primarly for magnetic monopoles
- can discover charged LLPs
- located ~2 m from IP8, outside LHCb VeLo detector
- mostly passive, no trigger, no pile-up
- sensitive to highly ionising particles with $\beta \leq 0.15 \quad Q/e$
- no SM background
- MoEDAL-MAPP consists of 4 subdetectors:
  - Magnetic Monopole Trappers
  - Nuclear Track Detectors
  - TimePix detector
  - MoEDAL Apparatus for Penetrating Particles

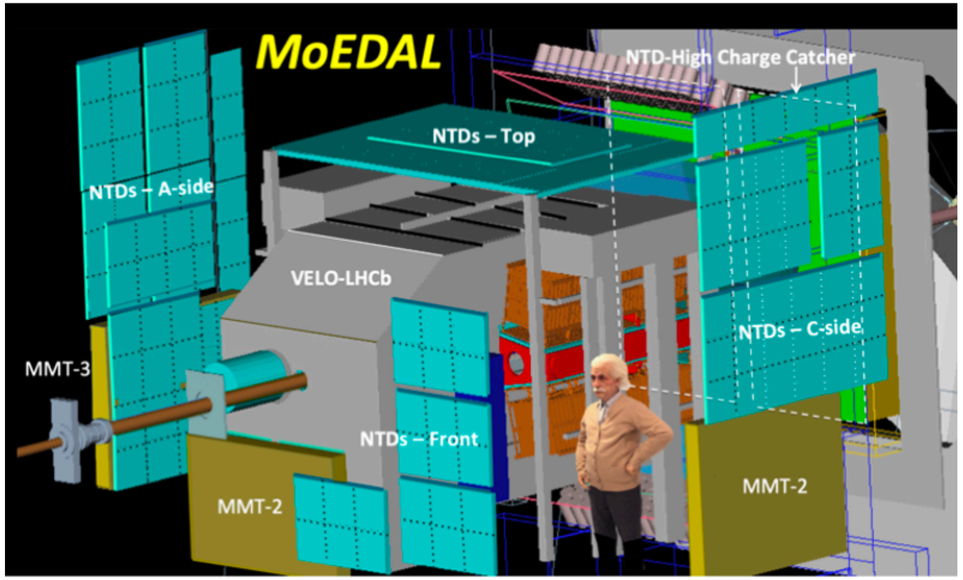

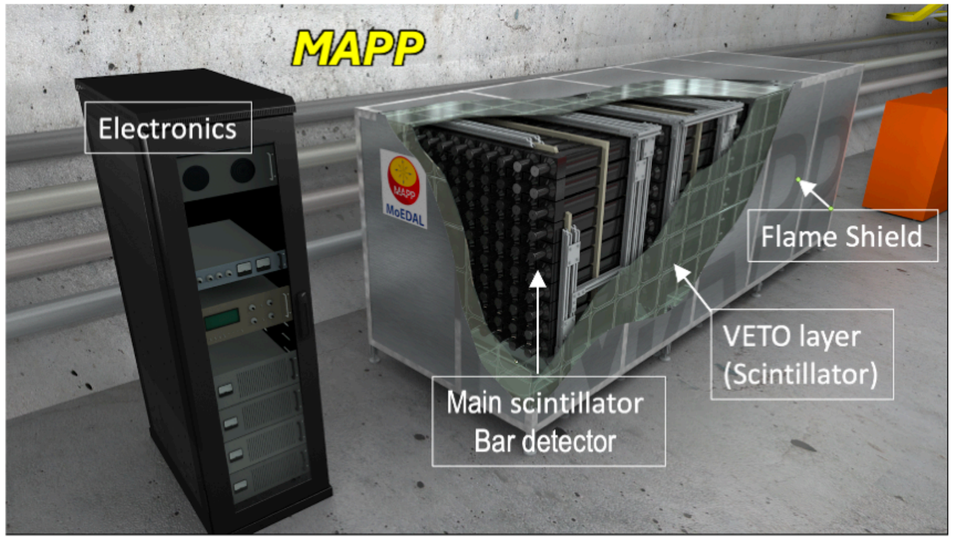

Nuclear Track Detector — layers

Detection of signal in 6 layers

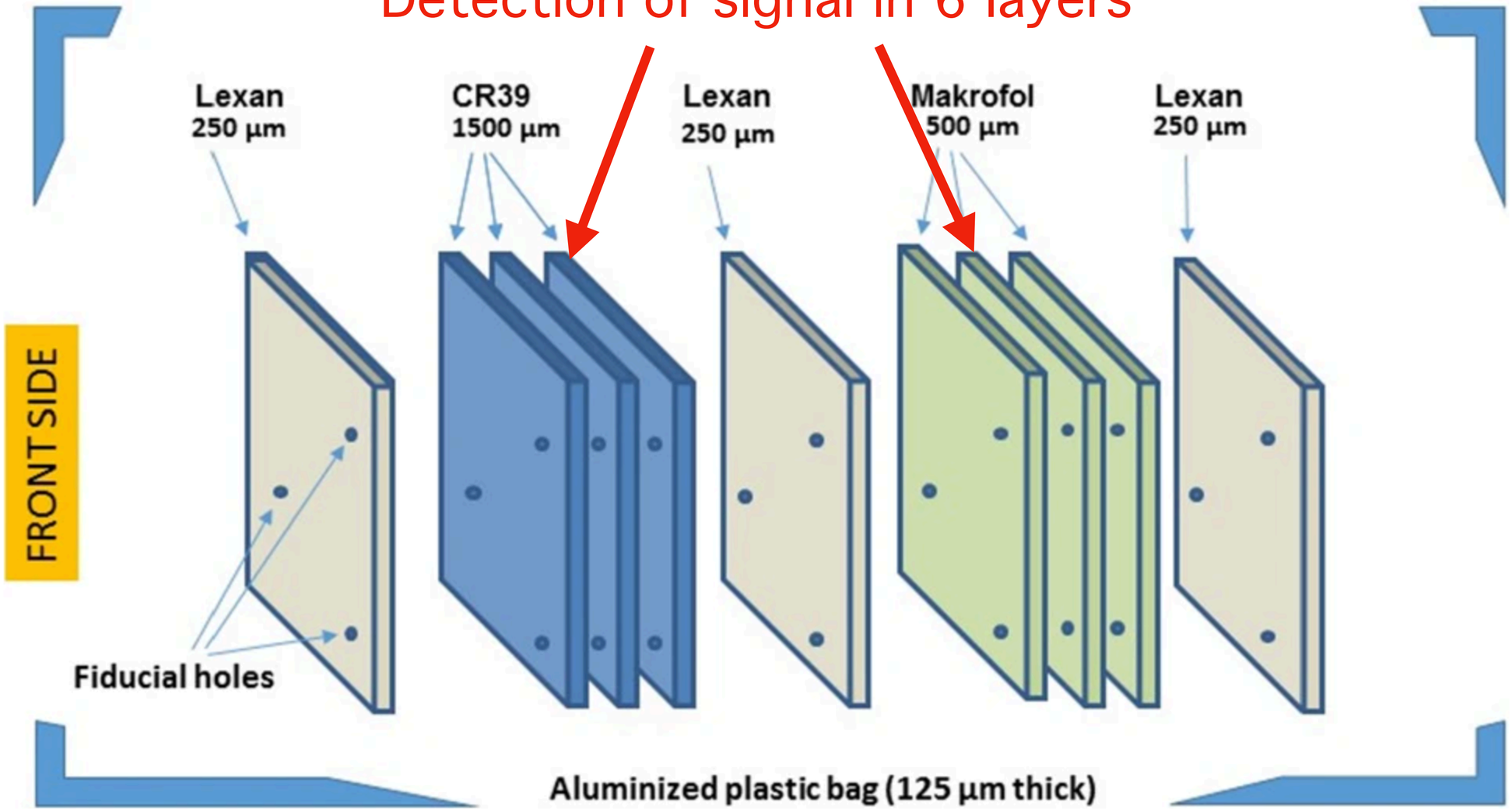

Nuclear Track Detector — etching

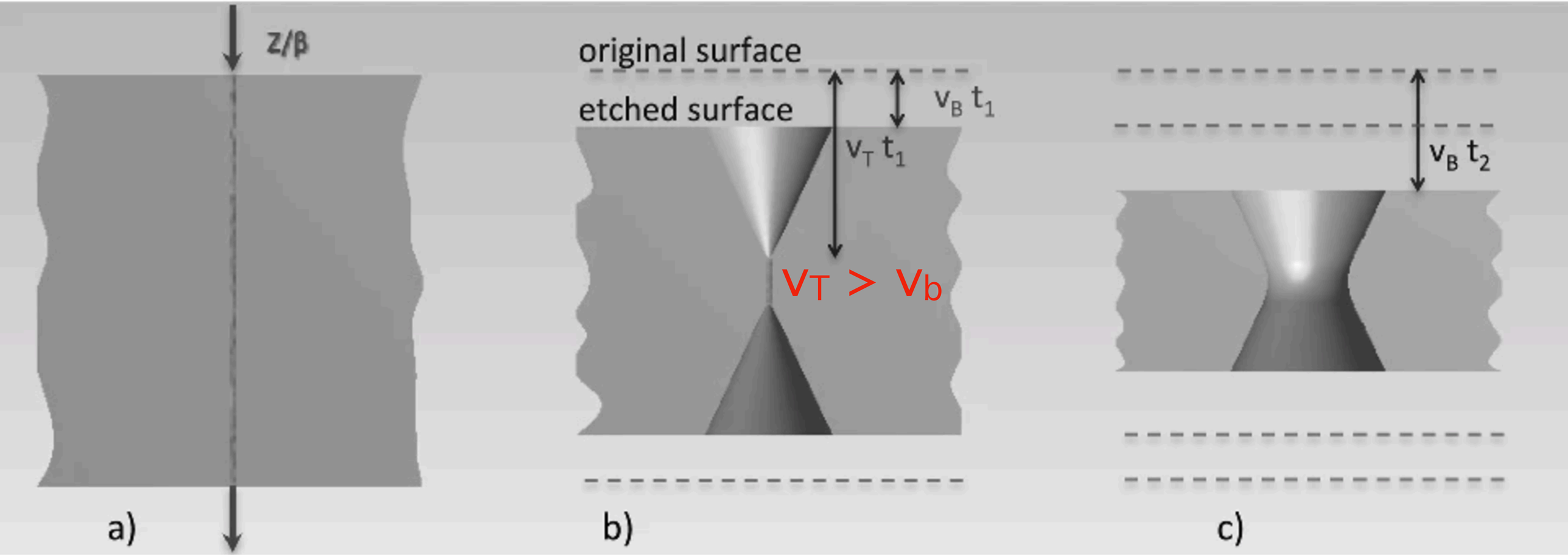

If $v_T \leq v_b$ track cannot be reconstructed!

Nuclear Track Detector — acceptance

The acceptance of the detector depends on:
- incidence angle
- electric charge
- velocity

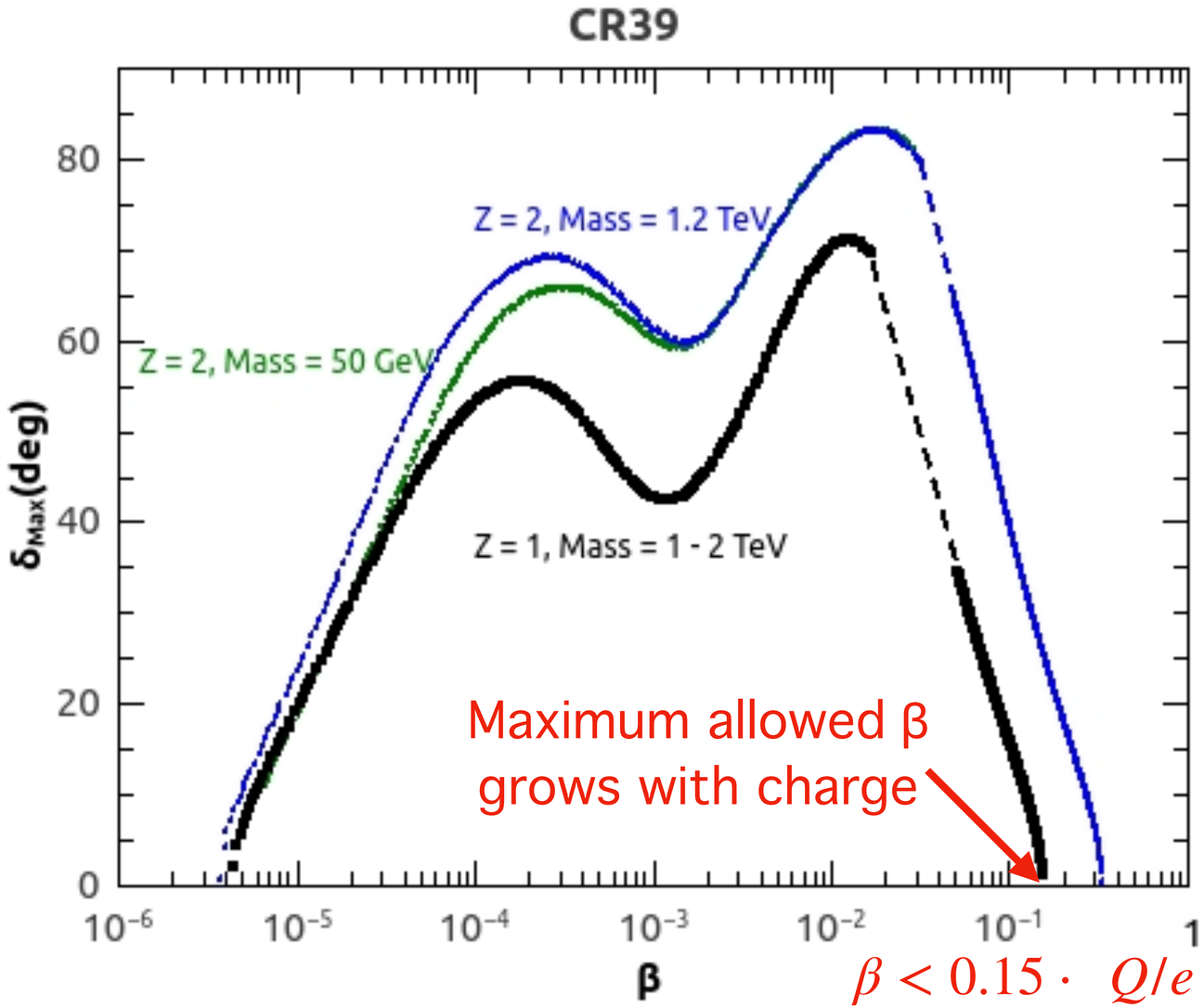

$$\beta < 0.15 \cdot \ Q/e$$

Signal at MoEDAL

- MoEDAL is sensitive only to highly-ionising particles with $c\tau \gtrsim \mathcal{O}(1\ \mathrm{m})$
- MoEDAL is sensitive only to slowly moving particles $\beta \leq 0.15 \cdot Z$
- Sensitivity grows for larger electric charges
- Signal = 6 highly-collinear double-sided etch-pits pointing towards the interaction vertex
- Effectively no SM background => observation of even few signal events marks BSM Physics discovery
- But lots of noise makes the analysis challenging

Signal estimation at MoEDAL

- The signal is estimated by

$$N_{sig}(m,\tau) = \sigma(m) \cdot L \cdot \left\langle \sum_i \Theta\left(\beta_{th} - \beta_i\right) P(\vec{\beta}_i, \tau) \right\rangle_{MC}$$

  - $\sigma(m)$ is the production cross-section for pair of particles of mass m
  - $\vec{\beta}_i$ is particle's three-velocity, β_{th} is its threshold value
  - summation over i includes two particles created in an event
  - $P(\vec{\beta}_i, \tau) = \epsilon(\vec{\beta}) \cdot \exp\left(-\frac{L_{NTD}(\vec{\beta})}{\gamma\beta c\tau}\right)$ is the probability to reach the detector, where $\epsilon(\vec{\beta})$ is 1 if particle's track crosses with and NTD panel, and 0 otherwise.
  - For neutralino mediator study, $P(\vec{\beta}_i, \tau) = 1 - \epsilon(\vec{\beta}) \cdot \exp\left(-\frac{L_{NTD}(\vec{\beta})}{\gamma\beta c\tau_{\tilde{\chi}_1^0}}\right)$
  - For Run 2 geometry, the incidence angle has to be considered

Signal at MoEDAL

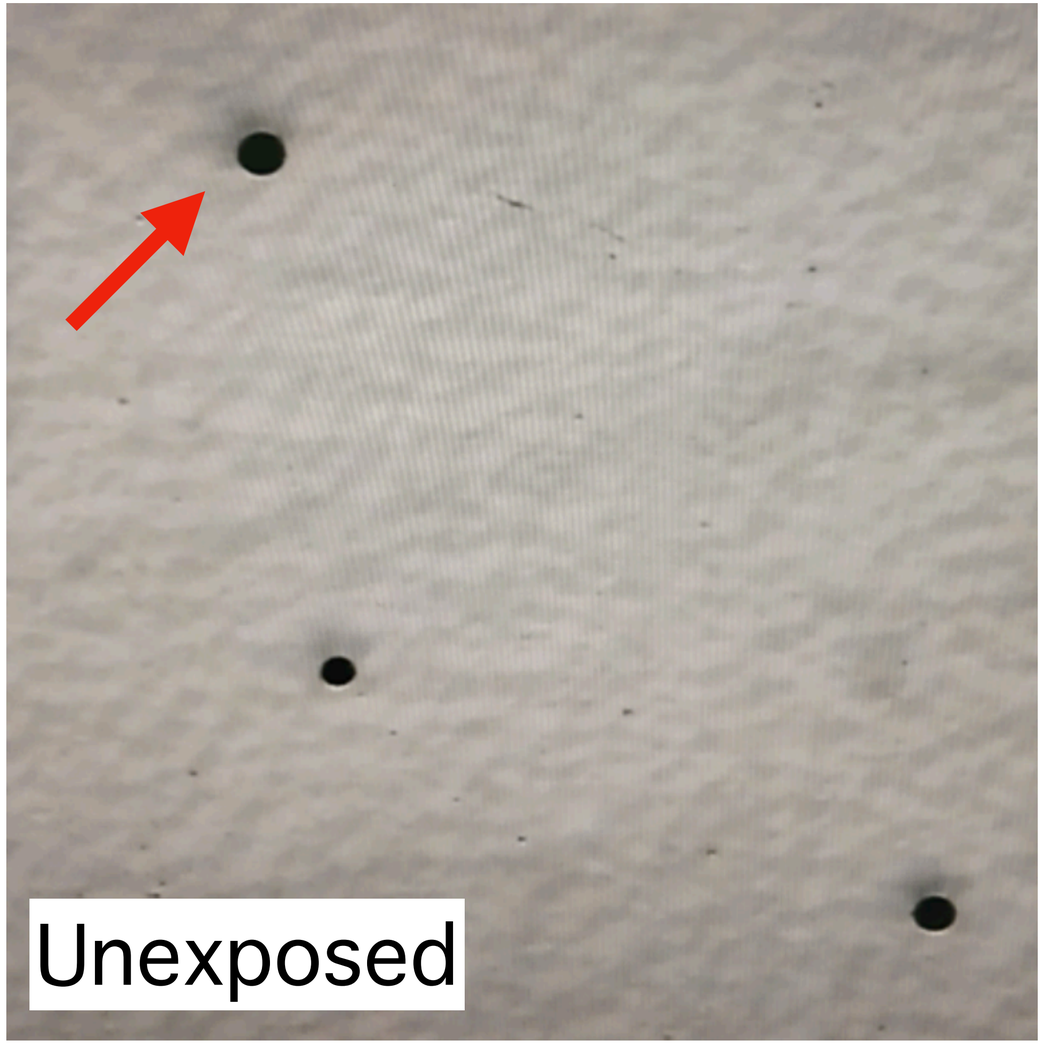

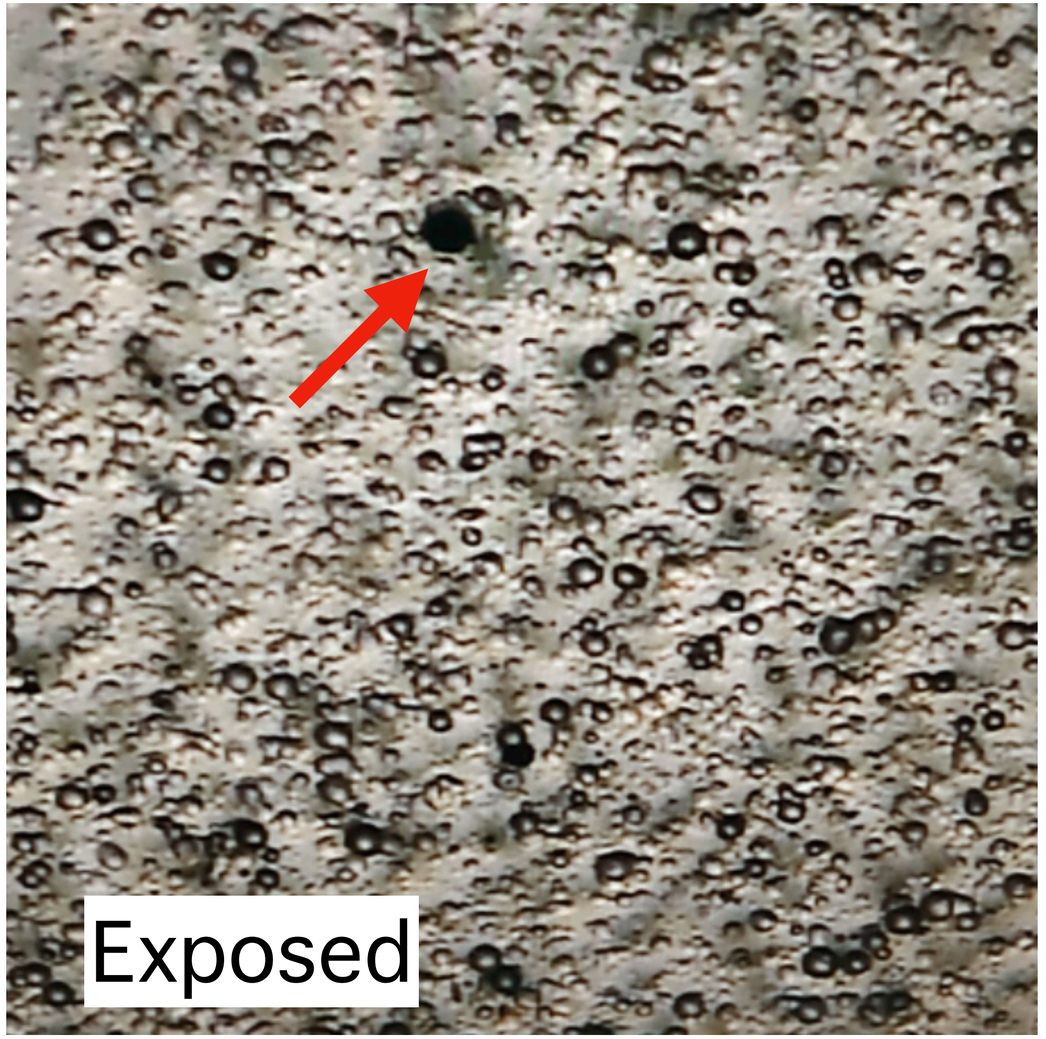

Prospects for discovering supersymmetric long-lived particles with MoEDAL

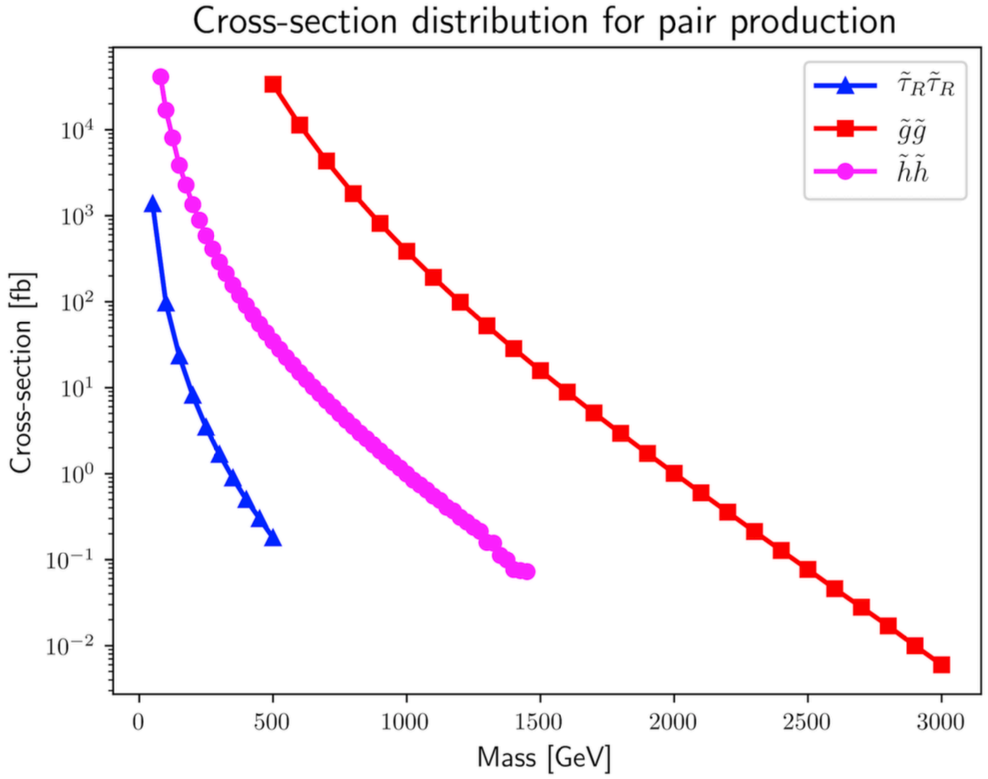

Figure 4.2: The cross section for pair production at 13 TeV LHC of staus (blue), gluinos (red), and higgsinos (magenta). Cross sections of staus and higgsinos were calculated at NLO + NLL level, while gluinos with $\text{NLLO}_{\text{approx}}$ + NNLL precision [198].

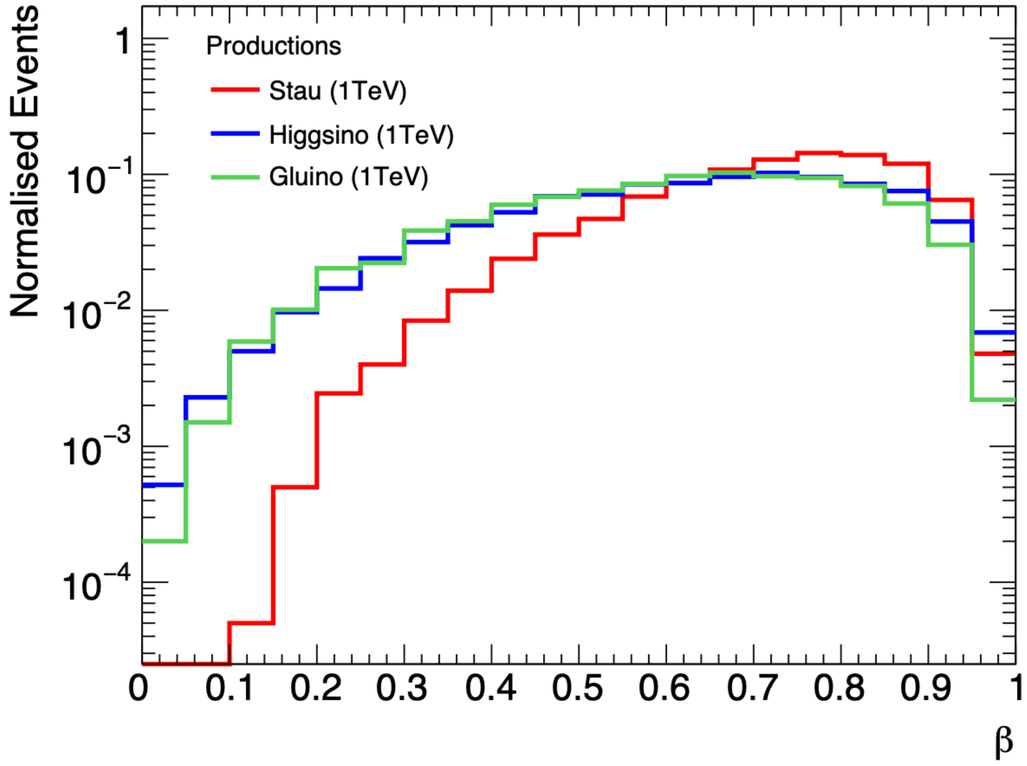

Figure 4.3: Comparison of velocity distributions of staus (red), higgsinos (blue), and gluinos (green). Pair production in 13 TeV pp collisions was simulated. All particles have $m = 1$ TeV.

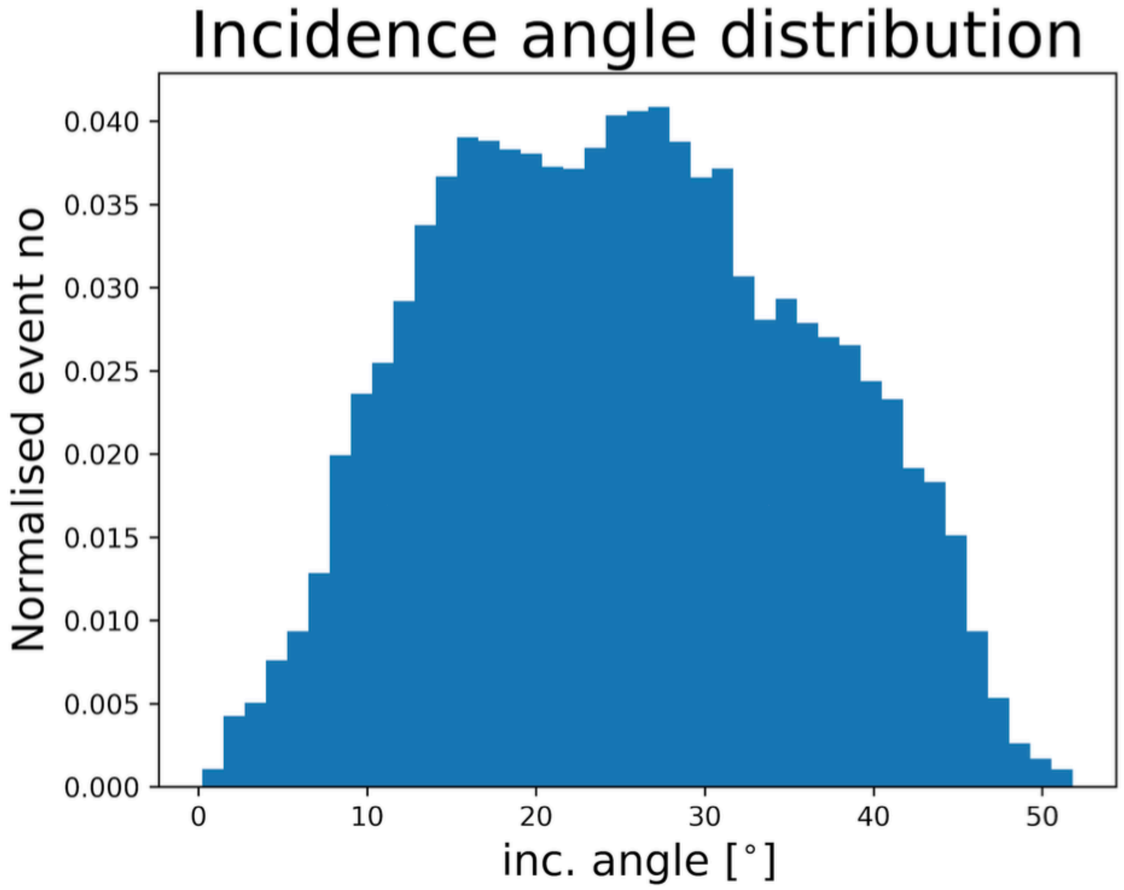

Figure 4.5: The distribution of incidence angle of staus hitting NTD panels assuming Run 2 geometry.

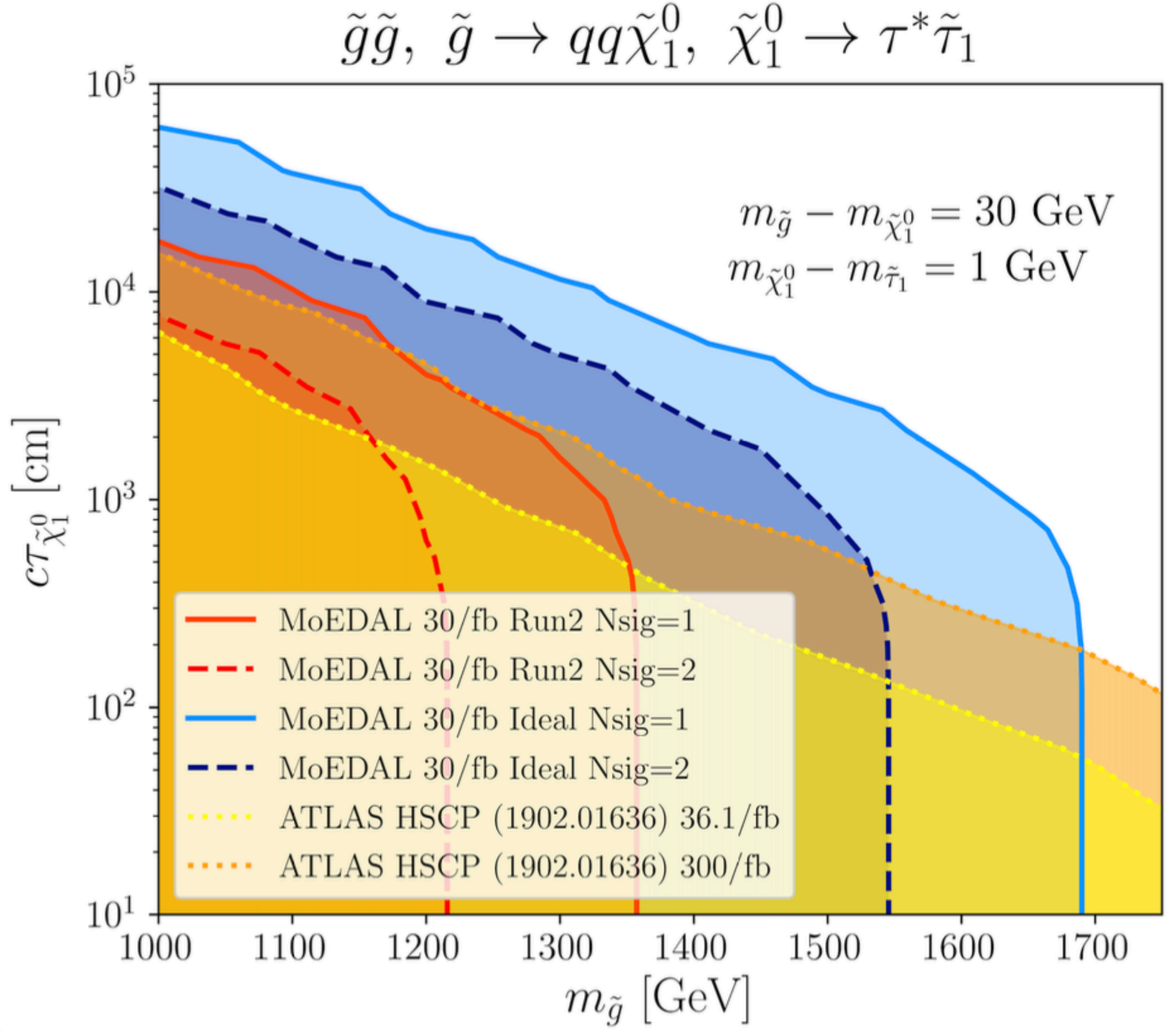

Figure 4.6: The sensitivity of the MoEDAL detector to the considered SUSY scenario, presented in the $m_{\tilde{g}}$ vs. $c\tau_{\tilde{\chi}_1^0}$ parameter plane. Solid contour lines correspond to $N_{\text{sig}} = 1$, while dashed contour lines to $N_{\text{sig}} = 2$. In the shaded area enclosed by the contour, the expected number of detected signal events is equal to or larger than at the contour line. Red contours correspond to Run 2 NTD geometry, while blue contours are obtained for an "ideal" geometry, for which all NTD panels face the interaction point. The latest experimental constraint coming from the ATLAS search [157] for Heavy (detector-)Stable Charged Particles (HSCPs) for $L = 36.1$ fb^{-1} 13 TeV is recast and plotted as a yellow contour with a dotted line. In addition, the exclusion contour by ATLAS is scaled up to $L = 300$ fb^{-1} and plotted in orange with a dotted contour line. For MoEDAL $L = 30$ fb^{-1} at the end of Run 3 is assumed.

Prospects of searches for long-lived charged particles with MoEDAL

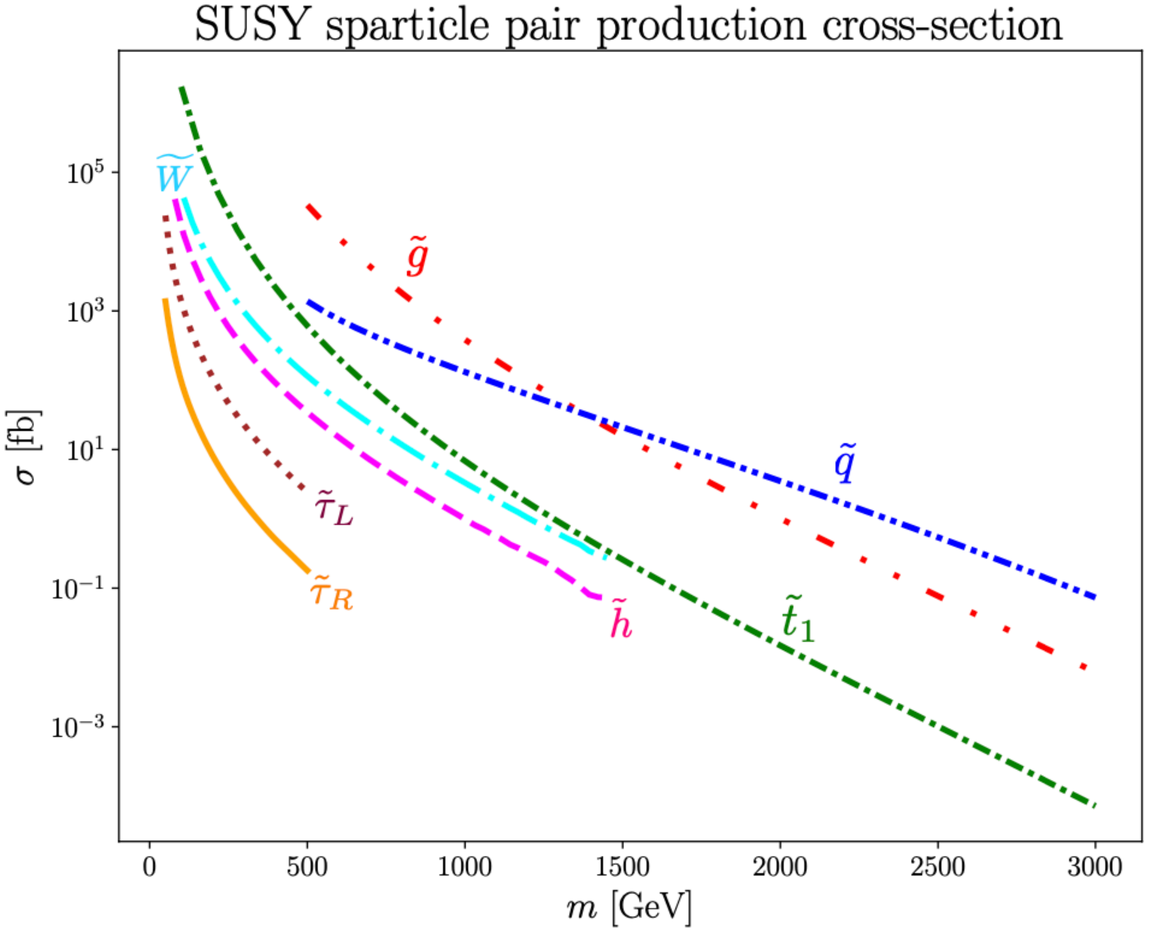

Figure 4.7: Pair production cross section for various sparticles as a function of their mass. For the coloured sparticles, ($\tilde{g}$, $\tilde{t}$, $\tilde{q}$), cross sections were calculated at the NNLO$_{\text{approx}}$+NNLL level [198, 222], while for the weakly interacting particles, ($\widetilde{W}$, $\tilde{h}$, $\tilde{\tau}_{L/R}$), the accuracy was at the NLO + NLL level [221, 222].

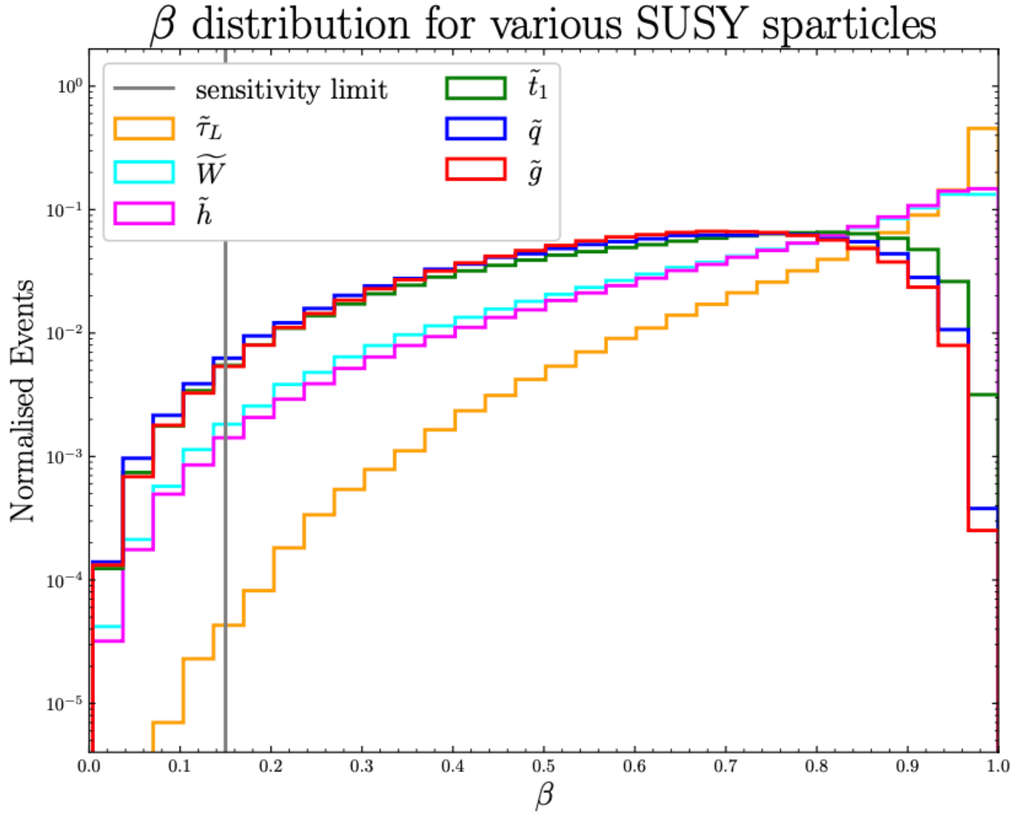

Figure 4.8: Velocity distributions for various SUSY particles. The vertical grey line corresponds to the MoEDAL sensitivity limit for singly charged particles, i.e. only particles with $\beta < 0.15$ can be registered by NTDs. The following representative masses were taken to produce the plot: $\tilde{g}$: 1010 GeV, $\tilde{q}$: 920 GeV, $\tilde{q}$: 720 GeV, $\widetilde{W}$: 300 GeV, $\tilde{\tau}_L$: 80 GeV.

Table 4.1: Comparison of the expected MoEDAL sensitivity at the end of Run 3 ($L = 30$ fb^{-1}, $\kappa = 0.7$, $N_{sig} = 1$) with the latest ATLAS and CMS constraints.

	MoEDAL	(ATLAS)	(CMS)
$\tilde{g}$	1600	(2000)	(1500)
$\tilde{q}$	1920	((2310))	-
$\tilde{t}$	920	(1350)	(1000)
$\widetilde{W}$	670	(1090)	-
$\tilde{h}$	530	((1170))	-
$\tilde{\tau}$	61	(430)	(230)

The gluino cannot be directly detected, because it rapidly hadronises into colour-neutral R-hadrons. If the colour charge of the gluino is neutralised by a gluon, the resulting R-hadron is electrically neutral and cannot be detected by MoEDAL. The other possibility is the formation of colour-neutral bound states involving gluino and two colour-octet quarks. By assuming that R-hadrons formed with the first-generation quarks are the lightest, we arrive at four possible bound states: $\tilde{g}u\bar{u}$, $\tilde{g}d\bar{d}$, $\tilde{g}u\bar{d}$, $\tilde{g}d\bar{u}$[4]. The former two states are electrically neutral and cannot be detected in the MoEDAL experiment, hence we will discuss the prospects for detection of the latter two charged R-hadrons. In the succeeding sections, we will introduce a parameter κ to represent the fraction of charged states among all of the produced R-hadrons, and study MoEDAL's sensitivity to charged R-hadrons for different values of κ.

In the case of squarks, we distinguish between two scenarios. In the first model, stop is the lightest squark forming a long-lived R-hadron, while the other five flavours are much heavier. In the second scenario the situation is reversed, stop is very heavy, while the other five squarks are nearly mass degenerate and form long-lived R-hadrons. In both cases we assume that heavy squarks decay to the lightest one on a time scale $\ll \mathcal{O}(1$ m/c). Similarly to the gluino, the lightest squark is assumed to form bound states with the first generation of SM quarks: $\tilde{u}u\bar{u}$, $\tilde{d}d\bar{d}$, $\tilde{u}d\bar{d}$, $\tilde{d}u\bar{u}$. The first two bound states are electrically neutral, while the other two are charged. Similarly to gluino R-hadrons, we will introduce a parameter κ to represent the fraction of charged states among all of the produced R-hadrons, and present prospects for detection of charged R-hadrons in MoEDAL for different values of κ.

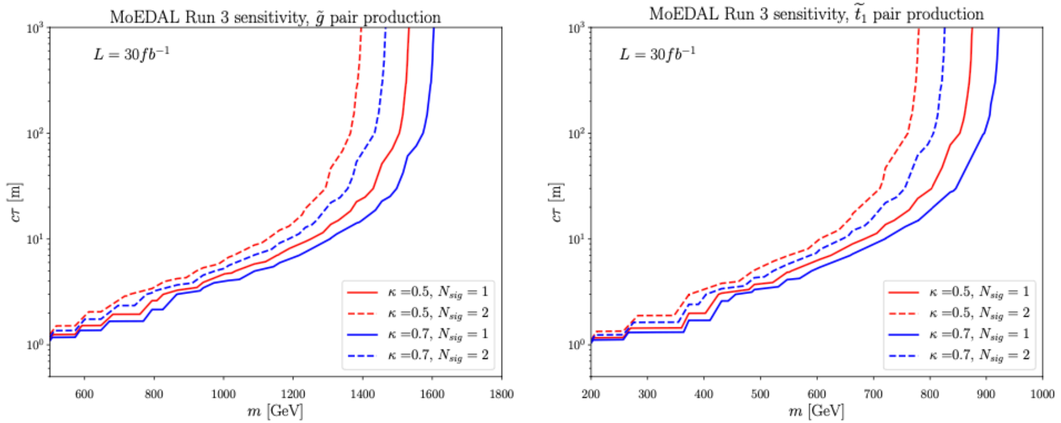

(a) gluino R-hadrons

(b) stop R-hadrons

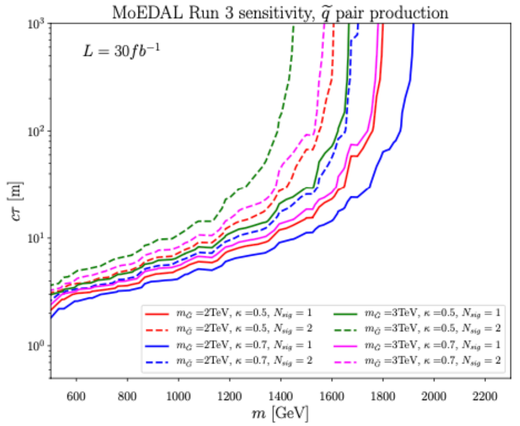

(c) squark R-hadrons

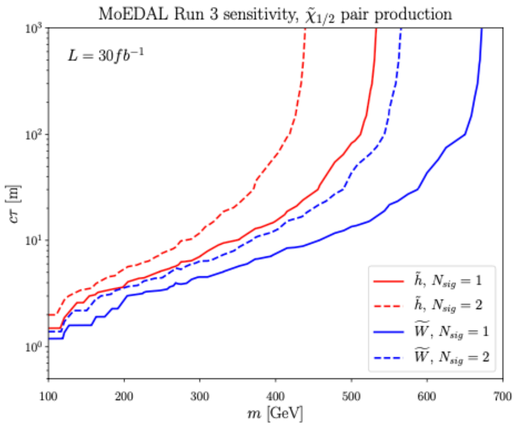

(d) charginos

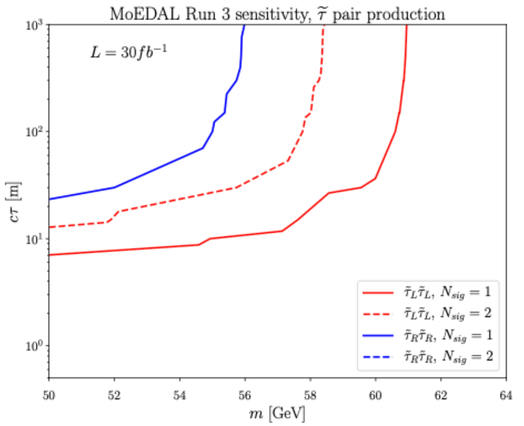

(e) staus

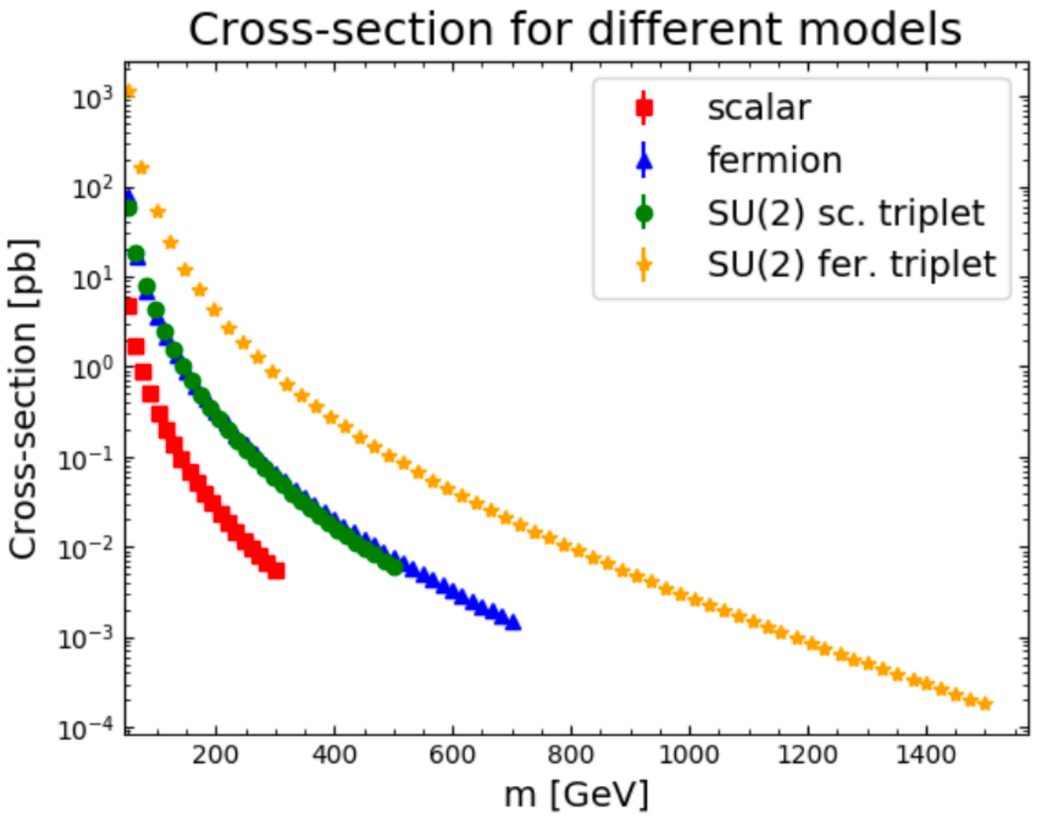

Figure 4.10: Leading order cross section for pair production of various doubly charged particles at 13 TeV LHC.

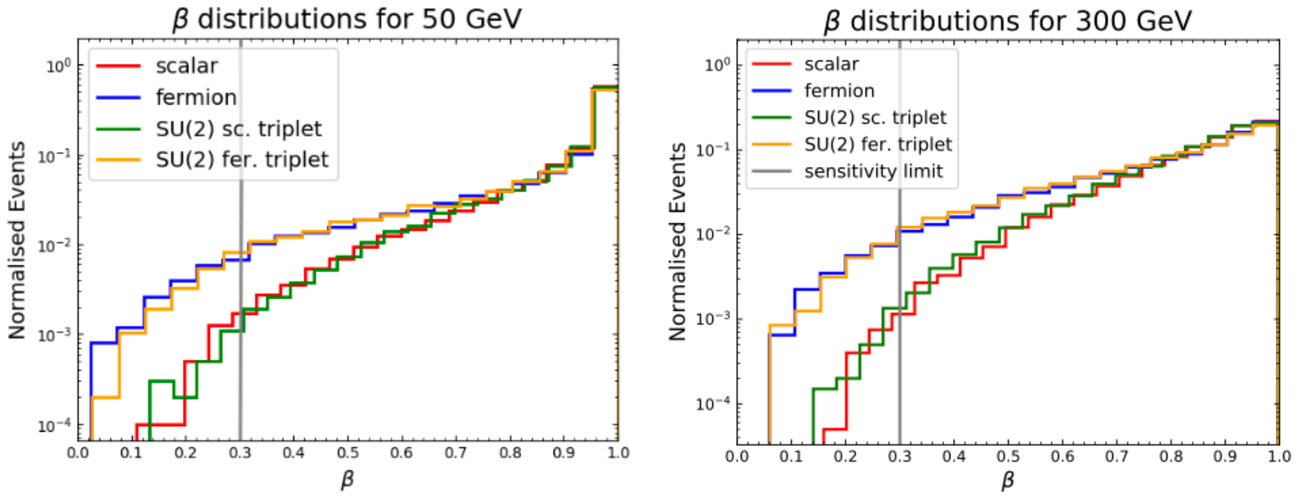

Figure 4.11: The velocity distributions of various doubly charged particles Y, with $m_Y = 50$ GeV (left) and $m_Y = 300$ GeV (right). The vertical grey line corresponds to the MoEDAL's sensitivity limit, i.e. the requirement that $\beta < 0.3$.

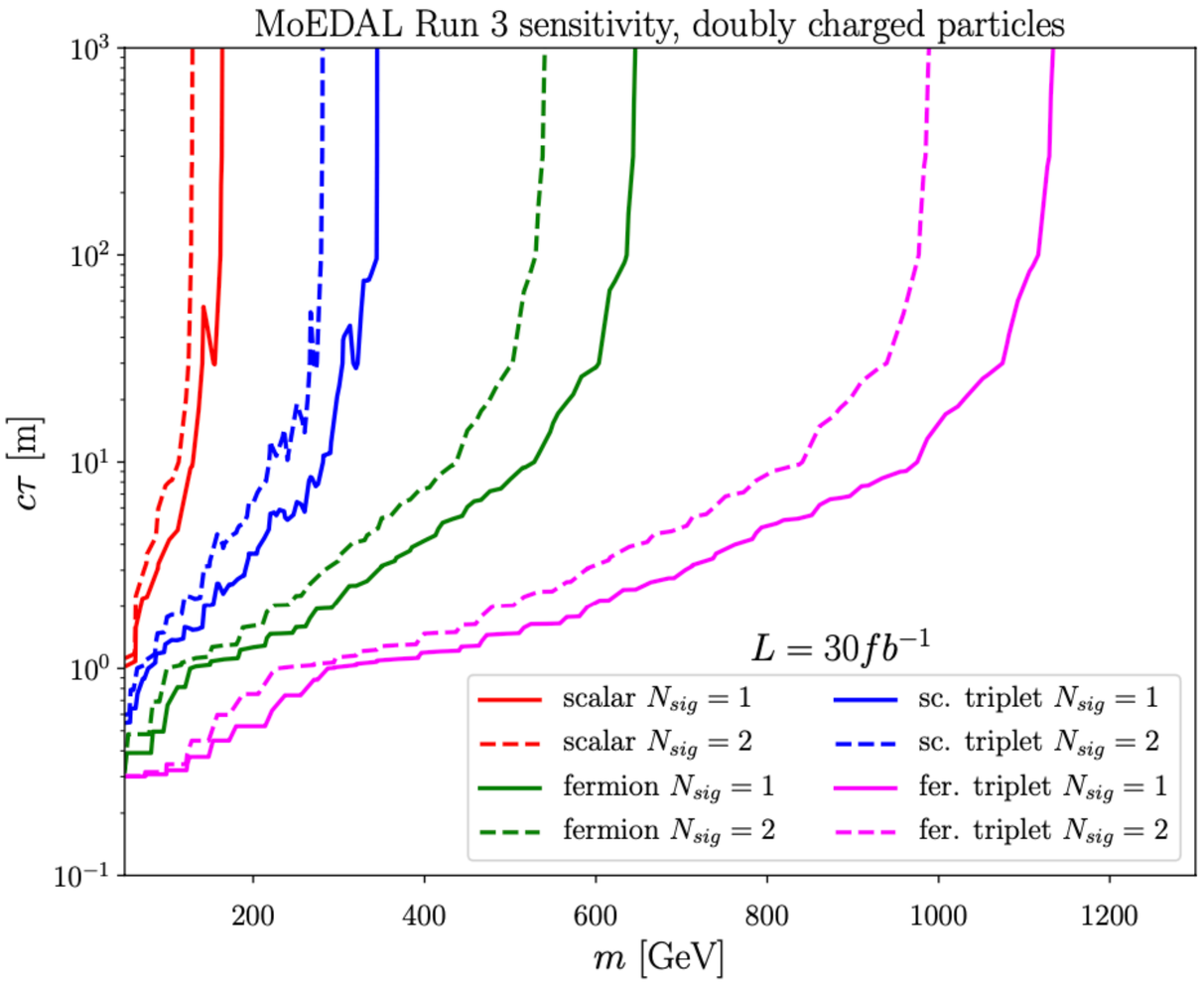

Figure 4.12: The expected sensitivity of the MoEDAL detector at the end of Run 3 to doubly charged singlet and triplet spin-0 and spin-1/2 particles. The integrated luminosity is assumed to be $L = 30$ fb^{-1}.

	MoEDAL	(CMS)
Scalar singlet	160	((320))
Fermion singlet	650	(680)
Scalar triplet	340	((590))
Fermion triplet	1130	((900))

Detecting long-lived multi-charged particles in neutrino mass models with MoEDAL

Uncoloured version

	S_1	S_3	F_i	$\bar{F}_i$
Spin	0	0	$\frac{1}{2}$	$\frac{1}{2}$
$SU(3)_C$	1	1	1	1
$SU(2)_L$	1	3	2	2
$U(1)_Y$	2	3	$\frac{5}{2}$	$-\frac{5}{2}$
Lepton number	-2	-4	-3	3

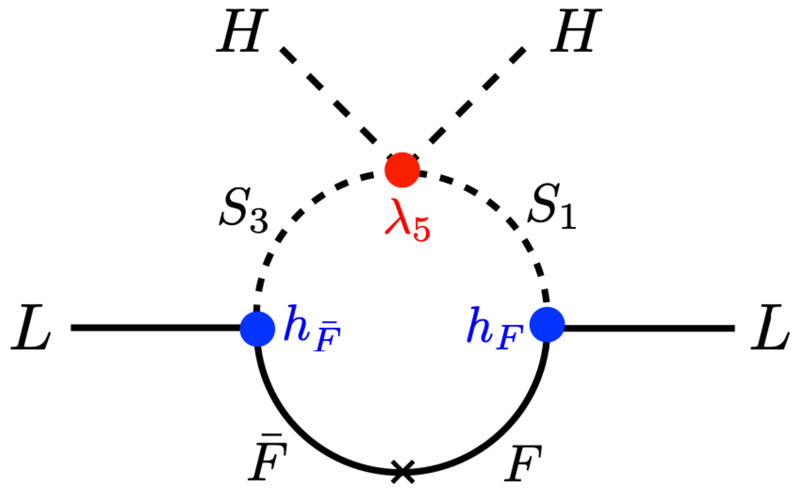

Figure 2.4: Neutrino mass generation diagram for a model from [118].

$$\mathcal{L}_{\text{BSM}} = \mathcal{L}_{\text{KIN}} - \Big[(h_{ee})_{ij}(e_R^i)^C(e_R^j)^C S_1^\dagger + (h_F)_{ij} L_i F_j S_1^\dagger + (h_{\bar{F}})_{ij} L_i \bar{F}_j S_3 + h.c.\Big] +$$
$$+ \lambda_2 |H|^2 |S_1|^2 + \lambda_{3a} |H|^2 |S_3|^2 + \lambda_{3b} |H S_3|^2 +$$
$$- \Big[\lambda_5 H H S_1 S_3^\dagger + h.c.\Big] +$$
$$+ \lambda_4 |S_1|^4 + \lambda_{6a} |S_3^\dagger S_3|^2 + \lambda_{6b} |S_3 S_3 S_3^\dagger S_3^\dagger| + \lambda_7 |S_1|^2 |S_3|^2,$$

Coloured version

	$\tilde{S}_1$	$\tilde{S}_3$	$\tilde{F}_i$	$\tilde{\tilde{F}}_i$
Spin	0	0	$\frac{1}{2}$	$\frac{1}{2}$
$\mathbf{SU(3)_C}$	$\bar{3}$	$\bar{3}$	3	$\bar{3}$
$\mathbf{SU(2)_L}$	1	3	2	2
$\mathbf{U(1)_Y}$	$\frac{4}{3}$	$\frac{7}{3}$	$\frac{11}{6}$	$-\frac{11}{6}$
Lepton number	-1	-3	-2	2

$$(h_{ee})_{ij}(e_R^i)^C(e_R^j)^C S_1^\dagger \to (h_{ed})_{ij}(d_R^i)^C(e_R^j)^C \tilde{S}_1^\dagger,$$

A non-zero value of λ_5 results in a violation of the lepton number, hence one can take λ_5 to be small and the theory will be technically natural in the sense of t'Hooft. Similarly, the absence of $(h_F)_{ij}$ or $(h_{\bar{F}})_{ij}$ leads to the conservation of the lepton number, and if both couplings are simultaneously zero, then BSM fermion number symmetry, i.e. $F_i \to e^{i\theta} F_i$, $\bar{F}_i \to e^{-i\theta} \bar{F}_i$, is restored. Therefore, a model in which both $(h_F)_{ij}$ and $(h_{\bar{F}})_{ij}$ are small is technically natural and radiatively stable.

In the discussed model, neutrino masses emerge radiatively from the one-loop diagram shown in Fig. 2.4. The Weinberg operator takes the form:

$$\frac{\lambda_5 N_C}{32\pi^2 \Lambda^2} \left[h_{\bar{F}}^T m_F h_F + h_F^T m_F h_{\bar{F}} \right]_{ij} \cdot L_i H L_j H, \tag{2.73}$$

where N_C is the number of colours of particles in the loop ($N_C = 1$ for now, but later a coloured version of the model will be discussed) and Λ is the mass scale of BSM fields. If we assume that all heavy masses are of the same order of magnitude, and that h_F and $h_{\bar{F}}$ are diagonal, one can roughly estimate neutrino masses by:

$$m_\nu \sim 0.05 \cdot N_C \cdot \left(\frac{\lambda_5}{10^{-6}} \right) \left(\frac{h_F h_{\bar{F}}}{10^{-4}} \right) \left(\frac{1 \text{ TeV}}{\Lambda} \right) \text{eV}. \tag{2.74}$$

Decays

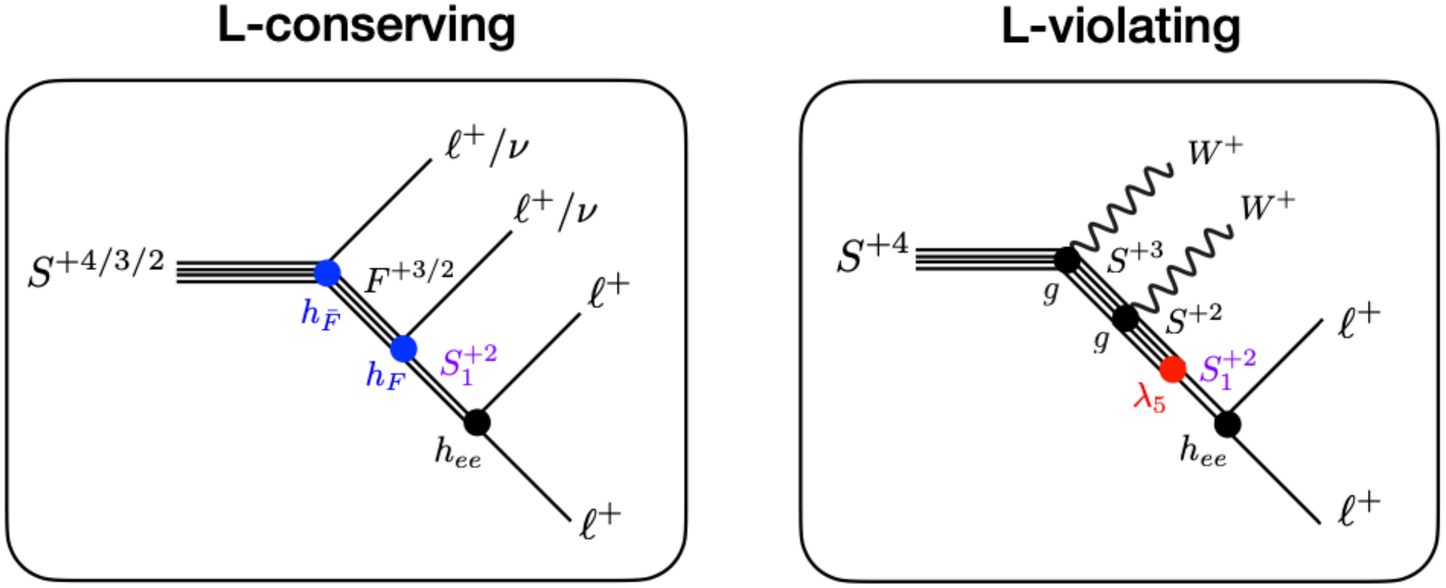

Figure 4.13: Diagrams for possible decays of S^{+4}, S^{+3} and S^{+2}. The same particle can decay into $L = -4$ final state (left) and $L = -2$ (right), hence its lepton number is not fixed unless λ_5 or $h_F \times h_{\bar{F}}$

$$\Gamma\left(S^{+4} \to l_\alpha^+ l_\beta^+ l_\gamma^+ l_\delta^+\right) \sim \frac{|(h_{ee})_{\alpha\beta}|^2}{192(4\pi)^5} \left|\left\langle \frac{h_{F\bar{F}}^{\gamma\delta}}{m_F} \right\rangle\right|^2 \frac{m_{S_3}^7}{m_{S_1}^4}, \tag{4.8}$$

$$\Gamma\left(S^{+4} \to W^+ W^+ l_\alpha^+ l_\beta^+\right) \sim \frac{|g_2^2 (h_{ee})_{\alpha\beta}|^2}{48(4\pi)^5} \left(\frac{\lambda_5 v^2}{m_{S_1}^2}\right)^2 \frac{m_{S_3}^5}{m_W^4}, \tag{4.9}$$

with

$$\left|\left\langle \frac{h_{F\bar{F}}^{\gamma\delta}}{m_F} \right\rangle\right| \equiv \left|\sum_k \frac{h_F^{\gamma k} h_{\bar{F}}^{\delta k} + h_F^{\delta k} h_{\bar{F}}^{\gamma k}}{m_{F_k}}\right|. \tag{4.10}$$

Decays, continuation

$$\Gamma\left(S^{+3}\to l_\alpha^+ l_\beta^+ l_\gamma^+ \nu_\delta^+\right)\sim \frac{|(h_{ee})_{\alpha\beta}|^2}{192(4\pi)^5}\left|\left\langle \frac{h^{\gamma\delta}_{F\bar{F}}}{m_F}\right\rangle\right|^2 \frac{m_{S_3}^7}{m_{S_1}^4}, \tag{4.11}$$

$$\Gamma\left(S^{+3}\to W^+ l_\alpha^+ l_\beta^+\right)\sim \frac{|g_2^2(h_{ee})_{\alpha\beta}|^2}{16(4\pi)^3}\left(\frac{\lambda_5 v^2}{m_{S_1}^2}\right)^2 \frac{m_{S_3}^3}{m_W^2}. \tag{4.12}$$

$$\Gamma\left(S^{+2}\to l_\alpha^+ l_\beta^+ \nu_\gamma^+ \nu_\delta^+\right)\sim \frac{|(h_{ee})_{\alpha\beta}|^2}{192(4\pi)^5}\left|\left\langle \frac{h^{\gamma\delta}_{F\bar{F}}}{m_F}\right\rangle\right|^2 \frac{m_{S_3}^7}{m_{S_1}^4}, \tag{4.13}$$

$$\Gamma\left(S^{+2}\to l_\alpha^+ l_\beta^+\right)\sim \frac{|(h_{ee})_{\alpha\beta}|^2}{4\pi}\left(\frac{\lambda_5 v^2}{m_{S_1}^2}\right)^2 m_{S_3}. \tag{4.14}$$

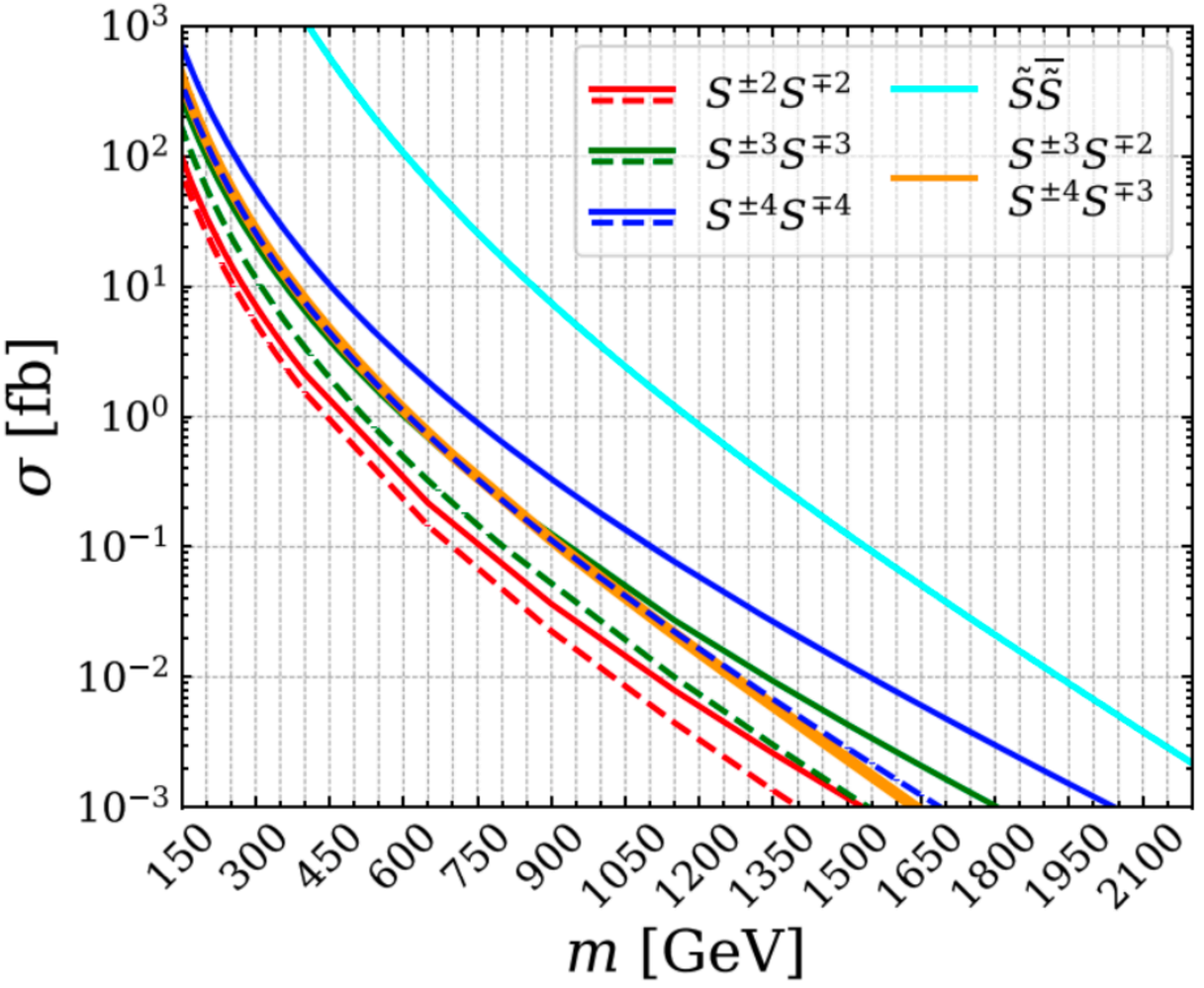

Figure 4.14: The leading order cross section for various modes of particle production in the coloured and uncoloured models introduced in Sec. 2.2.2. The dashed curves correspond to the cross section **without** the photon fusion process. The orange curve corresponds to the associated production: $pp \to S^{\mp 2e}S^{\pm 3e}$ (or $S^{\mp 3e}S^{\pm 4e}$ since the values are the same), mediated by the s-channel W boson. The cyan curve depicts the production cross section for a pair of coloured scalar particles, i.e. $pp \to \tilde{S}^{\pm 4/3}\tilde{S}^{\mp 4/3}$, $pp \to \tilde{S}^{\pm 7/3}\tilde{S}^{\mp 7/3}$, and $pp \to \tilde{S}^{\pm 10/3}\tilde{S}^{\mp 10/3}$.

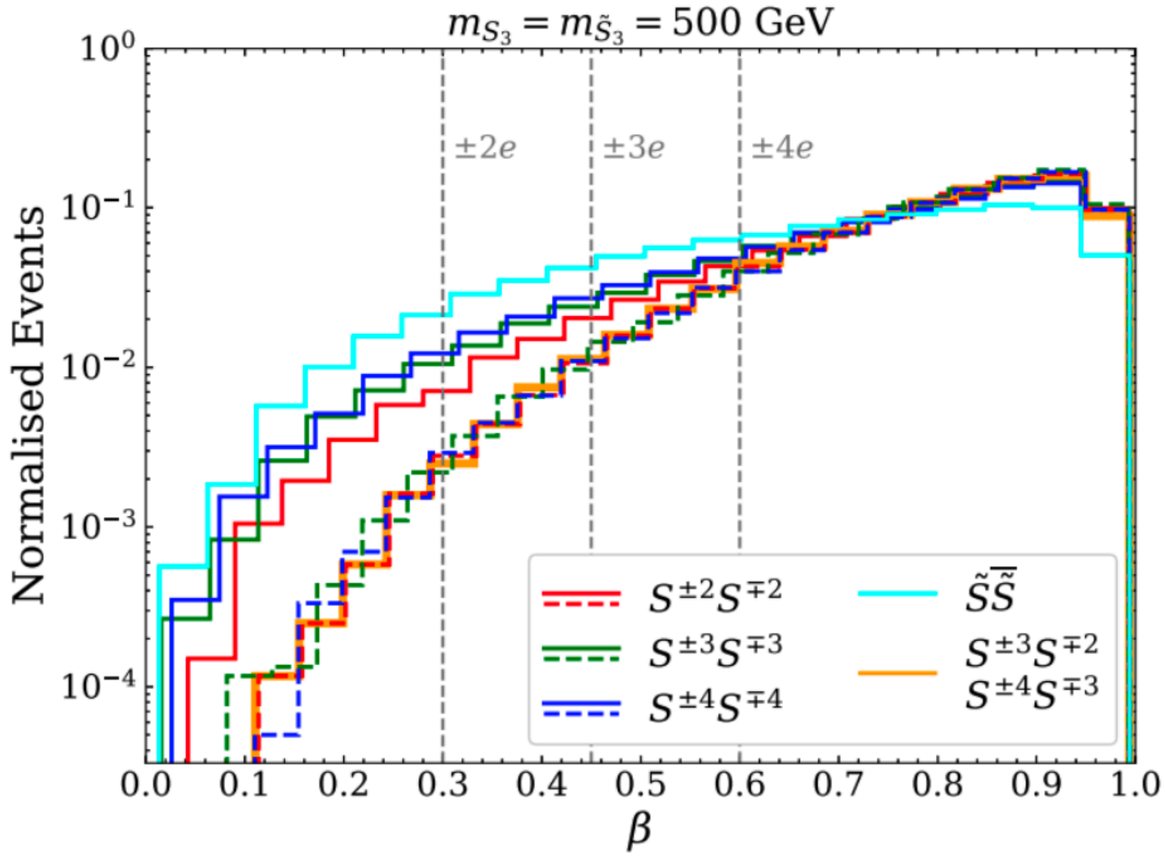

Figure 4.15: Velocity distributions for particles in various production modes. The dashed curves correspond to production **without** the photon fusion process included. The orange curve corresponds to the associated production: $pp \to S^{\mp 2e}S^{\pm 3e}$ (or $S^{\mp 3e}S^{\pm 4e}$ since the values are the same), mediated by the s-channel W boson. The cyan curve depicts the production cross section for a pair of coloured scalar particles, i.e. $pp \to \tilde{S}^{\pm 4/3}\tilde{S}^{\mp 4/3}$, $pp \to \tilde{S}^{\pm 7/3}\tilde{S}^{\mp 7/3}$, and $pp \to \tilde{S}^{\pm 10/3}\tilde{S}^{\mp 10/3}$. The masses of all particles were 500 GeV. Vertical grey lines depict MoEDAL NTD velocity thresholds for $|Q| \in \{2e, 3e, 4e\}$. Only particles moving below the appropriate velocity threshold can be detected.

Model independent

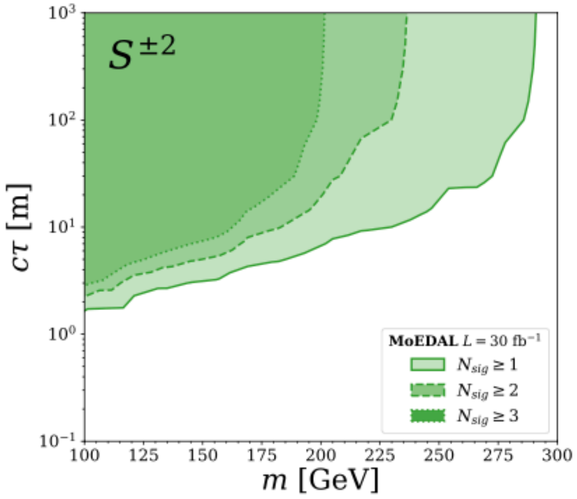

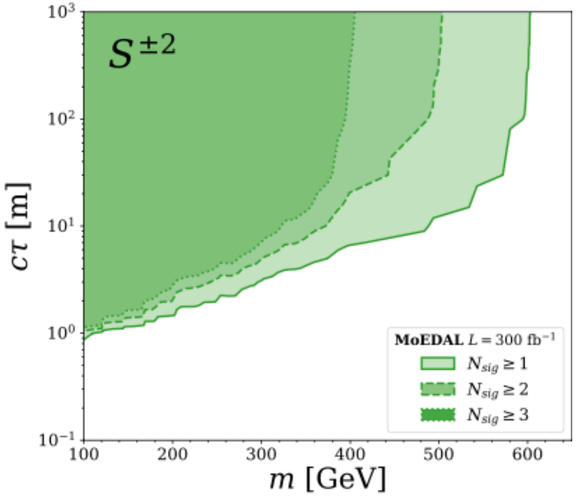

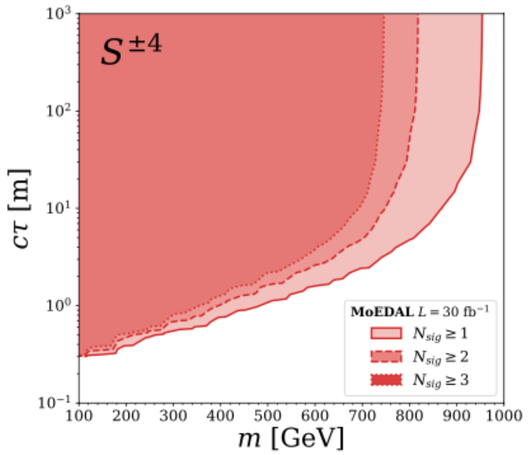

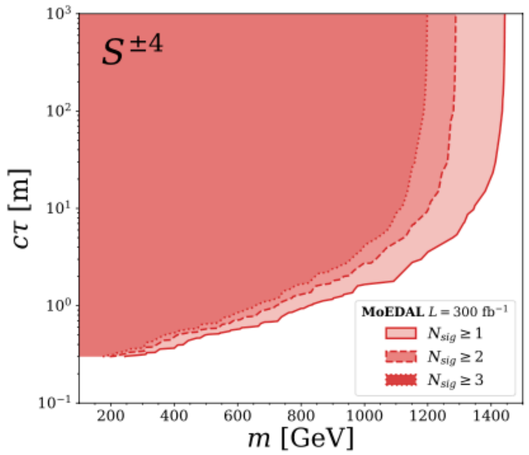

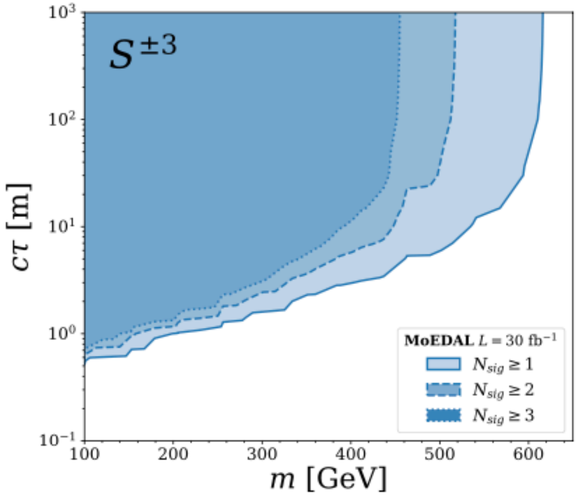

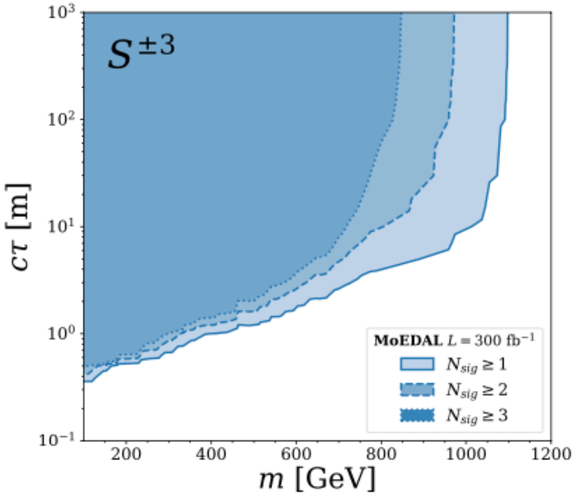

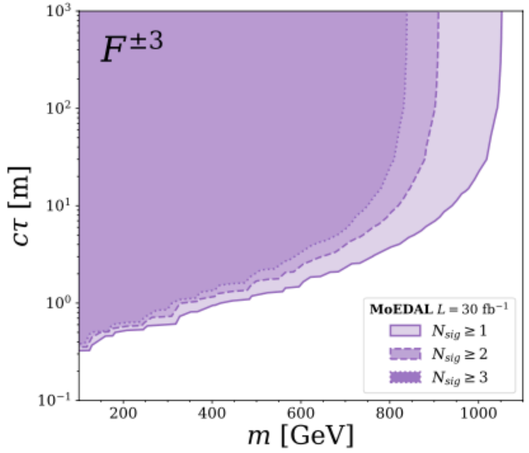

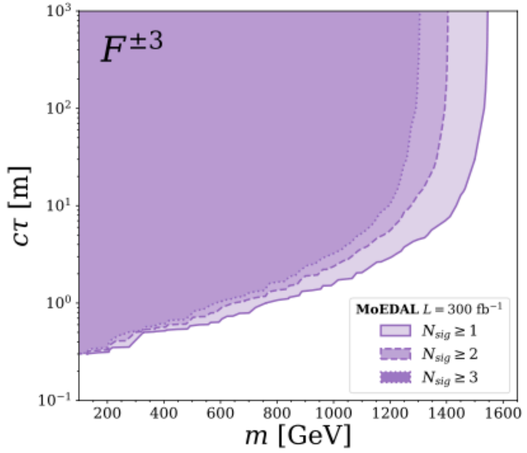

Figure 4.16: The model-independent detection reach of Run 3 (left, $L = 30$ fb^{-1}) and HL-LHC (right, $L = 300$ fb^{-1}) MoEDAL detector for colour-singlet multiply charged particles. Solid, dashed and dotted contours correspond to $N_{\rm sig} = 1$, 2, and 3, respectively.

Model independent

Table 4.3: Comparison of the most recent [159, 245] lower mass bounds on multiply charged particles from ATLAS for 36 fb^{-1} (column 1) and 300 fb^{-1} (column 2), with the detection reach by MoEDAL for 30 fb^{-1} (column 3) and 300 fb^{-1} (column 4). Values in double parentheses were obtained by recasting the ATLAS search [159]. MoEDAL reach outside (inside) the parentheses corresponds to $N_{\rm sig} = 3$ (1). All masses are in GeV units.

	current HSCP bound 36 fb^{-1} [159]	HSCP (Run-3) 300 fb^{-1} [245]	MoEDAL (Run-3) 30 fb^{-1}	MoEDAL (HL-LHC) 300 fb^{-1}
$S^{\pm 2}$	((650))	–	190 (290)	400 (600)
$S^{\pm 3}$	((780))	–	430 (610)	850 (1100)
$S^{\pm 4}$	((920))	–	700 (960)	1200 (1430)
$F^{\pm 3}$	1130	1500	800 (1030)	1300 (1550)

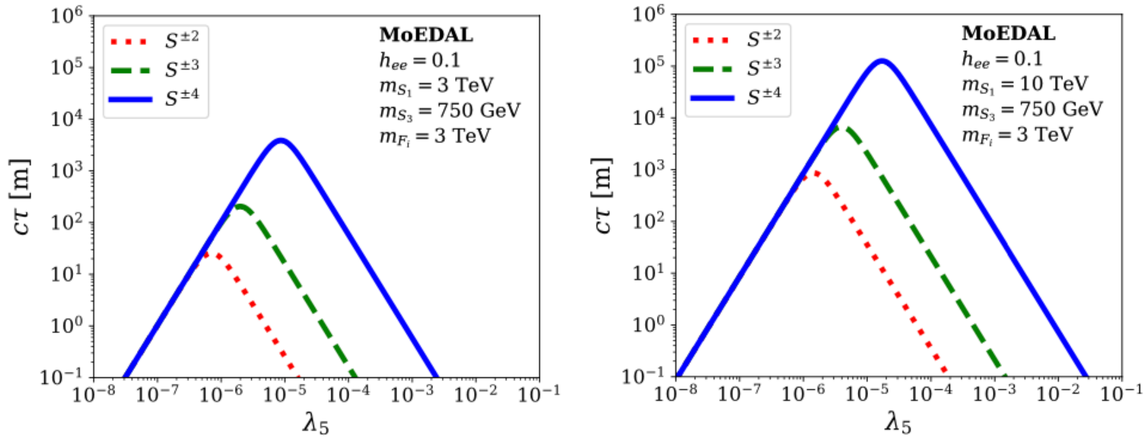

Figure 4.17: Decay lengths of $S^{\pm 4}$ (blue solid), $S^{\pm 3}$ (green dashed) and $S^{\pm 2}$ (red dotted) as a function of λ_5. Other parameters are set to $h_{ee} = 0.1$, $m_{S_3} = 750$ GeV, and $m_{S_1} = 3$ (10) TeV for the left (right) plot. For the given set of mass and λ_5 parameters, $h_F h_{\bar{F}}$ is obtained from fitting the neutrino data.

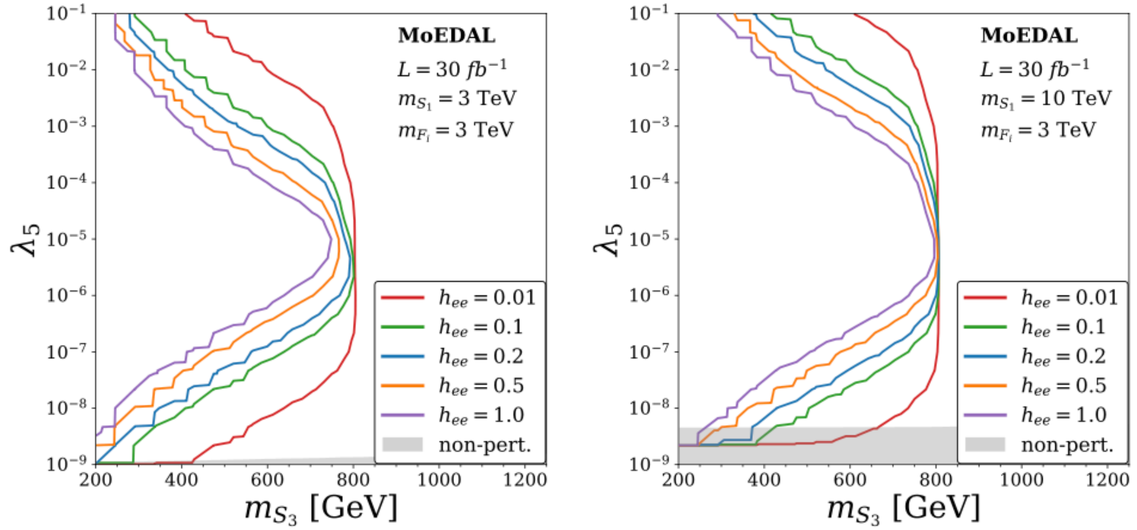

Figure 4.19: $N_{\rm sig} = 1$ contours for different values of the h_{ee} coupling, ranging from 0.01 to 1.0. The other parameters are assumed to take the following values:$m_{F_i} = 3$ TeV, (i = 1, 2, 3), $L = 30$ fb^{-1}, and $m_{S_1} = 3$ (10) TeV in the left (right) plot.

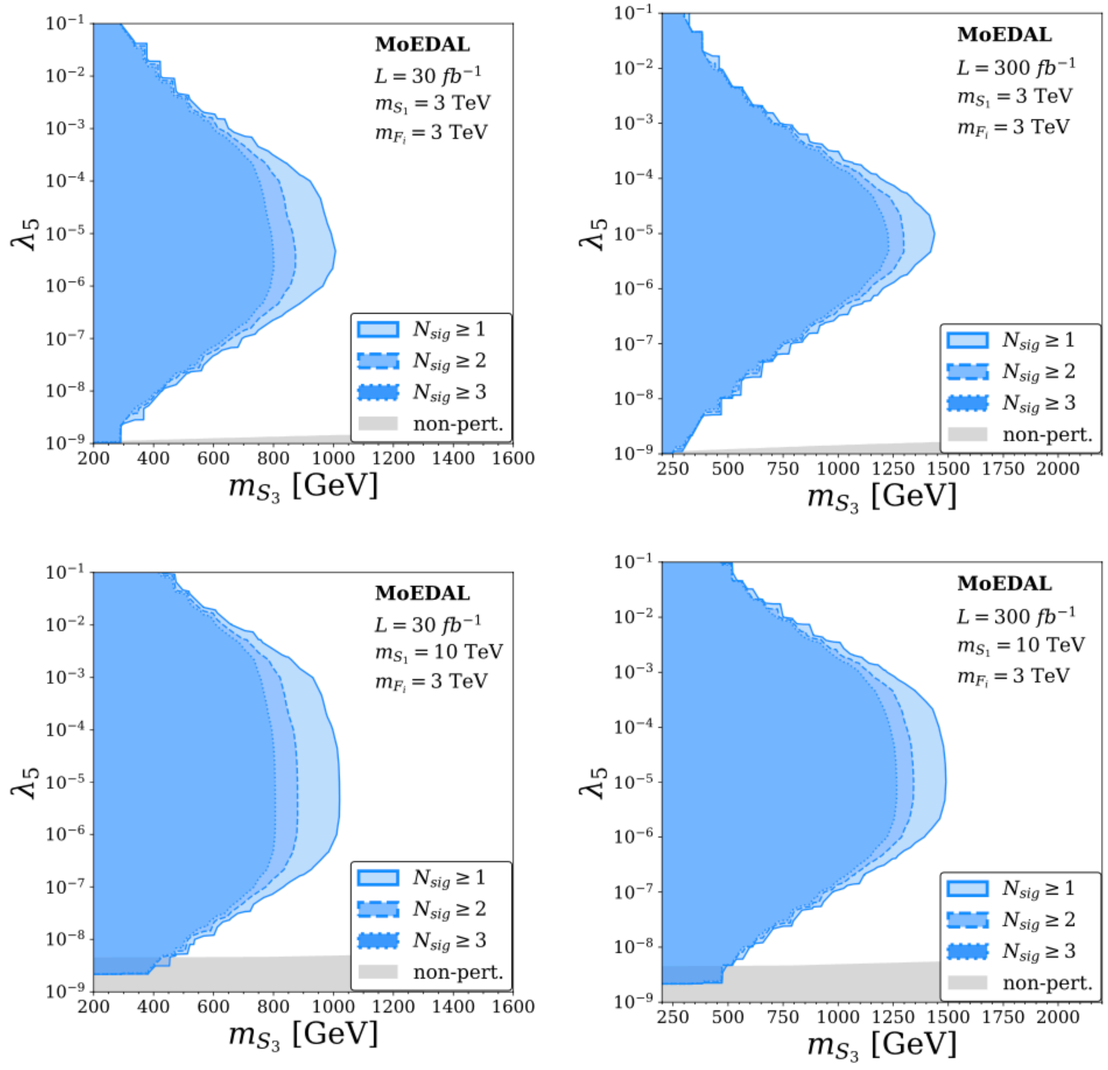

Figure 4.18: MoEDAL's sensitivity to the uncoloured version of the studied neutrino mass model on the (m_{S_3}, λ_5) parameter plane. Regions enclosed by solid, dashed and dotted contour lines correspond to $N_{\rm sig} \geq 1$, 2, and 3 signal event observations, respectively. The region with $N_{\rm sig} \geq 3$ will be excluded at 95% CL if MoEDAL observes no events. The left and right panels correspond to Run 3 ($L = 30$ fb^{-1}) and HL-LHC ($L = 300$ fb^{-1}). The upper (lower) two panels assume $m_{S_1} = 3$ (10) TeV. The h_F and $h_{\bar{F}}$ are fitted to neutrino data. The region shaded in grey, around $\lambda_5 \sim 10^{-9}$, is non-perturbative, because in that region $\max_{ij}(|(h_F)_{ij}|, |(h_{\bar{F}})_{ij}|) \geq 2$. Other parameters, common to all plots, are $m_{F_i} = 3$ TeV and $h_{ee} = 0.1$.

Spin-1/2 mesons: probability k

$$\tilde{S} + u_{L/R} \quad (+2/3)$$
$$\tilde{S} + d_{L/R} \quad (-1/3)\,,$$

Spin-0 baryons: probability $\frac{2}{3}(1-k)$

$$\tilde{S} + \bar{u}_L \bar{u}_R \quad (-4/3)$$
$$\tilde{S} + \bar{d}_L \bar{d}_R \quad (+2/3)$$
$$\tilde{S} + \bar{u}_L \bar{d}_R \quad (-1/3)$$
$$\tilde{S} + \bar{d}_L \bar{u}_R \quad (-1/3)$$

Spin-1 baryons: probability $\frac{1}{3}(1-k)$

$$\tilde{S} + \bar{u}_L \bar{d}_L \quad (-1/3)$$
$$\tilde{S} + \bar{u}_R \bar{d}_R \quad (-1/3)\,,$$

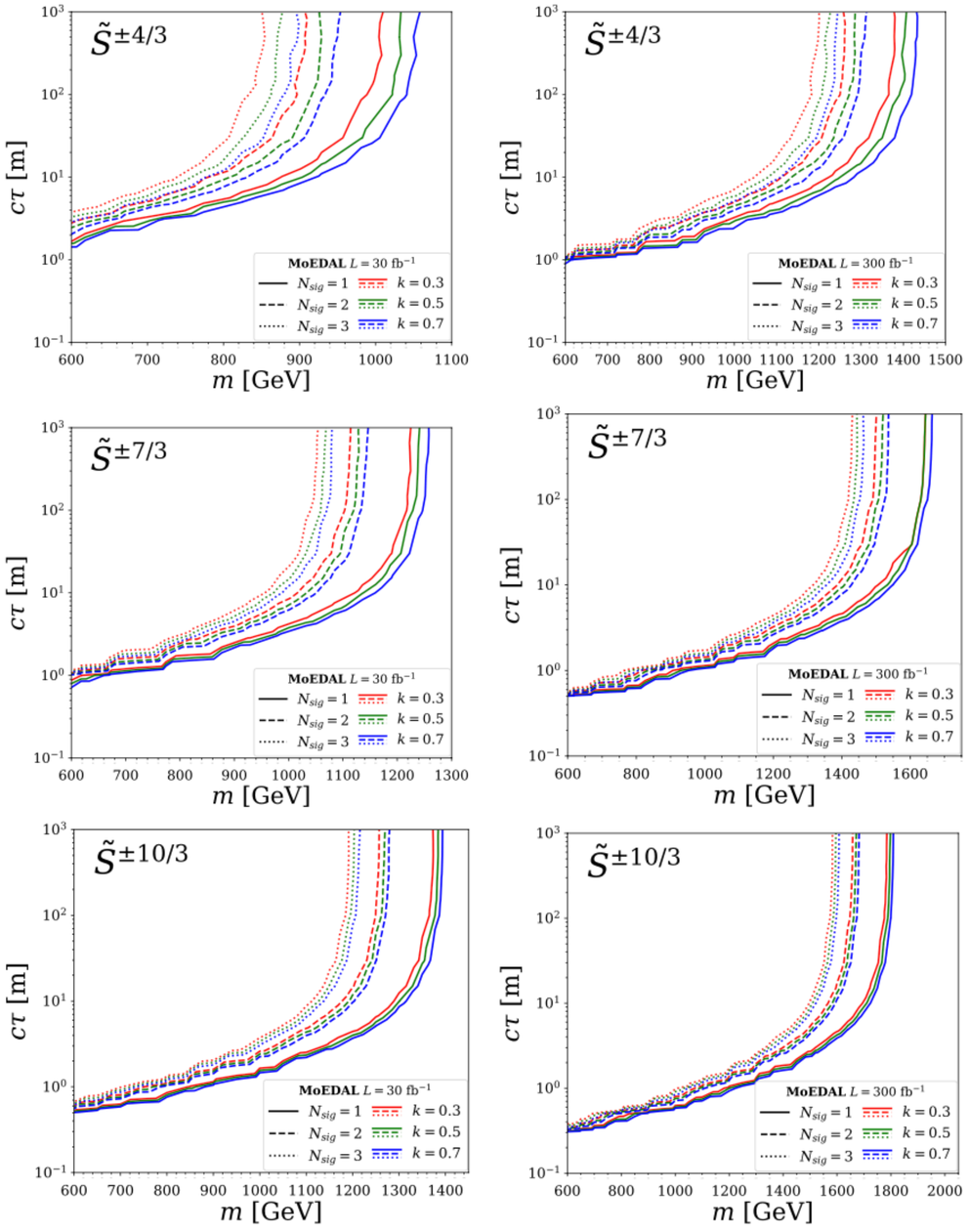

Figure 4.20: The model-independent detection reach of the MoEDAL detector. Results for the multiply charged colour-triplet particles are presented in the m vs. $c\tau$ parameter plane . Solid, dashed and dotted contours correspond to $N_{\rm sig} = 1$, 2, and 3, respectively. Red, green and blue colours represent $k = 0.3$, $k = 0.5$, and $k = 0.7$, respectively. The integrated luminosity is 30 fb^{-1} (left) and 300 fb^{-1} (right).

Table 4.4: Model-independent mass reaches (in GeV) of the multiply charged particles in the coloured model by MoEDAL (2nd and 3rd columns). In the first column, the numbers in the double parentheses correspond to the estimated mass bounds obtained in [245] by rescaling the 7 and 8 TeV CMS result [162] to 13 TeV with $L = 36$ fb^{-1}. The second column presents the projected mass reach for Run 3 (300 fb^{-1}) obtained in [245]. The numbers outside (inside) the brackets in the third and fourth columns represent MoEDAL's mass reaches with $N_{\rm sig} \geq 3$ (1) assuming $L = 30$ (Run 3) and 300 (HL-LHC) fb^{-1}, respectively.

	current HSCP bound 36 fb^{-1} [245]	HSCP (Run-3) 300 fb^{-1} [245]	MoEDAL (Run-3) 30 fb^{-1}	MoEDAL (HL-LHC) 300 fb^{-1}
$\tilde{S}^{\pm 4/3}$	((1450))	1700	880 (1050)	1250 (1400)
$\tilde{S}^{\pm 7/3}$	((1480))	1730	1080 (1250)	1450 (1650)
$\tilde{S}^{\pm 10/3}$	((1510))	1790	1200 (1400)	1600 (1800)

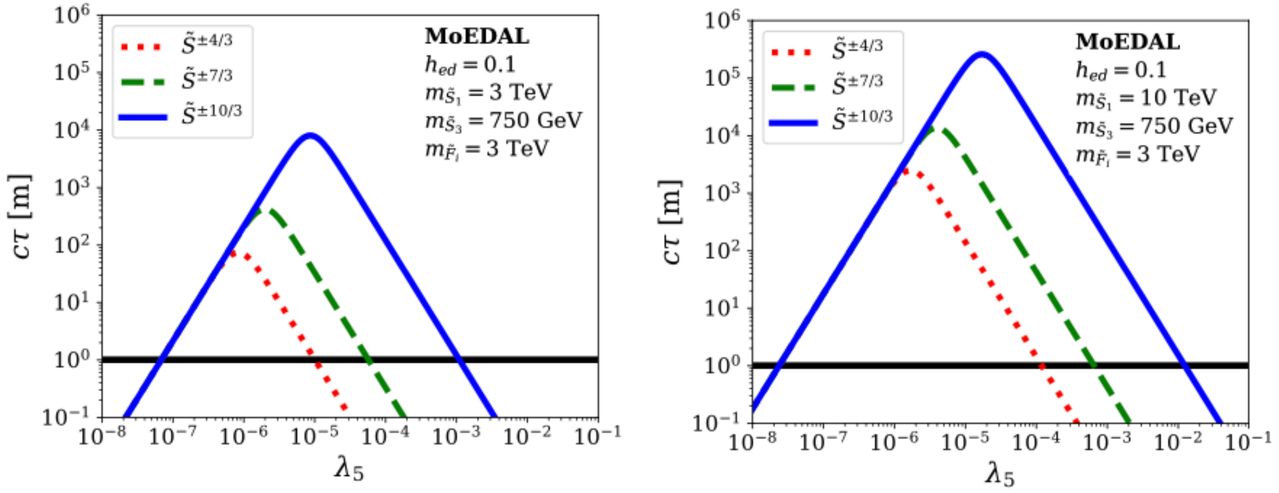

Figure 4.21: Decay lengths of $S^{\pm 10/3}$ (blue solid), $S^{\pm 7/3}$ (green dashed) and $S^{\pm 4/3}$ (red dotted) as a function of λ_5. Other parameters are set to $h_{ed} = 0.1$, $m_{S_3} = 750$ GeV, and $m_{S_1} = 3$ (10) TeV for the left (right) plot. For the given set of mass and λ_5 parameters, $h_F h_{\bar{F}}$ is obtained from fitting the neutrino data. The thick black horizontal line corresponds to $c\tau = 1$ m, which is a typical distance for the MoEDAL detector.

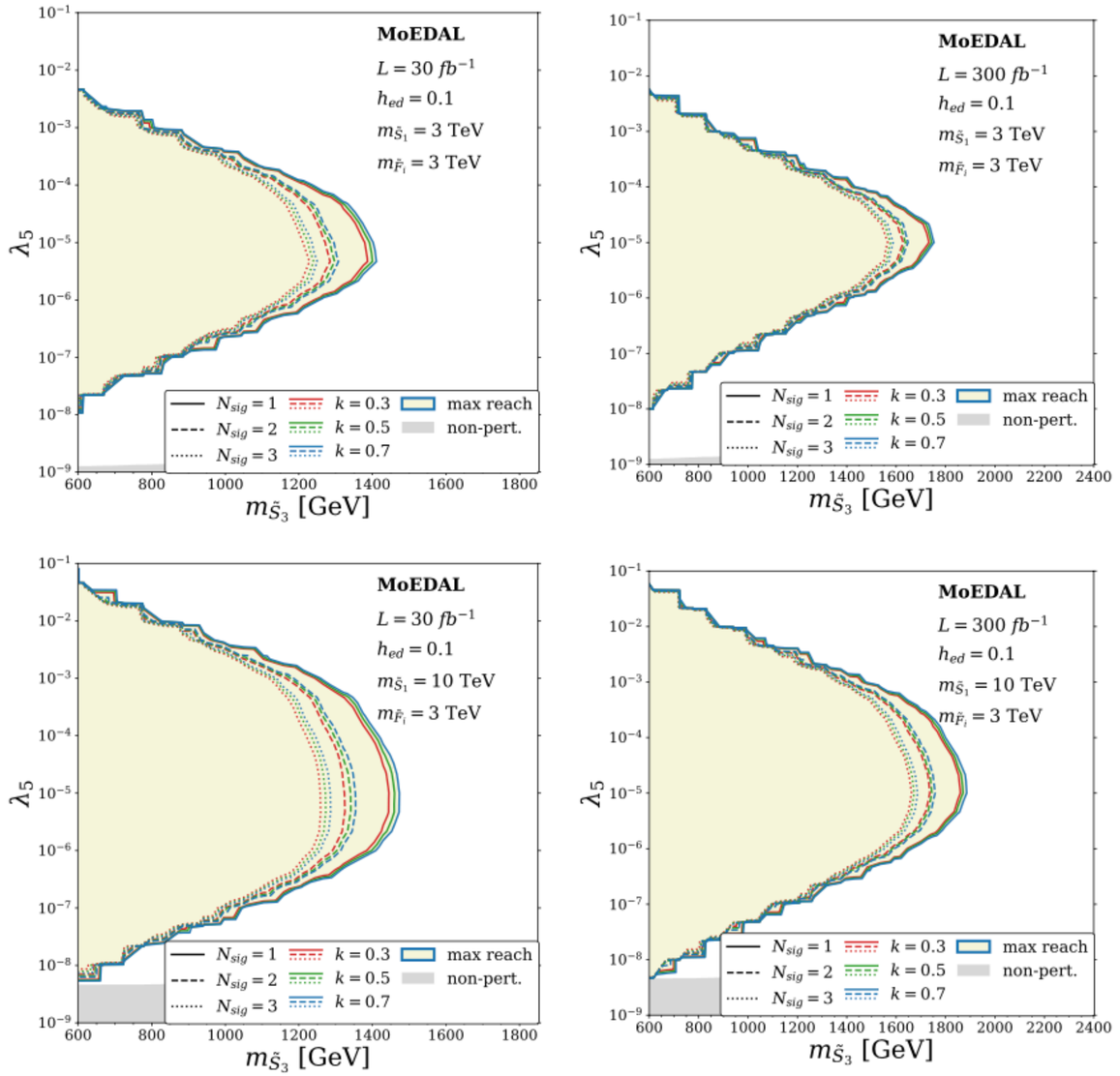

Figure 4.22: Sensitivity of the MoEDAL detector to the coloured version of the neutrino mass model studied in this project. Results are presented in $m_{\tilde{S}_3}$ vs. λ_5 parameter plane, with $h_F h_{\bar{F}}$ fitted to neutrino data. The top (bottom) panels correspond to $m_{\tilde{S}_1} = 3$ (10) TeV, while other parameters are set to $m_{\tilde{F}_i} = 3$ TeV and $h_{ed} = 0.1$ for all plots. Plots on the left (right) correspond to $L = 30$ fb^{-1} ($L = 300$ fb^{-1}) integrated luminosity. Solid, dashed and dotted contours represent $N_{\rm sig} = 1$, 2 and 3, respectively. Red, green and blue curves correspond to $k = 0.3$, $k = 0.5$, and $k = 0.7$, respectively. The grey region for small values of λ_5 is non-perturbative, because of a large coupling $\max_{ij}(|(h_F)_{ij}|, |(h_{\bar{F}})_{ij}|) \geq 2$, and cannot be trusted.

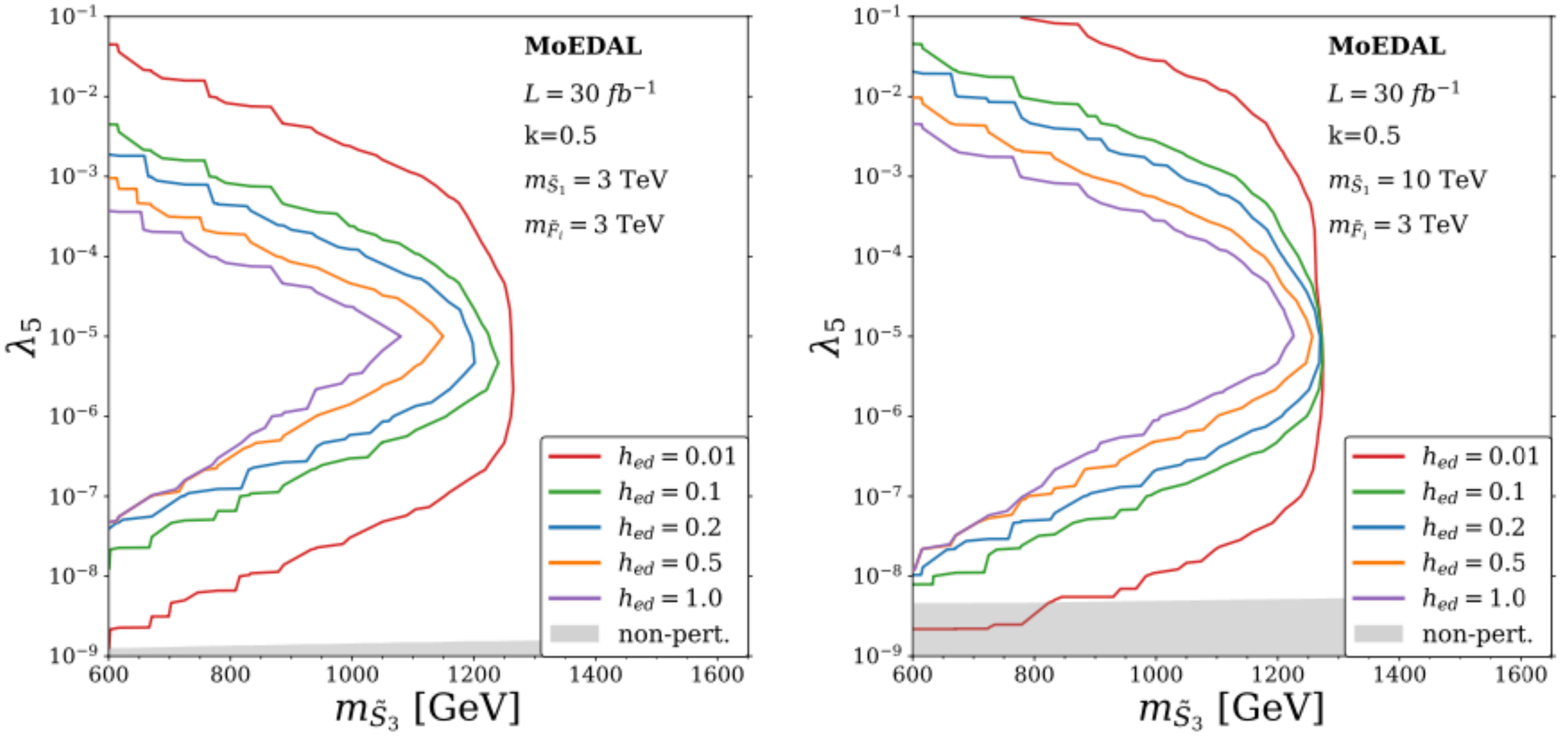

Figure 4.23: $N_{\text{sig}} = 1$ contours for different values of the h_{ed} coupling, ranging from 0.01 to 1.0. Other parameters were $m_{F_i} = 3$ TeV, (i $= 1, 2, 3$), $L = 30$ fb^{-1}, and $m_{S_1} = 3$ (10) TeV for the left (right) plot.

Discovery prospects for long-lived multiply charged particles at the LHC

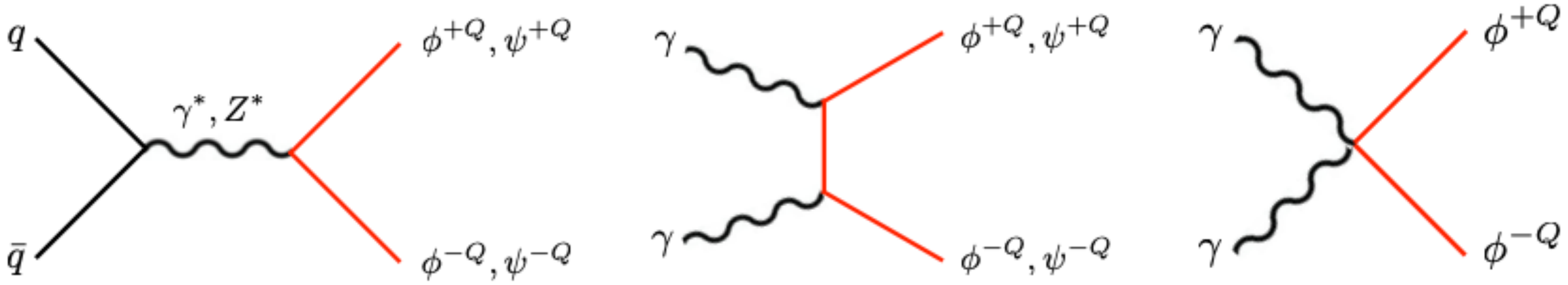

Figure 4.24: Feynman diagrams for colour-singlet open production modes.

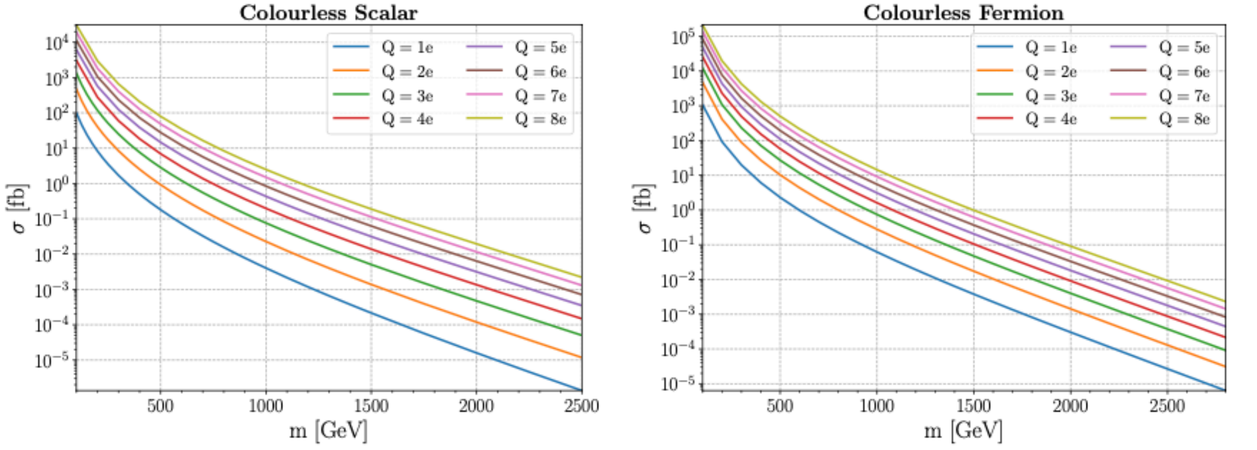

Figure 4.25: Leading order cross section for pair-production production of scalar (left) and fermion (right) particles. Curves with different colours correspond to particles with different magnitudes of the electric charge, Q, from $\pm 1e$ to $\pm 8e$.

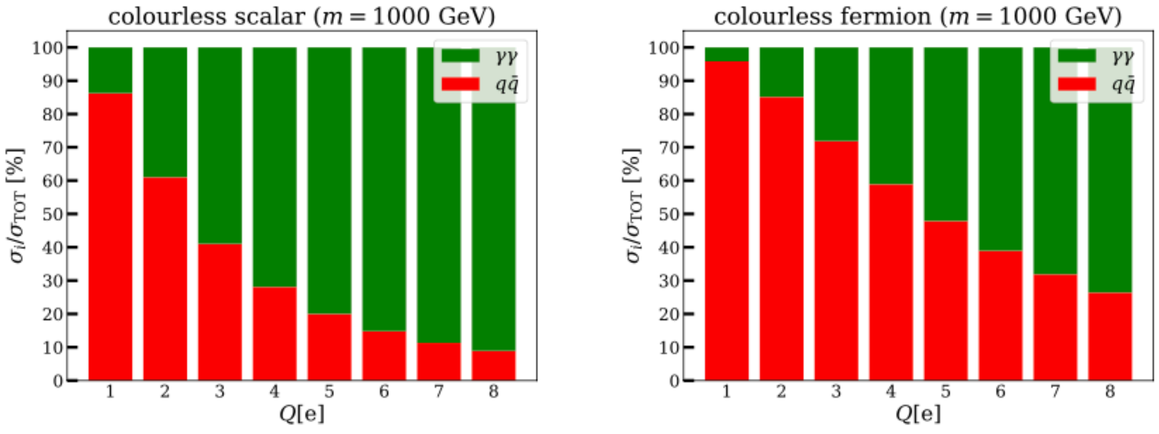

Figure 4.26: Relative contribution to the total production cross section of multiply charged scalars (left) and fermions (right) coming from $q\bar{q}$ (red) and $\gamma\gamma$ (green) initial states. All particles were assumed to have $m = 1$ TeV.

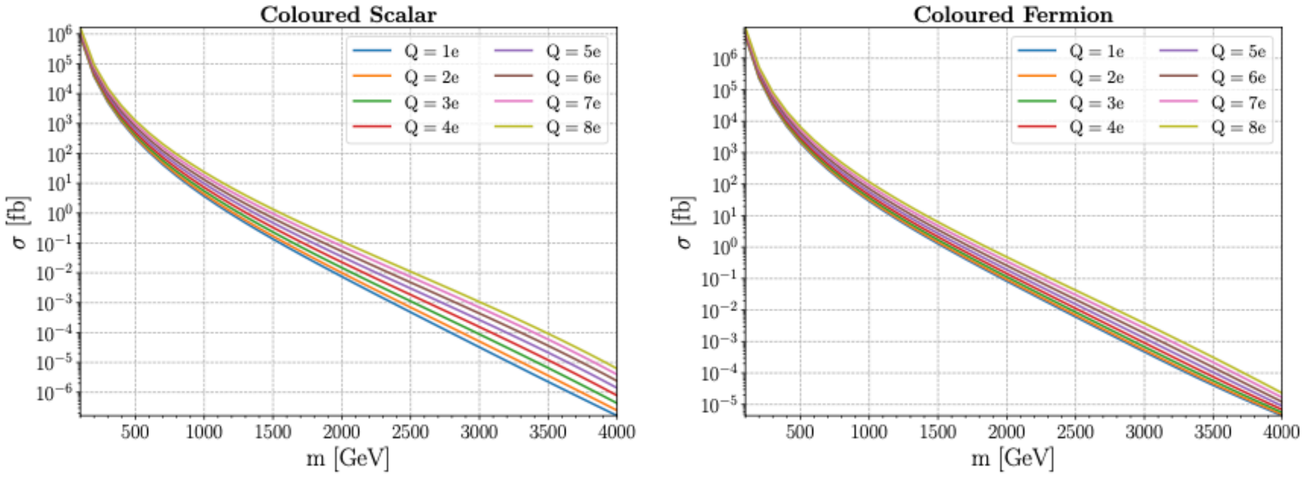

Figure 4.27: LO cross section for open mode production ($pp \to \xi^+\xi^-$) of colour-triplet scalars (left) and fermions (right). Curves with different colours correspond to particles with different magnitudes of the electric charge, Q, from $\pm 1e$ to $\pm 8e$.

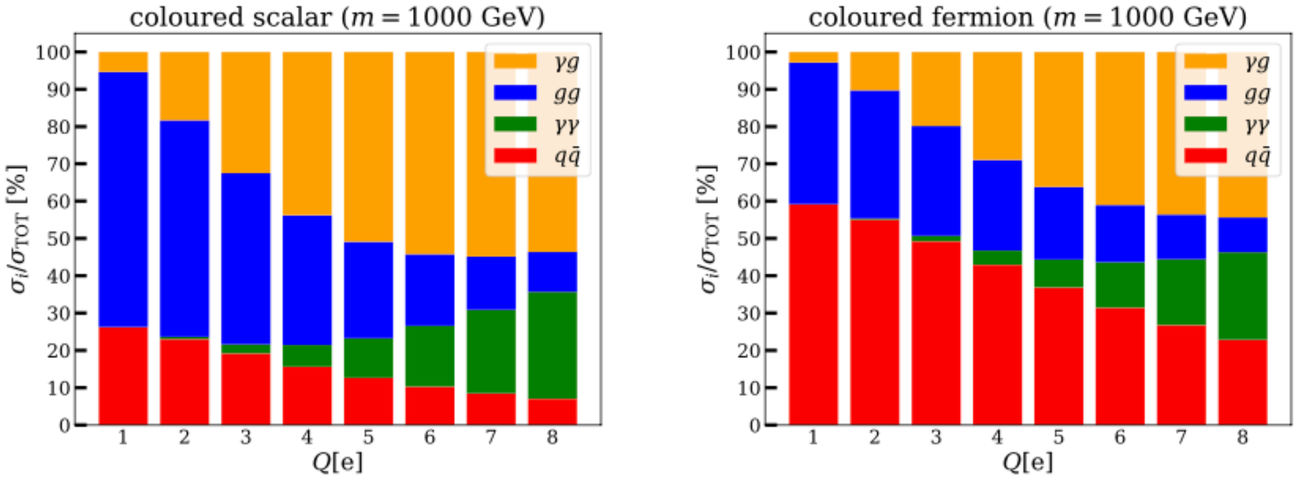

Figure 4.28: Relative contributions of different initial states, $q\bar{q}$ (red), $\gamma\gamma$ (green), gg (yellow), γg (blue), to the total production cross section of $SU(3)_C$-triplet scalars (left) and fermions (right), assuming $m = 1$ TeV.

Table 4.5: The hadronisation model for colour-triplet scalars (ϕ^{+Q}) explained. Possible spin-1/2, spin-0 and spin-1 colour-singlet states are listed in the left, centre and right tables, respectively. Each state has a probability of creation and charge shift assigned to it. The only free parameter of the model, k, being the probability to form a mesonic state, is varied between 0.3 and 0.7 when estimating the sensitivity of the LHC experiments to coloured LLPs.

spin 1/2 mesons

state	$\Delta Q/e$	p
$\phi^{+Q} + \bar{u}_{L/R}$	$-\frac{2}{3}$	$\frac{k}{2}$
$\phi^{+Q} + \bar{d}_{L/R}$	$+\frac{1}{3}$	$\frac{k}{2}$

spin 0 baryons

state	$\Delta Q/e$	p
$\phi^{+Q} + u_L u_R$	$+\frac{4}{3}$	$\frac{1-k}{6}$
$\phi^{+Q} + d_L d_R$	$-\frac{2}{3}$	$\frac{1-k}{6}$
$\phi^{+Q} + u_L d_R$	$+\frac{1}{3}$	$\frac{1-k}{6}$
$\phi^{+Q} + d_L u_R$	$+\frac{1}{3}$	$\frac{1-k}{6}$

spin 1 baryons

state	$\Delta Q/e$	p
$\phi^{+Q} + u_L d_L$	$+\frac{1}{3}$	$\frac{1-k}{6}$
$\phi^{+Q} + u_R d_R$	$+\frac{1}{3}$	$\frac{1-k}{6}$

Table 4.6: The hadronisation model for colour-triplet fermions (ψ^{+Q}) explained. Possible spin-1/2, spin-0 and spin-1 colour-singlet states are listed in the left, centre and right tables, respectively. Each state has a probability of creation and charge shift assigned to it. The only free parameter of the model, k, being the probability to form a mesonic state, is varied between 0.3 and 0.7 when estimating the sensitivity of the LHC experiments to coloured LLPs.

spin 0 mesons

state	$\Delta Q/e$	p
$\psi^{+Q} + \bar{u}_L$	$-\frac{2}{3}$	$\frac{k}{4}$
$\psi^{+Q} + \bar{d}_L$	$+\frac{1}{3}$	$\frac{k}{4}$

spin 1 mesons

state	$\Delta Q/e$	p
$\psi^{+Q} + \bar{u}_R$	$-\frac{2}{3}$	$\frac{k}{4}$
$\psi^{+Q} + \bar{d}_R$	$+\frac{1}{3}$	$\frac{k}{4}$

spin $\frac{1}{2}$ baryons

state	$\Delta Q/e$	p
$\psi^{+Q} + u_L u_R$	$+\frac{4}{3}$	$\frac{1-k}{5}$
$\psi^{+Q} + d_L d_R$	$-\frac{2}{3}$	$\frac{1-k}{5}$
$\psi^{+Q} + u_L d_R$	$+\frac{1}{3}$	$\frac{1-k}{5}$
$\psi^{+Q} + d_L u_R$	$+\frac{1}{3}$	$\frac{1-k}{5}$
$\psi^{+Q} + u_L d_L$	$+\frac{1}{3}$	$\frac{1-k}{5}$

[ATLAS, 1812.03182]

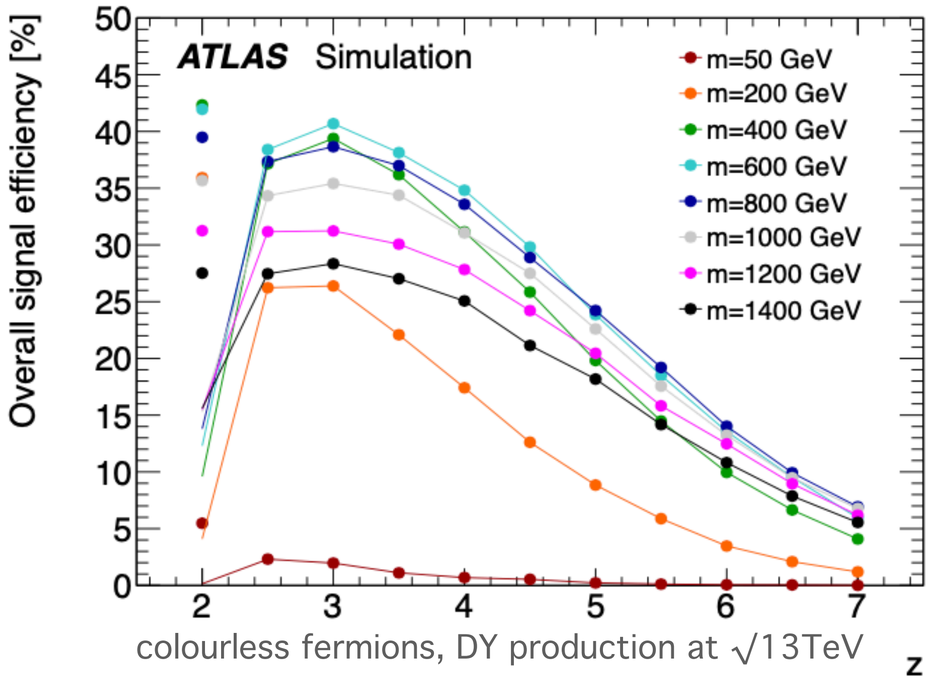

$$p_T^{MEAS} = \frac{p_T^{TRUTH}}{Q}$$

$Q = 1e, \;\; p_T = 50\text{GeV}$

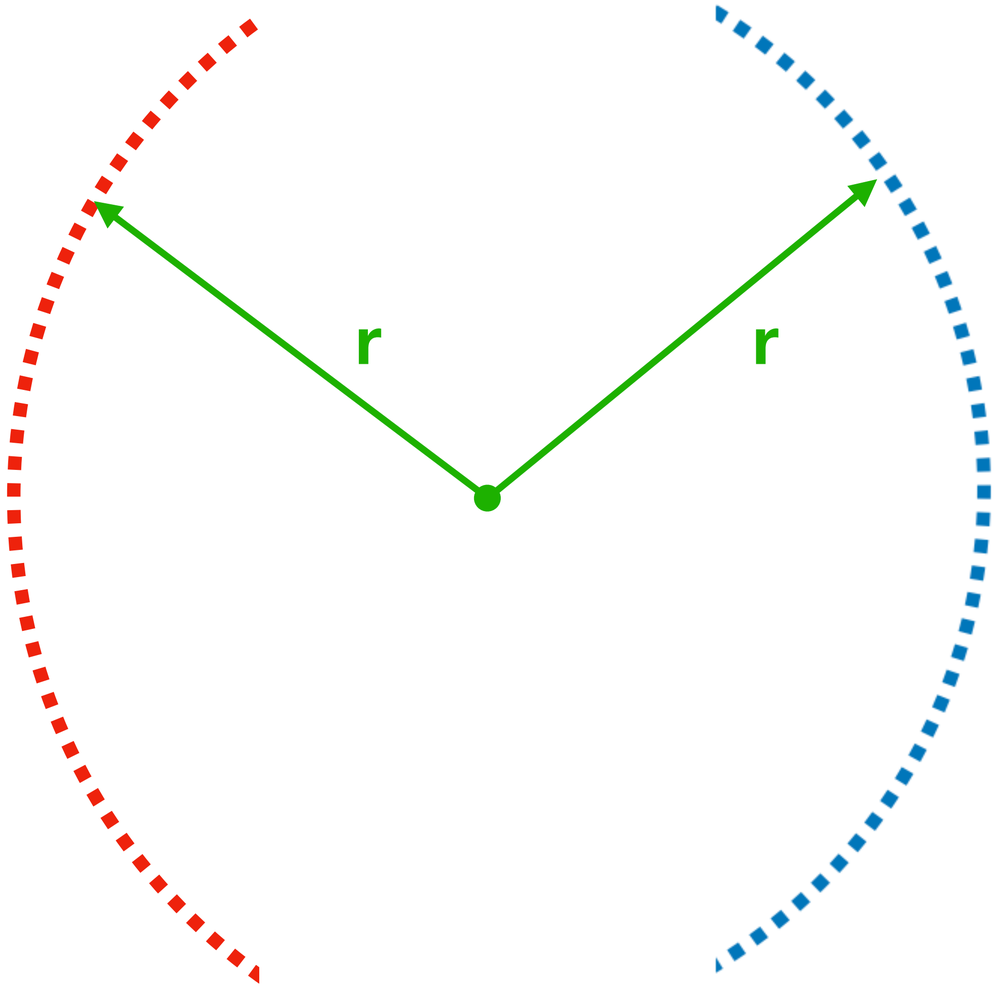

$Q = -8e, \;\; p_T = 400\text{GeV}$

Recasting open channel searches

1. Simulate muon trigger (online selection)

$$\eta \leq 2.1, \quad p_T^{MEAS} \geq 50 GeV, \quad t_{TOF} - \frac{x_{trigger}}{c} \leq 50\ ns\ (25\ ns)$$

$$r = \frac{p_T}{0.3 \times Q \times B} \longrightarrow p_T^{TRUTH} = Q \times p_T^{MEASURED}$$

reconstruction algorithm
assumes Q=1

online selection

$$p_{\mathrm{T}} > 50 \cdot |Q/e| \text{ GeV}\,, \quad |\eta| < 2.1\,,$$

$$t_{\mathrm{TOF}} - \frac{x_{\mathrm{trigger}}}{c} < \begin{cases} 50 \text{ ns} & \cdots\ |\eta| < 1.6 \\ 25 \text{ ns} & \cdots\ 1.6 \leq |\eta| < 2.1 \end{cases}$$

offline selection

$$p_{\mathrm{T}} > 65 \cdot |Q/e| \text{ GeV}\,,$$

$$\frac{1}{\beta_{\mathrm{MS}}} \equiv \frac{c \cdot t_{\mathrm{TOF}}}{x_{\mathrm{trigger}}} > 1.25\,,$$

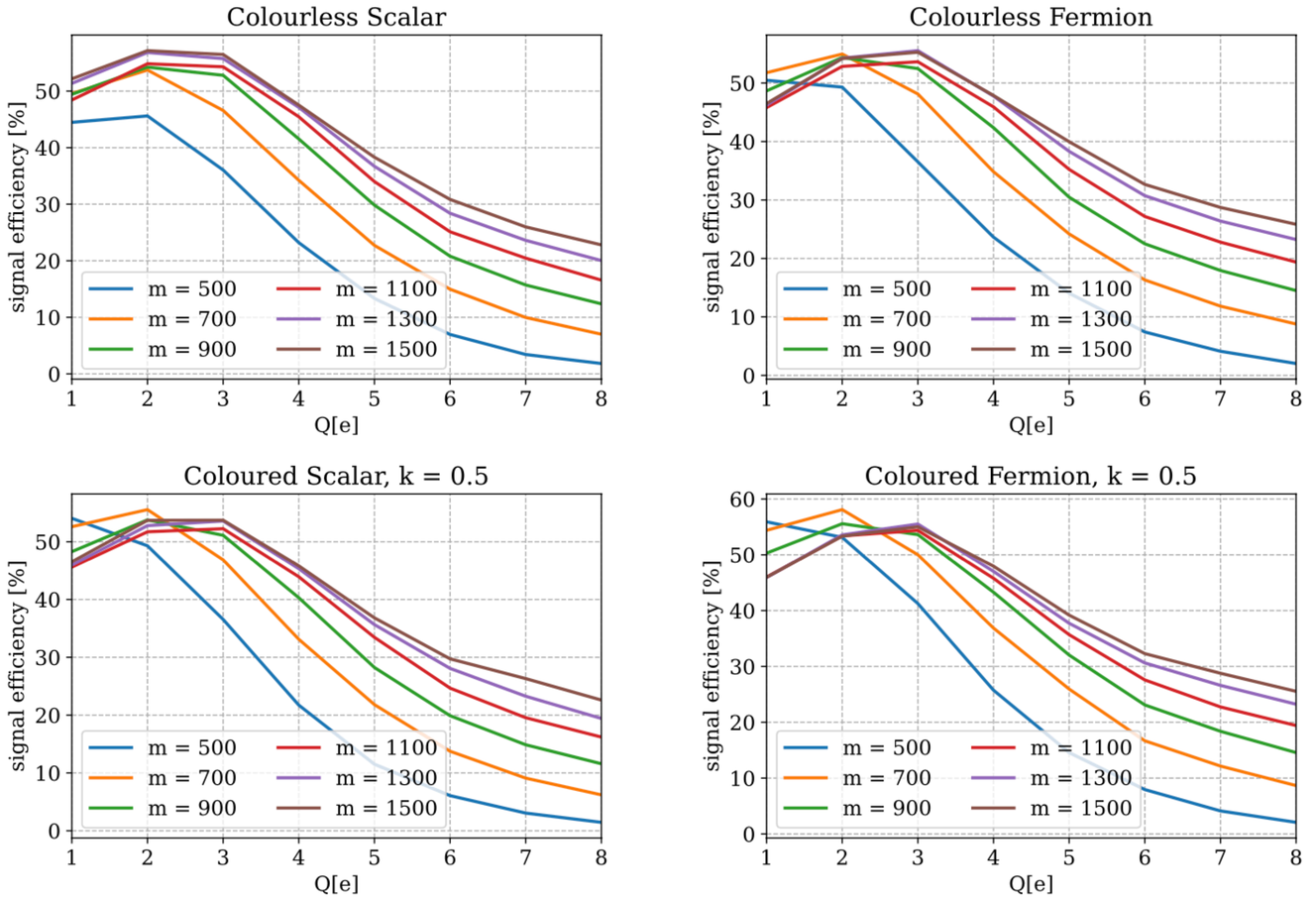

Figure 4.29: Signal efficiency as a function of BSM particle's charge Q, for scalar (left) and fermionic (right) particles. The panels in the bottom (top) correspond to colour-triplet (singlet) particles. Curves with different colours represent different masses.

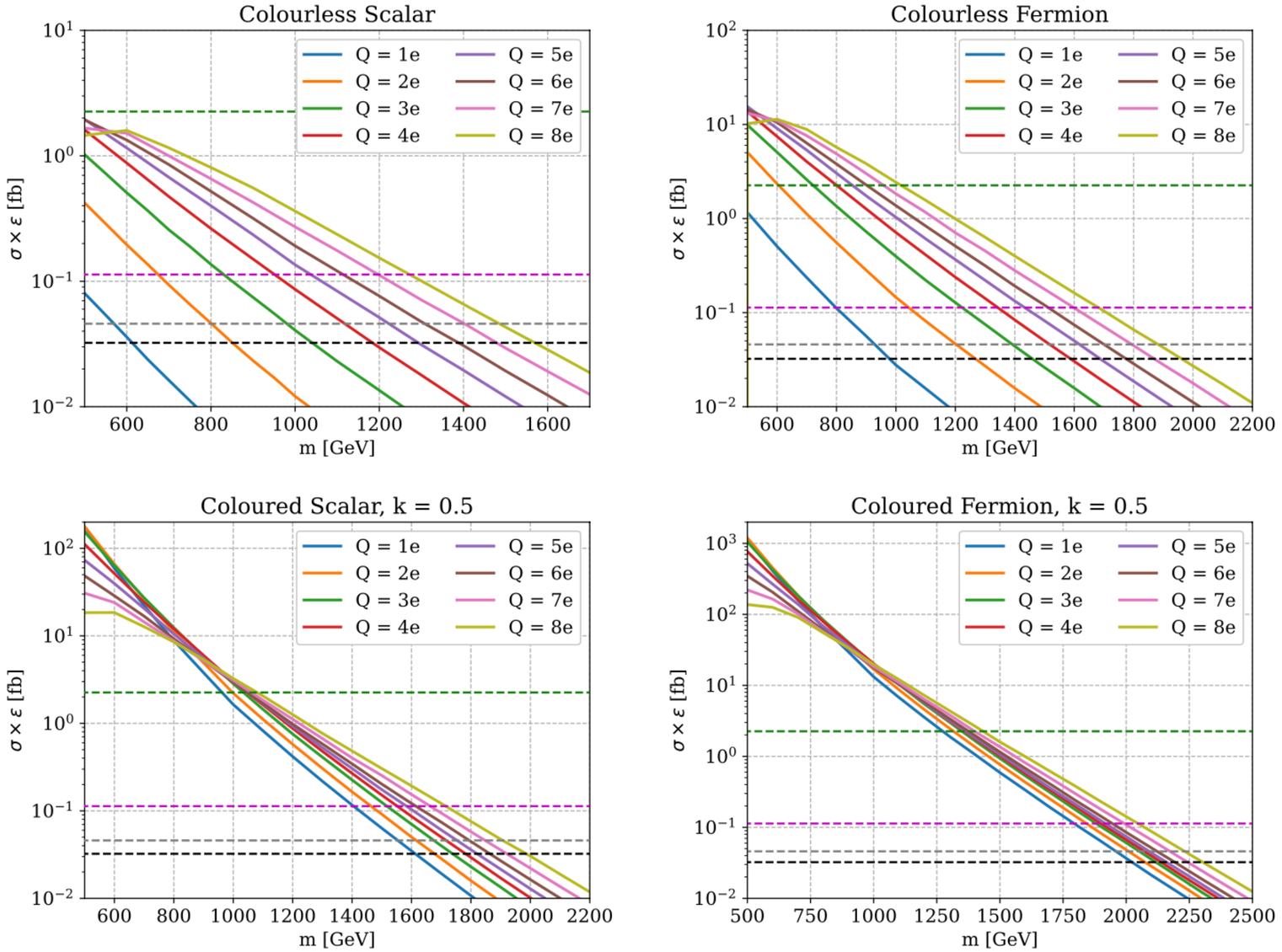

Figure 4.30: Effective cross section, $\sigma_{\text{eff}} \equiv \sigma \cdot \epsilon_{\text{eff}}$, for colourless scalars (top left), colourless fermions (top right), coloured scalars (bottom left), and coloured fermions (bottom right). Distinct colours of solid lines correspond to the effective cross section of particles with different electric charges. The dashed green, magenta, grey and black lines correspond to upper bounds for 2.5 fb^{-1}, 138 fb^{-1}, 300 fb^{-1}, and 3000 fb^{-1}, respectively. Limits were obtained by re-interpreting the CMS analysis [163].

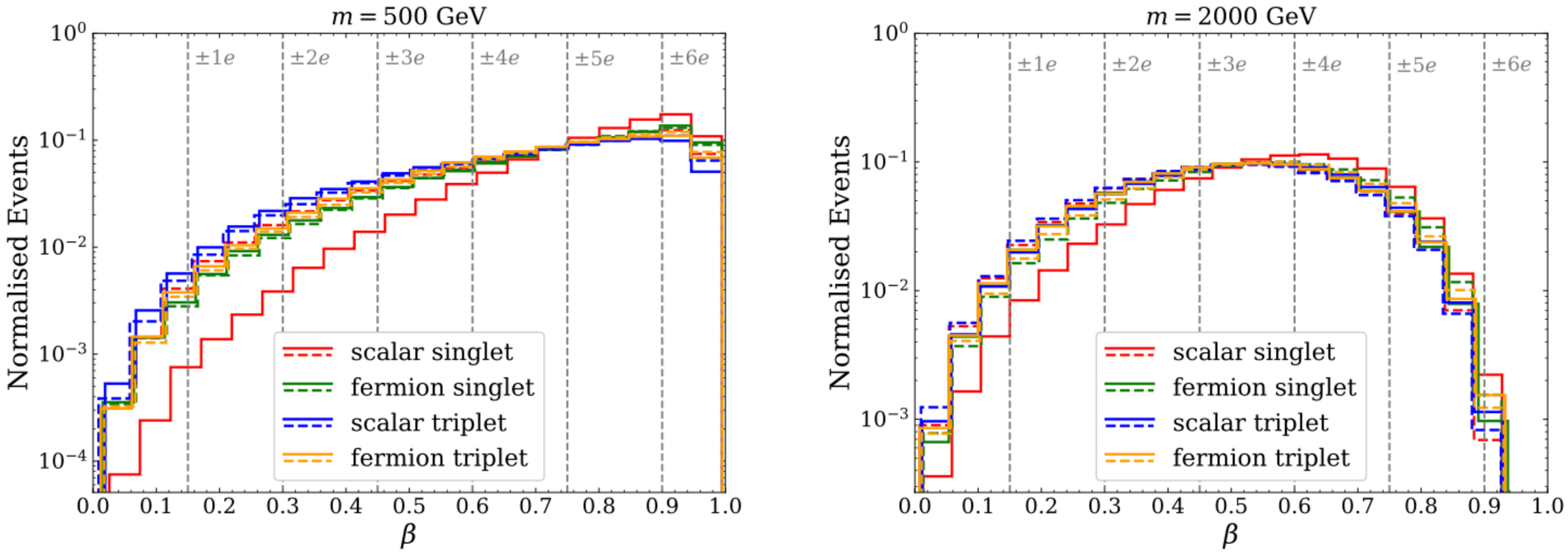

Figure 4.31: Velocity distributions of multiply charged long-lived particles with mass 500 GeV (left) and 2 TeV (right). Solid (dashed) histogram lines correspond to particles with $Q = 1e$ ($8e$). Vertical dashed grey lines correspond to MoEDAL velocity thresholds for different magnitudes of the electric charge.

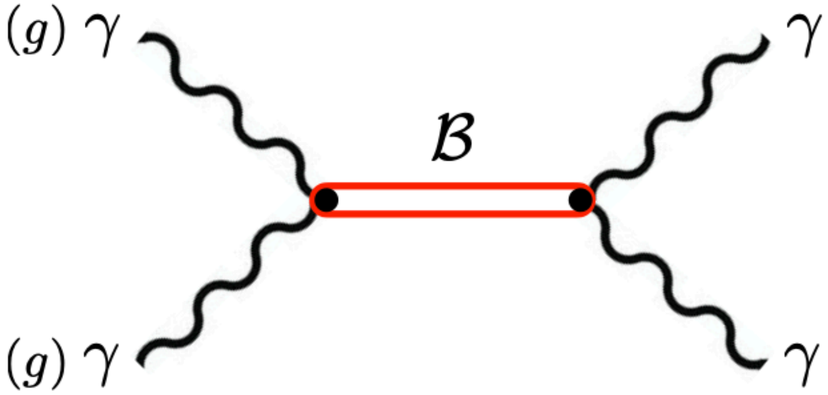

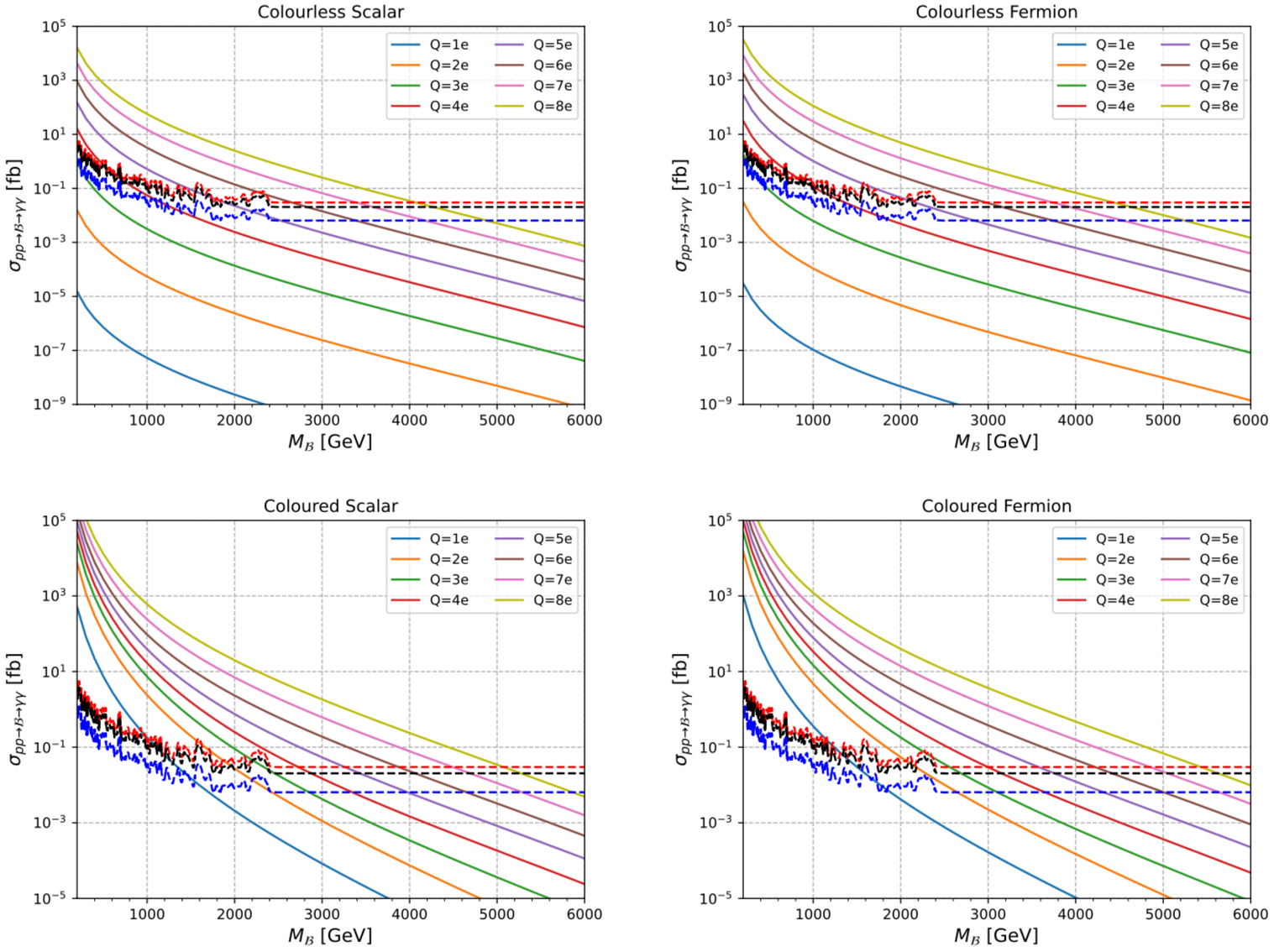

Figure 4.33: Diphoton resonant production cross section for colourless (top row) and coloured (bottom row) particles, with spin-0 (left column) and spin-1/2 (right column). The cross section is presented as a function of the mass of the formed bound state, $M_{\mathcal{B}} \approx 2m$. Dashed lines represent exclusion (sensitivity) upper limits for 139 (red), 300 (black), and 3000 (blue) fb^{-1} ATLAS, based on [251].

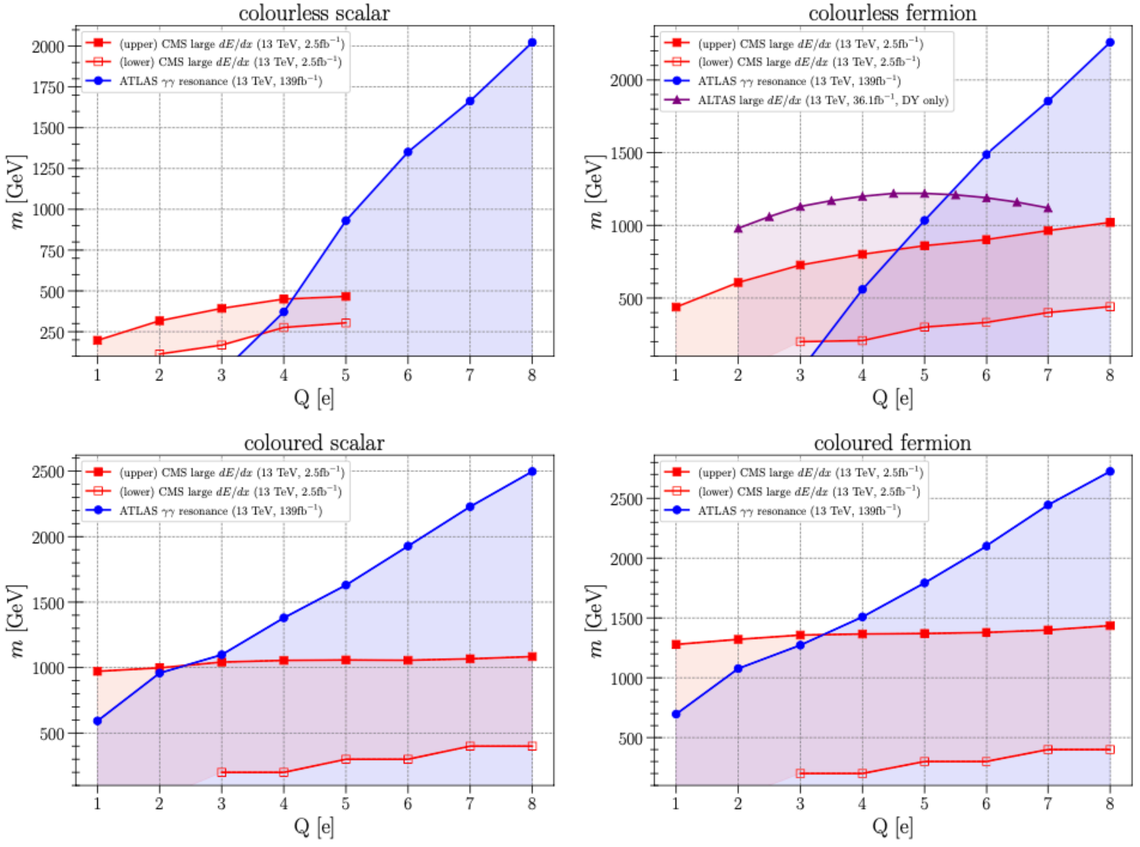

Figure 4.34: Current lower limits on masses of multiply charged particles: colourless scalars (top left), colourless fermions (top right), coloured scalars (bottom left), and coloured fermions (bottom right). The limits were recast to include production processes with initial state photons. The region shaded in red is excluded by the large dE/dx CMS search [163], based on 13 TeV 2.5 fb^{-1} data set. For colourless fermions with $2e \leq |Q| \leq 7e$ there is an additional constrain from the ATLAS search [159] for large dE/dx based on 13 TeV 36.1 fb^{-1} data. The region shaded in blue is excluded by the diphoton resonance search by ATLAS [251], based on 13 TeV 139 fb^{-1} data set.

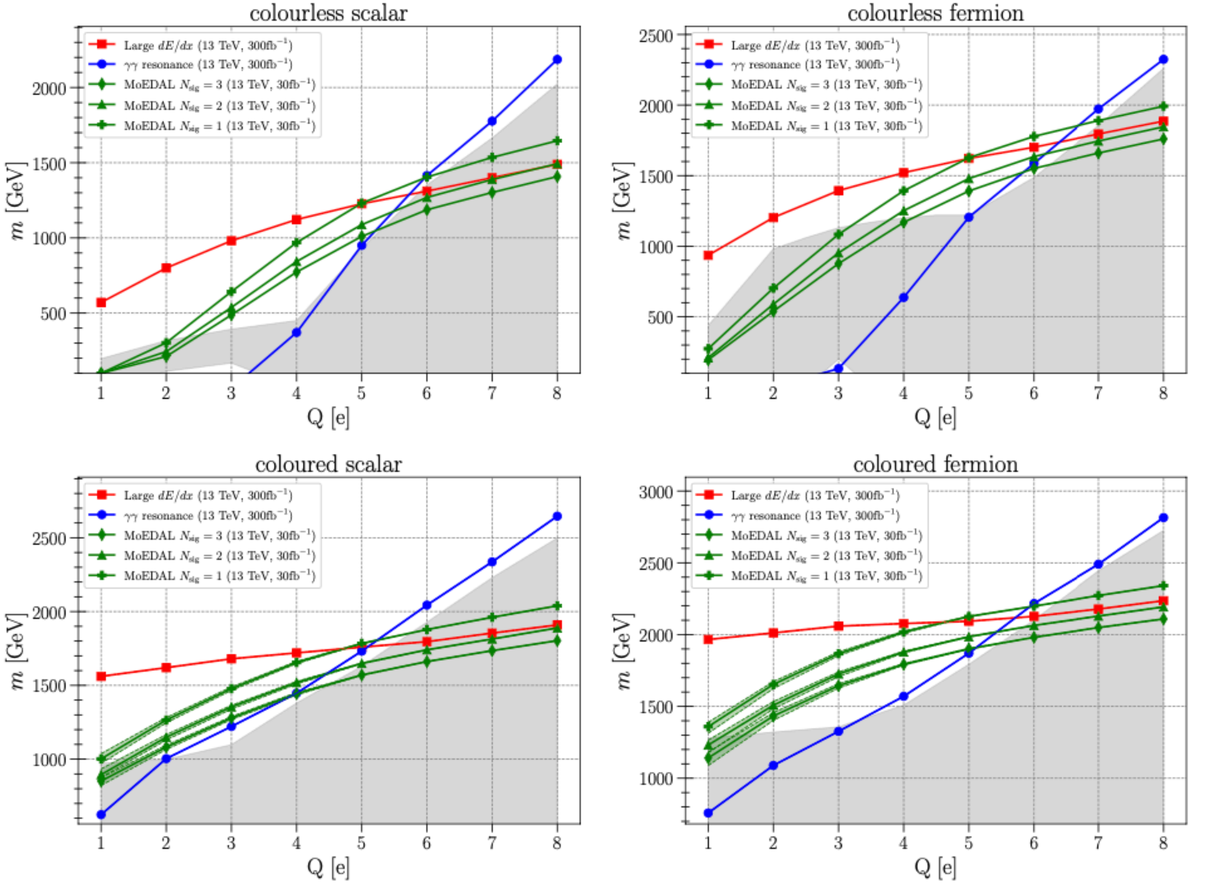

Figure 4.35: Sensitivities of the Run 3 LHC experiments to multiply charged long-lived BSM particles: colourless scalars (top left), colourless fermions (top right), coloured scalars (bottom left), and coloured fermions (bottom right). The integrated luminosity is assumed to be 30 fb^{-1} for MoEDAL, and 300 fb^{-1} for ATLAS and CMS. The region shaded in grey colour is already excluded (cf. Fig. 4.34). Red, blue and green curves correspond to limits provided by large dE/dx, diphoton resonance, and MoEDAL searches, respectively. The uncertainty of the hadronisation model for colour-triplet particles is depicted as the variable width of the curves. This effect is visible only for MoEDAL and particles with $Q \leq 3e$.

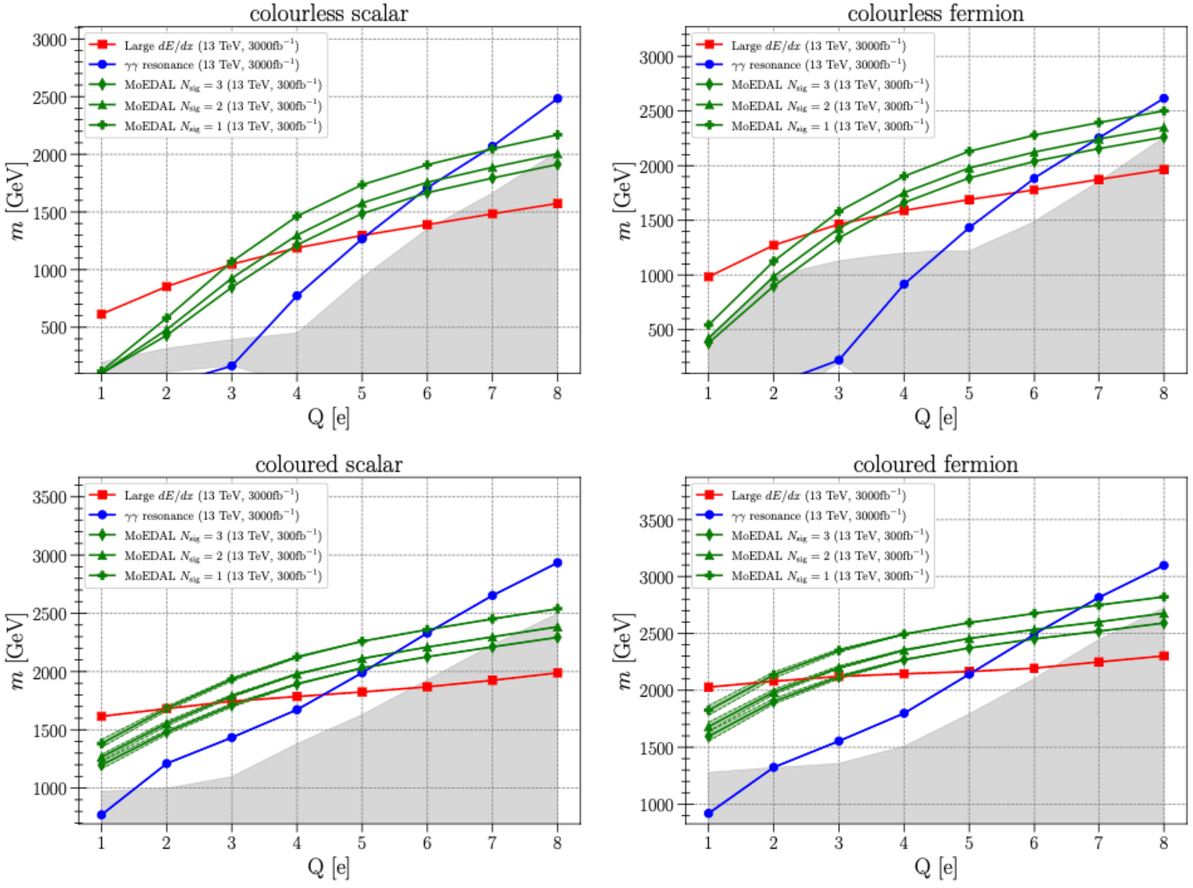

Figure 4.36: Sensitivities of the HL-LHC experiments for multiply charged long-lived BSM particles: colourless scalars (top left), colourless fermions (top right), coloured scalars (bottom left), and coloured fermions (bottom right). The integrated luminosity is assumed to be 300 fb^{-1} for MoEDAL, and 3 ab^{-1} for ATLAS and CMS. The region shaded in grey colour is already excluded (cf. Fig. 4.34). Red, blue and green curves correspond to limits provided by large dE/dx, diphoton resonance, and MoEDAL searches, respectively. The uncertainty of the hadronisation model for colour-triplet particles is depicted as the variable width of the curves. This effect is visible only for MoEDAL and particles with $Q \leq 3e$.

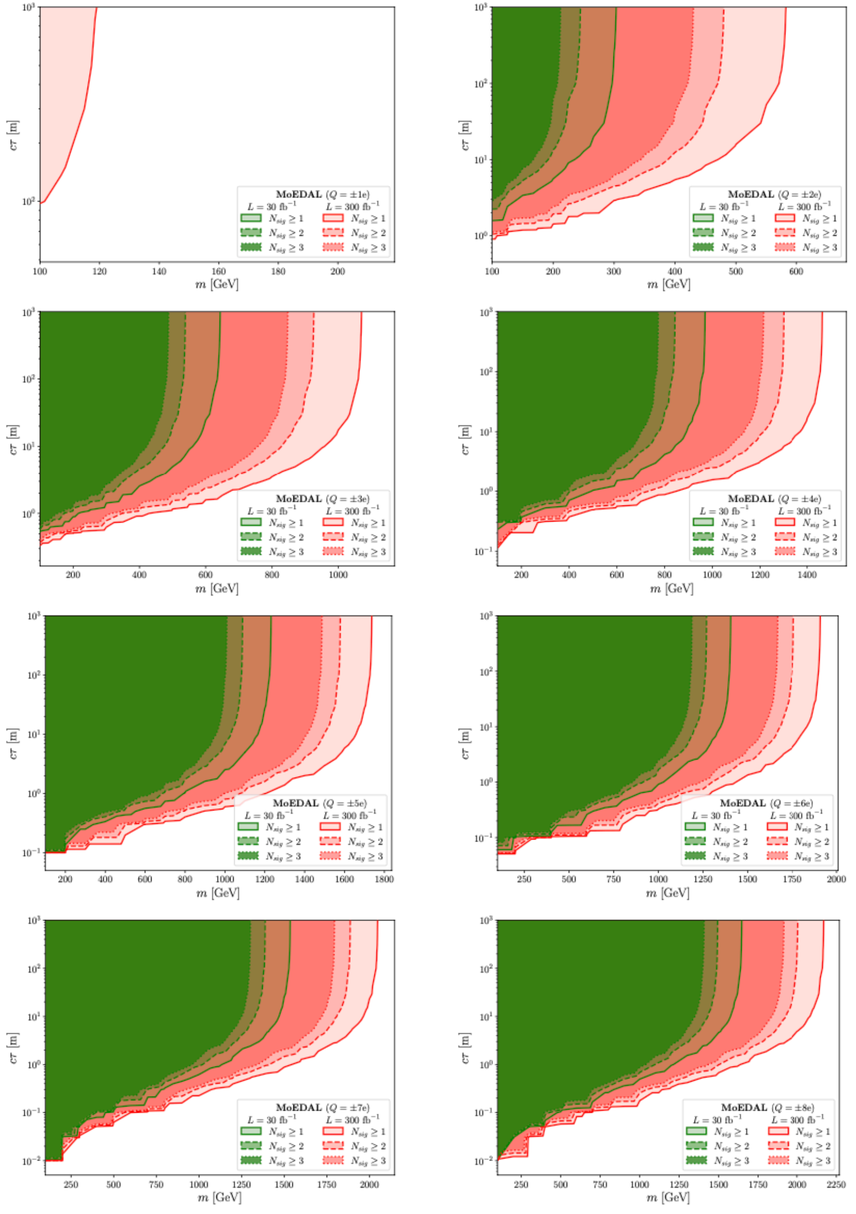

Figure 4.37: Model-independent detection reach of MoEDAL in the (m, $c\tau$) parameter plane for $SU(3)_C$-singlet scalars. Solid, dashed, and dotted contour lines correspond to $N_{\rm sig} = 1$, 2 and 3, respectively. Green and red colours represent results for Run 3 ($L = 30$ fb^{-1}) and HL-LHC ($L = 300$ fb^{-1}) data taking phases, respectively.

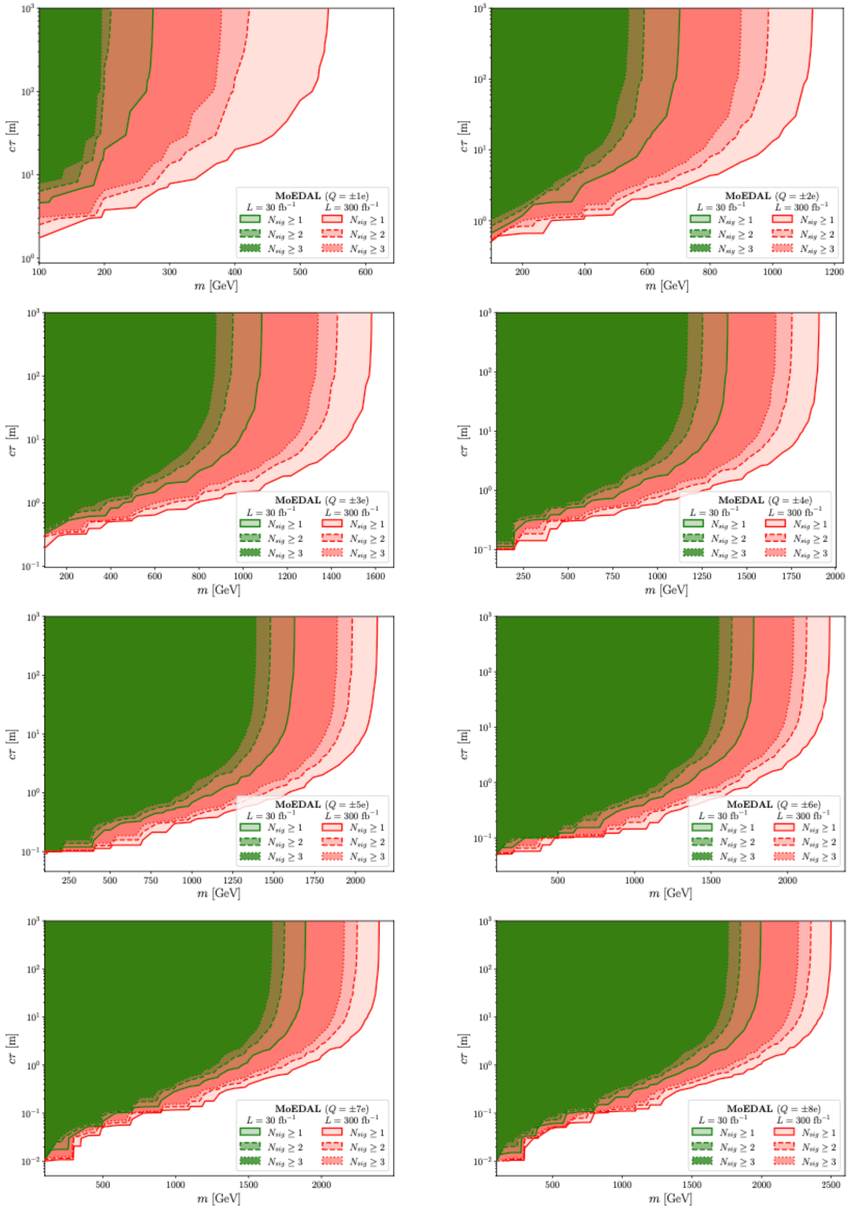

Figure 4.38: Model-independent detection reach of MoEDAL in the (m, $c\tau$) parameter plane for $SU(3)_C$-singlet fermions. Solid, dashed, and dotted contour lines correspond to $N_{\rm sig} = 1$, 2 and 3, respectively. Green and red colours represent results for Run 3 ($L = 30$ fb^{-1}) and HL-LHC ($L = 300$ fb^{-1}) data taking phases, respectively.

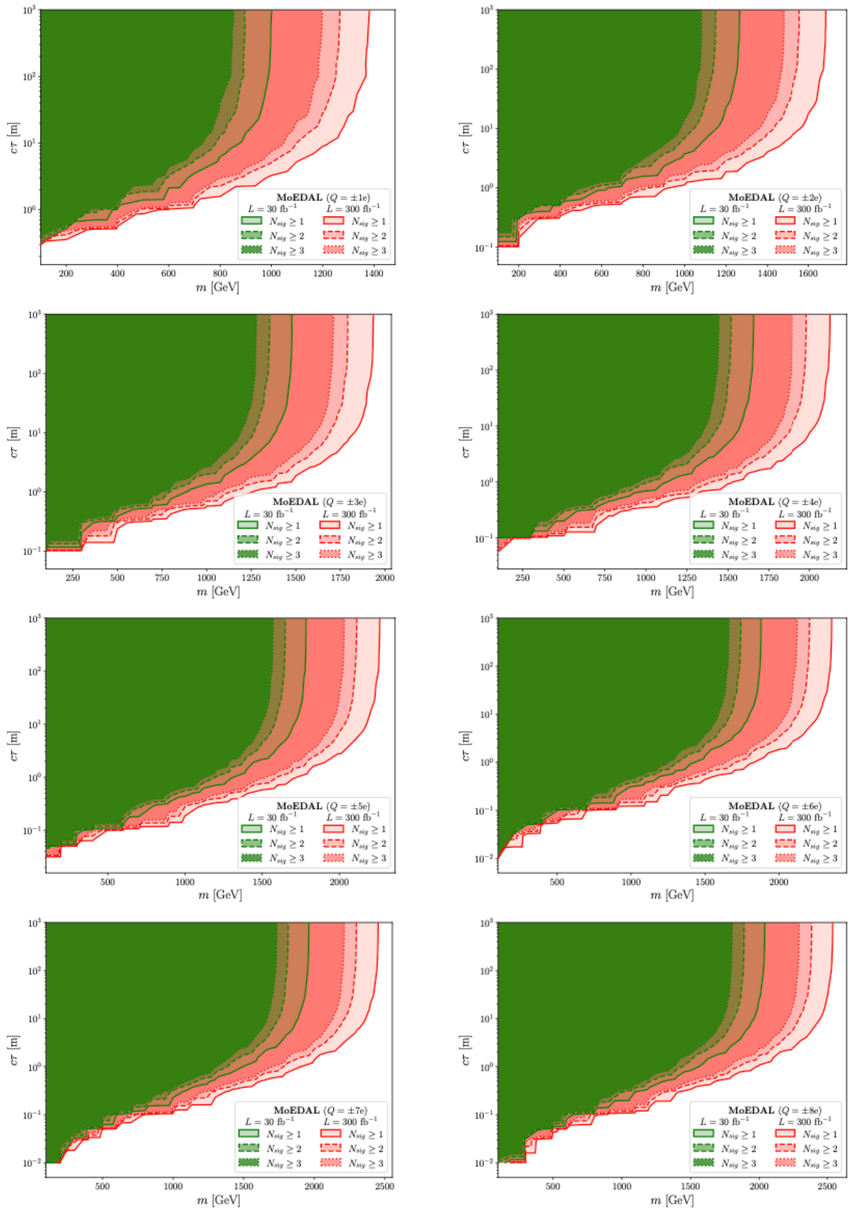

Figure 4.39: Model-independent detection reach of MoEDAL in the (m, $c\tau$) parameter plane for $SU(3)_C$-triplet scalars. Solid, dashed, and dotted contour lines correspond to $N_{\rm sig} = 1$, 2 and 3, respectively. Green and red colours represent results for Run 3 ($L = 30$ fb^{-1}) and HL-LHC ($L = 300$ fb^{-1}) data taking phases, respectively.